Frequency Control of Virtual Power Plants

Weilin Zhong

17209048

A thesis submitted to University College Dublin
in fulfilment of the requirements for the degree of

Doctor of Philosophy

College of Engineering and Architecture
School of Electrical & Electronic Engineering
Head of School: Prof. John Sheridan

Supervisor: Prof. Federico Milano

December 2021

I hereby certify that the submitted work is my own work, was completed while registered as a candidate for the degree stated on the Title Page, and I have not obtained a degree elsewhere on the basis of the research presented in this submitted work.

Acknowledgements

The content of this thesis is the result of my four-year-long research in Dublin, Ireland, working under the supervision of Prof. Federico Milano and within the ESIPP (Energy Systems Integration Partnership Programme) project, Grant No. SFI/15/SPP/E3125.

First, I wish to thank my brilliant supervisor and mentor, Prof. Federico Milano, for the constant technical and financial support, motivation, and feedback throughout my PhD. Working with him has been a great experience. His immense knowledge of power systems always helps me to solve challenging research and engineering problems. On the other hand, his passion and endless motivation for research worked as a source of inspiration and made me always try to give my best. What I have learned from him, e.g. the way to do research, write papers, and focus on details, will advance my entire reach and working life.

Special thanks to my friends Dr. Mohammed Ahsan Adib Murad and Dr. Muyang Liu, for the assistance and collaboration at the beginning of my PhD. Special thanks also to my pals Dr. Georgios Tzounas and Dr. Taulant Kërçi, with whom I had extended collaboration within the group. In addition, I would like to thank all the group members, Dr. Álvaro Ortega, Dr. Guðrún Margrét Jónsdóttir, Dr. Ioannis Dassios, Dr. Junru Chen, and Mr. Muhammad Adeen, as well as the visiting students, Dr. Kaiyao Wan and Dr. Yong Wan, for their invaluable help, our stimulating discussions, and mostly, for sharing everyday life on and off campus.

Finally, I am very grateful to my parents and family for their never-ending support and encouragement throughout my entire life, without which I could not get this far.

Weilin Zhong

Dublin, December 2021

致我的父母，钟振华和刘辉。

Abstract

The Virtual Power Plant (VPP) concept refers to the aggregation of Distributed Energy Resources (DERs) such as solar and wind power plants, Energy Storage Systems (ESSs), flexible loads, and communication networks, all coordinated to operate as a single generating unit.

Using as starting point a comprehensive literature review of the VPP concept and its frequency regulation technologies, the thesis proposes a variety of frequency control and state estimation approaches of VPPs, as follows.

First, the thesis studies the impact of coordinated frequency control of VPPs on power system transients, in which ESSs are utilized to provide fast frequency regulation. The thesis also proposes a simple yet effective coordinated control of DERs and ESSs able to integrate the total active power output of the DERs, and, thus, to improve the overall power system dynamic performance.

The impact of topology on the primary frequency regulation of VPPs is also investigated. With this regard, two types of VPPs topologies are considered, that is, a topology where the DERs that compose the VPP are scattered all-over the transmission grid; and a topology where the DERs are all connected to the same distribution system that is connected to the rest of the transmission grid through a single bus.

Next, the thesis proposes a control scheme to improve the dynamic response of power systems through the automatic regulators of converter-based DERs. In this scheme, both active and reactive power control of DERs are varied to regulate both frequency and voltage, as opposed to current practice where frequency and voltage controllers are decoupled. To properly compare the proposed control with conventional schemes, the thesis also defines a metric that captures the combined effect of frequency/voltage response at any given bus of the network.

Finally, the thesis presents an on-line estimation method to track the equivalent, time-varying inertia as well as the fast frequency control droop gain provided by VPPs. The proposed method relies on the estimation of the rate of change of the active and reactive power at the point of connection of the VPP with the rest of the grid. It provides, as a byproduct, an estimation of the VPP's internal equivalent reactance based on the voltage and reactive power variations at the point of connection.

Throughout the thesis, the proposed techniques are duly validated through time domain simulations and Monte Carlo simulations, based on real-world network models that include stochastic processes as well as communication delays.

Contents

List of Figures

List of Tables

List of Acronyms and Abbreviations

AC	Alternating Current
AGC	Automatic Generation Control
AIITS	All-Island Irish Transmission System
AVR	Automatic Voltage Regulator
CoI	Center of Inertia
CSMA	Carrier Sense Multiple Access
CVPP	Commercial Virtual Power Plant
DAE	Differential-Algebraic Equation
DB	Deadband
DC	Direct Current
DDAE	Delay Differential-Algebraic Equation
DER	Distributed Energy Resource
DFIG	Doubly-Fed Induction Generator
DG	Distributed Generator
DMS	Data Management System
DS-VPP	Distribution System Virtual Power Plant

EMS Energy Management System

ESS Energy Storage System

EV Electric Vehicle

FCR Frequency Containment Reserve

FFR Fast Frequency Response

ICT Information and Communications Technology

IEC International Electrotechnical Commission

IEEE Institute of Electrical and Electronics Engineers

IP Internet Protocol

ISO International Organization for Standardization

LF Loop Filter

LFC Load Frequency Control

LPF Low-Pass Filter

MG Microgrid

MILP Mixed-Integer Linear Programming

MPPT Maximum Power Point Tracking

PD Phase Detector

PDC Phasor Data Concentrator

PDF Probability Density Function

PFC Primary Frequency Control

PI Proportional-Integral

PID Proportional-Integral-Derivative

PLL Phase-Locked Loop

PMU Phasor Measurement Unit

PoC Point of Connection

PSS Power System Stabilizer

PV Photo-Voltaic

RES Renewable Energy Source

RoCoF Rate of Change of Frequency

RTU Remote Terminal Unit

SDDAE Stochastic Delay Differential-Algebraic Equation

SDE Stochastic Differential Equation

SFC Secondary Frequency Control

SIL Storage Input Limiter

SM Synchronous Machine

SoC State of Charge

SPVG Solar Photo-Voltaic Generation

SRF-PLL Synchronous Reference Frame Phase-Locked Loop

SVC Static Var Compensator

TG Turbine Governor

TSO Transmission System Operator

TS-VPP Transmission System Virtual Power Plant

TVPP Technical Virtual Power Plant

UC Unit Commitment

UDP User Datagram Protocol

ULTC Under-Load Tap Changer

VCO Voltage Controlled Oscillator

VDL Voltage-Dependent Load

VPP Virtual Power Plant

VSC Voltage-Sourced Converter

VSG Virtual Synchronous Generator

WAC Wide-Area Communication

WG Wind Generator

WiFi Wireless Fidelity

WLAN Wireless Local Area Network

WSCC Western Systems Coordinating Council

Notation

This section states the notation adopted throughout the thesis.

Vectors and Matrices

a, A	scalar
$\boldsymbol{a}$, $\mathbf{a}$	vector
$\boldsymbol{a}^*$, $\mathbf{a}^*$	vector conjugate
$\boldsymbol{A}$, $\mathbf{A}$	matrix
$\boldsymbol{A}^*$, $\mathbf{A}^*$	matrix conjugate

Sets and Units

$\mathbb{C}$	complex numbers
$\jmath$	unit imaginary number
$\mathbb{R}$	real numbers

Time Domain

$a(t)$	time domain quantity
$\dot{a}(t)$	first order derivative
$\ddot{a}(t)$	second order derivative

Common Parameters

B	susceptance
$\mathcal{B}$	data packet size
D	damping coefficient
G	conductance
K	control gain

M	mechanical starting time
$\mathcal{P}$	data packet lose rate
R	resistance
$\mathcal{R}$	droop constant of primary frequency control
$\mathcal{S}$	transmission channel bandwidth
T	time constant
X	reactance
Y	admittance
Z	impedance
α_p	voltage exponent of active power in load models
α_q	voltage exponent of reactive power in load models
τ	time delay

Common Variables and Functions

a	drift term of stochastic process
b	diffusion term of stochastic process
E	stored energy
P, p	active power
Q, q	reactive power
S, s	complex power
t	time
u	input signal
v	voltage magnitude
x	state variable
y	algebraic variable
Γ	Gamma function
Δ	variation of quantity
ϵ	input error signal
η	stochastic perturbations
θ	voltage phase angle
μ	mean value
ξ	white noise
ϱ	rate of change of the voltage with respect to the magnitude
σ	standard deviation

ω	angular frequency

Common Superscripts and Subscripts

CoI	center of inertia
d	direct axis of the dqo transform
d	delayed quantity
D, h	device connected to bus h of the grid
f	low-pass filter
G	generator
inj	power injection
L, h	load connected to bus h of the grid
loc	local bus
m	mechanical
min	minimum
max	maximum
o	initial condition
PoC	point of connection
q	quadrature axis of the dqo transform
ref	reference
W	Weibull distribution
w	washout filter

Chapter 1

Introduction

1.1 Research Motivation

The electric power system is currently undergoing deep structural transformations. Arguably, the most significant change is the gradual replacement of conventional fossil fuel-based power plants with Renewable Energy Sources (RESs) due to the environmental and sustainability concerns [65, 100]. Most of the RESs, such as Wind Generator (WG) and Solar Photo-Voltaic Generation (SPVG) connected to the grid through power electronic converters and contribute to the reduction of the overall available rotational inertia in the system which, in turn, may lead to large frequency variations and threat the dynamic performance and stability of the grid. Other notable changes are the increased flexibility of energy generation/consumption - partially due to the steady growth of Energy Storage Systems (ESSs), controllable loads and Electric Vehicles (EVs), as well as the integration of power networks with communication systems through the Information and Communications Technology (ICT).

The Virtual Power Plant (VPP) concept refers to the aggregation of the elements above, including Distributed Energy Resources (DERs), ESSs, flexible loads, ICTs, all coordinated to operate as a single generating unit [57]. As the power generations of VPPs are intermittent and stochastic, how to regulate VPPs to maintain the system dynamic and stability is a challenging task.

The primary purpose of a VPP is to optimize the performance of its constituent parts by coordinating the production and consumption [71]. For operation purposes, the active power output of a VPP is scheduled similarly to conventional generators, e.g. through the solution of a daily-ahead unit-commitment problem [93]. In transient conditions, e.g. following a contingency, VPPs have to provide frequency support [54]. The active power scheduling and the frequency control are generally decoupled due to their different time scales. Moreover, the devices that form a VPP can be geographically dispersed or combined as a cluster in a distribution network, which has different requirements for ICT. In this vein, the impact on the dynamic performance of the VPP of topology and communication delays due to communication networks should also be taken into account.

An option to improve the VPP dynamic performance is to enhance the frequency control capability of the DERs. However, the capability of DERs to regulate the frequency through the available power reserve is limited because (i) they are typically designed to achieve a (near) maximum power extraction; and (ii) the availability of a certain power reserve is hard to be ensured, since a large portion of DER generation is stochastic, e.g. wind and solar Photo-Voltaic (PV) [58].

Frequency regulation in power systems is traditionally provided through the active power, while the reactive power is employed to regulate the voltage. This is an intuitive choice for conventional large-scale systems, where the active (P) and reactive (Q) power flows are largely decoupled due to the highly inductive nature of transmission lines [48]. On the other hand, DERs are often integrated within distribution networks, where the resistance/inductance (R/X) ratio of feeders is large, thus leading to a strong interaction of P and Q with voltage and frequency, respectively. In this vein, effectively exploiting the P-Q coupling has the potentiality to improve the frequency and voltage regulation provided by DERs.

As already mentioned, the backbone of today's power grids, i.e. the conventional Synchronous Machines (SMs), are being replaced by power-electronic driven RESs, with RESs is reducing the overall system inertia. Therefore, apart from the control strategies, the estimation of inertia provided by VPPs is also an interesting topic. Compared to the conventional power plants, the main characteristic of converter-interfaced VPPs is that they do not provide mechanical inertia to the system. Still, the controls of their power converters can be designed so that they emulate the inertial response of SMs, leading to the concept of *equivalent* or *virtual* inertia. It is relevant to note that, in contrast to the inertia constant of a SM, the virtual inertia provided by a VPP may be time-varying. Monitoring the equivalent inertia provided by VPPs becomes a key feature towards a reliable and flexible grid in a low-inertia power system, which helps operators to apply suitable control strategies to mitigate stability challenges.

The objective of this thesis is to explore all three above directions. In particular, the thesis features novel aspects in coordinated frequency control of VPPs, combined voltage-frequency control of DERs, and inertia and fast frequency control estimation of VPPs.

1.2 Thesis Overview

1.2.1 Contributions

The main goal of this thesis is to contribute to the stability analysis and control of VPPs by developing a handful of novel control techniques for the DERs within VPPs. In particular, the main contributions of the thesis are in three directions, namely, coordinated frequency control of VPPs, combined voltage-frequency control of DERs, and inertia and fast frequency control estimation of VPPs.

Coordinated Frequency Control of Virtual Power Plants

Proper control of VPPs is crucial to ensure a stable operation of the power grid. This thesis employs coordinated frequency control schemes for the purpose of VPPs control in two ways: (i) by coordinating ESS with the VPP active power output to provide fast frequency regulation to the grid; (ii) by coordinating the RESs within VPP to improve power system short-term dynamics.

1. *Coordinated* ESS*:*

   ESSs are expected to become crucial elements of the fast frequency control in low-inertial systems and, in turn, of VPPs. With this regard, during the last decade, there has been a growing interest in the modeling and control of ESSs [68, 84, 85]. The main objective of the ESS is to regulate a measured quantity of the system, e.g., the frequency of the bus of connection of the ESS with the grid, based on common and practical control schemes, such as the Proportional-Integral (PI), Proportional-Integral-Derivative (PID), and lead-lag controllers. This is due to the fact that these kinds of control schemes combine a simple structure, which is easy tuning and has overall a good performance. With this in mind, this thesis investigates an extension control structure for the ESS, based on the common control scheme.

In this thesis, a centralized frequency control scheme of the ESS included in a VPP is developed. This scheme coordinates the active power output from the VPP by taking into account the information sharing from the DERs.

2. *Coordinated* RES*:*

   The ability of ESSs to provide frequency control is limited by their capacity and State of Charge (SoC) at any given time. As a consequence, ESS might not always be effective and improve the dynamic performance and stability of the grid [65,127]. To address this problem, apart from ESSs, other RESs within a VPP, such as WGs and SPVGs, can be coordinated to provide fast frequency regulation.

   In this thesis, a simple yet effective coordinated control technique of VPPs is proposed, which is able to integrate the total active power output of the RESs and, thus, improves the power system dynamic response and maintains frequency stability.

Combined Voltage-Frequency Control of Distributed Energy Resources

Apart from investigating the control structure of the overall VPPs, developing novel control approaches of the DERs can also enhance the dynamic response of power systems. DERs are often integrated within distribution networks, where the resistance/inductance (R/X) ratio of feeders is large, thus leading to a strong interaction of P and Q with voltage and frequency, respectively. In this vein, references indicate that voltage and reactive power regulation can contribute to the improvement of the frequency response [23, 111], and active power regulation can also be utilized to improve the voltage response of the system [29, 120].

This thesis proposes a simple yet practical control scheme that enhances the dynamic response of power systems through the automatic controllers of converter-based DERs. In the proposed scheme, the regulation of both frequency and voltage is provided through both the active and reactive power control loops of DERs. This is in contrast to current practice, where active and reactive control loops are partially or fully decoupled. As a byproduct, a novel scalar metric is proposed to capture the combined effect of frequency/voltage response provided at a bus of a power network. This metric is sensitive to the rate of change of the frequency and the voltage and thus captures and is able to evaluate the transient performance of the proposed DER active/reactive control scheme under a variety of disturbance scenarios.

Inertia and Fast Frequency Control Estimation of Virtual Power Plants

In contrast to SMs, most VPPs consist of devices connected to the grid through power electronic converters and contribute to the reduction of the overall available rotational inertia in the system which, in turn, may lead to large frequency variations and threat the dynamic performance and stability of the grid [57,65]. On the other hand, if properly controlled, VPPs can provide, as an ancillary service, an inertial response that is similar to that provided by conventional SMs [125]. The goal of this thesis is to provide a novel method to estimate the equivalent inertia and FFR provided by VPPs, a tool that can help system operators to better plan, monitor, and control their network.

This thesis proposes a technique to track in real-time the equivalent inertia of a VPP. The estimator relies on a novel approach to determine the VPP's internal equivalent reactance. The SM model imposed to the VPP for the estimation takes into account the machine's damping, which, first, leads to improved accuracy of the estimation and, second, allows estimating the VPP's equivalent FFR droop gain.

* * *

The simulation results presented in this thesis were obtained with a co-simulation framework for power systems and communication networks, which integrates the Python-based power system analysis software tool Dome [60] and the communication network simulator NS-3 [92]. A detailed description of the framework is provided in Appendix C. The models and techniques developed in the course of this thesis were implemented and included in Dome.

1.2.2 Organization

The remainder of the thesis is organized as follows.

Chapter 2 provides the overview of the VPP concept and its frequency regulation technologies. The VPP is a paradigm that aggregates widely dispersed resources over an electrical grid or part of it thereof and aspires to emulate the behavior of conventional generators. In this sense, VPPs are expected to contribute to system services. One of the most typical and important system services is frequency control. Frequency control ensures the continuous balance of generation and demand and acts so to preserve it in real-time as imbalances occur. To realize this service, proper reserves, defined as regulating reserves, must be procured and retained to respond to any imbalance during a given planning time-frame. As VPPs comprise multiple, different resources, which are dispersed over potentially vast areas, procuring regulating reserves and realizing frequency control is a challenging task. This chapter defines frequency control as a service offered by VPPs, and also illustrates the ways this service may be planned and realized.

Chapter 3 focuses on the coordinated frequency control of VPPs. A simple yet effective coordinated control technique of VPPs to improve the short-term dynamic response of the overall power system is first validated for the ESS, and then tested for other DERs. The robustness of the proposed control is evaluated through a Monte Carlo analysis that leverages a detailed modeling of stochastic disturbances of loads, wind speed, and solar irradiance. The impact of communication delays of a variety of realistic communication networks with different bandwidths is also discussed and evaluated. Moreover, the impact of topology on the primary frequency regulation of VPPs utilized the coordinated frequency control structure is also evaluated in this chapter.

Chapter 4 presents a control scheme to improve the dynamic response of power systems through the automatic regulators of converter-based DERs. In this scheme, both active and reactive power control of DERs are varied to regulate both frequency and voltage, as opposed to current practice where frequency and voltage controllers are decoupled. To assess the proposed control against the current state-of-art, the chapter also defines a metric that captures the combined effect of frequency/voltage response at any given bus of the network. Results indicate that the proposed control strategy leads to a significant improvement in the stability and performance of the overall power system. The impact on the proposed control of load models, the R/X ratio of network lines, as well as the level of DER penetration to the grid, are properly evaluated.

Chapter 5 proposes a method to estimate, in transient conditions, the equivalent inertia constant and fast frequency control droop gain of VPPs. The estimations are obtained based on the frequency and active power variations at the point of connection of the VPP with the power grid. The accuracy of the estimator is enhanced by a novel technique employed to approximate the VPP's equivalent internal reactance, based on the voltage and reactive power variations at the Point of Connection (PoC).

Finally, Chapter 6 summarizes the most relevant conclusions of the thesis and suggests directions for future work.

1.2.3 Publications

This section provides the list of publications that gave rise to the work presented in this thesis.

Journal papers

1. **W. Zhong**, M. A. A. Murad, M. Liu, and F. Milano, Impact of virtual power plants on power system short-term transient response, Electric Power Systems Research, Elsevier, vol. 189, 106609, December 2020.
   DOI: 10.1016/j.epsr.2020.106609

2. **W. Zhong**, J. Chen, M. Liu, M. A. A. Murad, and F. Milano, Coordinated control of virtual power plants to improve power system short-term dynamics, Energies, MDPI, vol. 14, no. 4, 1182, February 2021. *Special Issue: Frequency Regulation in Low Inertia Renewable Energy Dominated Grid 2021.*
   DOI: 10.3390/en14041182

3. **W Zhong**, G. Tzounas, and F. Milano, Improving the power system dynamic response through a combined voltage-frequency control of distributed energy resources, IEEE Transactions on Power Systems, accepted in January 2022, in press.
   DOI: 10.1109/TPWRS.2022.3148243

4. **W. Zhong**, G. Tzounas, M. Liu, and F. Milano, On-line inertia estimation of virtual power plants, Electric Power System Research, Elsevier, accepted in February 2022, in press. Will be presented at the 2022 Power Systems Computation Conference (PSCC), Porto, Portugal, 27 June – 1 July 2022.

Book Chapter

4. T. Kërçi, **W. Zhong**, A. Moghassemi, F. Milano, and P. Moutis, *Frequency Control and Regulating Reserves by VPPs*, in *Scheduling and Operation of Virtual Power Plants*, editors A. Zangeneh and M. Moeini-Aghtaie, Elsevier, February 2022. ISBN: 9780323852678.

Conference Papers

5. **W. Zhong**, M. Liu, and F. Milano, A co-simulation framework for power systems and communication networks, IEEE PowerTech, Milano, Italy, 23-27 June 2019. DOI: 10.1109/PTC.2019.8810936.

6. **W. Zhong**, T. Kërçi, and F. Milano, On the impact of topology on the primary frequency control of virtual power plants, IEEE PowerTech, Madrid, Spain, 27 June - 2 July 2021. DOI: 10.1109/PowerTech46648.2021.9494801.

7. **W. Zhong**, G. Tzounas, and F. Milano, Real-Time Estimation of VPP Equivalent Inertia and Fast Frequency Control, IEEE PES General Meeting, Denver, CO, 17-21 July 2022.

Deliverables

9. G. Tzounas, F. Milano, J. Chen, T. Kërçi, **W. Zhong**, D. Nouti, and G. Lipari, Scenario Description for Frequency and Inertia Response Control for VPPs, Project Name: edgeFLEX, March 2021, available at: https://www.edgeflex-h2020.eu/progress/work-packages.html.

10. G. Tzounas, J. Chen, T. Kërçi, **W. Zhong**, and F. Milano, Frequency Control Concepts for Current VPPs in Large Scale Deployment, Project Name: edgeFLEX, March 2021, available at: https://www.edgeflex-h2020.eu/progress/work-packages.html.

Chapter 2

Frequency Regulation by Virtual Power Plants: Overview and Technologies

2.1 Introduction

Keeping the frequency as close to the nominal value as possible everywhere in the system is one of the main objectives of Transmission System Operators (TSOs). However, this is challenging as frequency fluctuates due to the variations of demand, stochastic noise and harmonics, events such as line connection and disconnections and, last but not least, contingencies [66].

Frequency variations are caused by SMs that inextricably link frequency to power imbalances, as the following simplified swing equation:

$$M\frac{d}{dt}\omega(t) \approx p_{\text{gen}}(t) - p_{\text{load}}(t) - p_{\text{loss}}(t)\,, \tag{2.1}$$

where $\omega(t)$ represents the system frequency, M represents the total inertia of the SMs, $p_{\text{gen}}(t)$ represents the total power generation, $p_{\text{load}}(t)$ represents the total power consumption and $p_{\text{loss}}(t)$ represents the total losses. Notably, equation (2.1) shows that the magnitude of frequency variations depends on the value of M. This means that the greater the system inertia, the smaller the frequency variations and vice versa. The role of inertia has been the focus of intense research in recent years as the high penetration of large rotating non-synchronous renewable sources has significantly reduced the amount of inertia in the system and increased the level of stochastic fluctuations of power [65].

Large frequency deviations may lead to blackouts. For example, they were the main cause of the Italian power system blackout in September 2003 [13]. The partial blackout of the European interconnected power system in November 2006 was caused by overloading cascading effects and the geographic unbalance of the production and the load split [20]. Other frequency related events that led to power system blackouts can be found in [28].

In conventional power systems, the frequency is controlled hierarchically. After a power imbalance occurs, the inertia of the SMs inherently responds (no control needed) to constrain the magnitude of the frequency deviation. Intuitively, it may be described as the response of the rotating machines to the rate of change of the imbalance. Following, the Primary Frequency Control (PFC) is realized. PFC is a local actuation process that measures the rotor speed of the generator (as an equivalent of the electrical frequency), compares it to a reference to calculate the deviation and controls the unit to increase or decrease its output proportionally to that deviation. This control takes place in the time scales of tens of seconds and up to a few minutes, and in most cases is a mandatory service for multiple generating units with an installed capacity greater than a specified threshold. The generating units involved in PFC and the threshold for their eligibility to participate in PFC is defined by TSOs or regulating authorities. Typically, generating units that provide PFC must guarantee an active power reserve greater than $\pm 1.5\%$ of their nominal for interconnected systems and $\pm 10\%$ of their nominal for islanded (or low-inertia) systems [9]. Apart from the PFC, Frequency Containment Reserve (FCR) is another concept in the European Union Internal Electricity Balancing Market that means operating reserves necessary for constant containment of frequency deviations from the nominal value to constantly maintain the power balance in the whole synchronously interconnected system. After PFC, the Secondary Frequency Control (SFC), also known as Automatic Generation Control (AGC), follows and reinstates both frequency and FCR to the nominal value, while it may also restore power exchanges between different areas to their scheduled values, in case they have contributed to PFC. The SFC is planned centrally (although it may be realized by local controllers) and takes place in the time scales of several seconds and up to around 15 minutes. The generating units that provide SFC must guarantee an active power reserve that ranges from $\pm 6\%$ of their nominal for thermal units to $\pm 15\%$ of their nominal for hydroelectric units [9] A typical frequency response in power systems following a loss of a generating unit is shown in Figure 2.1.

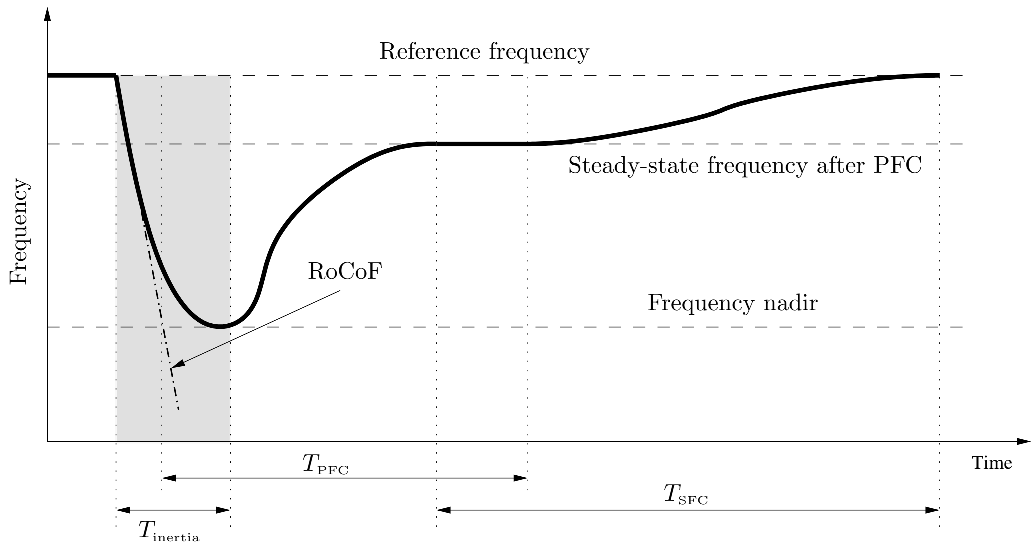

Figure 2.1: Qualitative transient behavior of the frequency in power systems following a loss of a generating unit [51].

Traditionally, TSOs have relied on large conventional power plants connected at the transmission network to provide primary and secondary frequency regulation. As these generators are being gradually decommitted and substituted with small DERs, that are mainly connected at the distribution network, it becomes apparent that the latter ones have to provide these services as well. This chapter discusses the primary and secondary frequency control of VPPs.

The remainder of the chapter is organized as follows. Having already summarized the need for frequency control in power systems, the rest of this Section 2.1 provides a comprehensive review of the most relevant works on VPP frequency regulation. In the review, particular emphasis is given to the role of storage systems, including both large scale batteries and EVs. Section 2.2 expands on the literature review and offers a detailed taxonomy of VPP components, frequency control and reserves frameworks, as well as control and operation strategies.

2.1.1 Literature Review

While the concept of VPP is relatively recent, there is already a fair number of studies on the implementation and impact of frequency control of VPPs on the performance of power systems. This section is divided into three parts, namely DERs, Microgrids (MGs) and ESSs.

2.1.1.1 Distributed Energy Resources

DERs are the main feature of VPPs, as they allow the scheduling of the VPP and define its capacity. The integration, coordination and feasibility of the DERs that compose the VPP has thus been extensively studied.

Regarding the integration of DERs and VPPs, reference [3] explores the matter of frequency regulation by wind and PV energy resources through battery storage systems. The proposed algorithms incorporate large numbers of all aforementioned resources and properly coordinate them for the purpose. The aim is to deliver the service without relying on considerable upgrades of storage capacity. The studies in [72, 91, 107] specify that the electric generators of WGs that are not directly connected to the grid are largely decoupled from the electric frequency, i.e. they cannot contribute to frequency regulation. Deloading such WGs to retain frequency reserves for frequency drops is the way they may be enabled to participate in this service. At the same time a short-term release of active power by drawing kinetic energy from the WG rotor is the means to emulate an inertial response by said assets.

The control of power converters used with DERs plays a key role in the potential of VPPs in offering grid services. A control design for an inverter-interfaced PV system that decouples the dynamics of the generation from those of the grid, is presented in [119]. The method ensures proper control across various operating scenarios and is largely unaffected by whether the grid is more resistive or reactive. In [73] the authors specify that the deloading of a PV plant may be realized by Direct Current (DC) switches controlling groups (strings) of PV modules per each inverter. Frequency regulation signals can accordingly drive more DC breakers to reconnect, thus increasing PV power at an occurrence of a frequency drop and vice versa. Fields tests have shown negligible effect on PV inverter operation and fast response times. A Voltage-Sourced Converter (VSC) interfaced battery storage model is developed in [84] in order to accommodate dynamic and transient behavior studies of such systems. It is a crucial modeling block for the assessment of battery interactions with the grid when the offer of grid services will be considered.

Over-frequency is another problem in modern power systems which can happen every so often. This problem is addressed in [75] that proposes a decision tree based method to reduce the active power output of VPPs and, consequently, mitigate the over-frequency occurrences.

The impact of the frequency control of DERs connected at the distribution level on the dynamic behavior of high voltage transmission systems is studied in [87]. The paper compares three strategies to generate the input signal used by the DER frequency regulators, namely, decentralized, centralized and average. It is shown that the centralized approach leads to a better dynamic performance of the system. However, communication delays can significantly impact the noted performance. The impact of VPPs on power system transient response is analyzed in [127]. This work considers two strategies for the frequency control of the DERs included in the VPP, namely, coordinated and non-coordinated. The paper shows that the coordinated control approach leads to a better dynamic response of the system as compared to that without coordination. The paper also shows that communication delays associated with the coordinated control approach have a negligible impact on the dynamic response of the VPP.

For practical implementation purposes, the frequency response should be straightforward to apply. Reference [81] proposes a test system for easy and dependable determination of frequency response from a VPP connected to a utility grid and including many distinct power plants. The test system includes a module providing a frequency test sequence that is composed of a set of values and a unit injecting them simultaneously to all nodes of the VPP. Each node includes at least one of either a single generating unit, a single storage unit, or a combination of generating and storage units supervised by a plant controller.

The power output control of VPPs is also important in the context of frequency regulation. The control method proposed in [54] aims to provide primary frequency regulation and, at the same time, carefully adjust the aggregated power output of the VPP comprising PVs and controllable loads (ice machines in this paper). This is done by coordinating the power output of the PVs and power consumption of the ice machines; namely, curtailing a certain amount of PV power and adjusting the number of controllable loads by solving a mixed-integer program. PFC is achieved with a quadratic interpolation-based active power control strategy. Each PV can operate in a power dispatch mode and simultaneously estimate its maximum available power.

The aggregation of resources within a VPP is another aspect of frequency control because it concerns generation-demand imbalances that the VPP itself may cause. The researchers in [93] propose to operate a VPP with loads with thermal inertia. The control algorithm acts directly on these loads by optimizing their consumption in a specified period, as well as minimizing the difference between generation and demand. In [97], the definition and numerical simulation methods for three aggregation control strategies of distributed generation units in a VPP are proposed. The strategies seek to maximize the efficiency of VPPs as well as minimize the power deviation during dynamic load conditions. Similarly, [117] proposes a VPP model which integrates Distributed Generators (DGs), ESSs and flexible loads. This VPP performs frequency regulation by decomposing the AGC signal and distributing it to its integrated assets.

The impact of the aggregate response of DERs on the power system dynamic behavior is studied in [42]. The VPP concept is utilized to effectively aggregate the DERs. Two VPP control strategies are proposed, namely, AGC approach and Mixed-Integer Linear Programming (MILP). A case study shows that the AGC-based VPP limits the frequency excursions of the system more efficiently as compared to the MILP-based VPP. The work in [102] develops a semi-empirical lifetime model of lithium-ion batteries operated to provide primary frequency regulation in the Danish energy market. The model is proposed as a tool to study the economic profitability of the investment in lithium-ion battery energy storage system. A feasibility study of VPPs that provide ancillary services, including active and reactive power control, for a 50-kV distribution network in Sweden, is presented in [21]. The paper provides a quantification of the economic profits simulated via measuring the variations in the hourly production and consumption at the network nodes. Some authors have emphasized the importance of the configurations, architectures, and the components/model of VPPs like different types of VPPs, the integration of VPP with DERs like PV or WG, ICT systems, etc.

A comprehensive review of the types, architectures, operations, optimization algorithms, communication requirements and current implementations of VPPs, is provided in [118]. A method of operating a MG as VPP, based on artificial intelligence methods is outlined. The paper anticipates that VPPs will become common solutions for grid operations.

In [43] a DG inverter controller is developed to manage active and reactive power transfer over any type of line, either resistive or reactive. The approach enables complete power control regardless of the type of network (transmission or distribution) to which the generator is connected to. This study, although not explicitly addressing generation-demand imbalances, it describes how dispersed VPP resources can ensure the maximum power transfer when contributing to frequency regulation services.

In [90], the authors present how a Commercial Virtual Power Plant (CVPP) can integrate distributed resources and trade them in the energy market, while accounting for the network constraints and other operating constraints imposed by the Technical Virtual Power Plant (TVPP). An overall algorithm to combine these two aspects of a VPP is proposed and the challenges forward are identified. The ICT requirements in light of enabling VPPs to procure, offer and realize ancillary services, are presented in [22]. The current standards frameworks need to be rethought and/or enhanced according to new directions. Based on the example of International Electrotechnical Commission (IEC) 61850, ancillary services from VPPs will be enabled if additional interactions among the various actors are defined and the data are properly determined.

The work in [45] proposes a capability-coordinated frequency control method for a VPP including an adjustable-speed pumped storage hydroelectric plant, a wind power plant, and an ESS, to improve the controllability of the VPP. The method can reduce the frequency nadir, with a signal of frequency correction distributed among the VPP assets, and decrease the steady-state error of system frequency with a SFC type of coordination. This, in turn, provides flexible ancillary service to the frequency regulation of a power system.

2.1.1.2 Microgrids

VPPs are not MGs, as the latter, usually have complete sensing and control of the grid among the controlled assets [96]. Yet, MGs have several aspects in common with VPPs, one of them being the ability to provide frequency and voltage support. The researchers in [25] study the impact of high shares of MGs on the Load Frequency Control (LFC) of power systems. The paper develops a dynamic model of MGs to study its contribution to LFC. MGs are classified into two categories of different features with respect to the LFC. The work in [35] proposes a coordinated frequency control approach for the EVs and RESs included in a MG. The approach is based on an adaptive PI controller. The paper shows that the proposed controller is robust to the volatility of the RESs. In [24], an extended Virtual Synchronous Generator (VSG) is presented for MGs based on the concept of virtual rotor, to procure primary, and secondary control. This virtual asset is inspired by the conventional synchronous generator. Its effectiveness is verified via of an MG test system.

In [114] the authors propose a distributed secondary frequency and voltage control approach for islanded MGs. The effectiveness of the proposed controller is evaluated by means of small-signal stability and time domain analysis. The paper shows that the controller can restore the frequency and bus voltage to their nominal value and ensure proper reactive power-sharing. Also, a power control strategy for Doubly-Fed Induction Generator (DFIG) in an MG is introduced in [121]. The control strategy makes use of a 10% wind power margin to provide frequency support. Moreover, reference [121] proposes a variable coefficient strategy in order to utilize different control parameters at different wind speeds and, in this way, improve the DFIG frequency support.

Some works have presented hierarchical controllers in MGs and VPPs to provide frequency support. The work in [122] proposes a hierarchical controller for an MG comprising WGs and battery units. The aim is to provide primary and secondary frequency support to a weak grid by regulating the power flow over the tie-line. In [89], a control strategy based on the IEC/International Organization for Standardization (ISO) 62264 standard for hierarchical control for MGs and VPPs with ESS is presented. The paper also reviews MG design principles, as well as the types and roles of VPPs. The authors in [14] propose a model-free based generalized droop control. The control uses an adaptive neuro-fuzzy inference system for voltage coexistent and frequency regulation in the islanded MGs. This control structure can help reduce the imbalance between generation and consumption.

2.1.1.3 Energy Storage Systems

ESSs and Energy Management Systems (EMSs) are crucial elements of the frequency control of non-synchronous devices and, in turn, of VPPs. If properly controlled, energy storage can also be utilized to provide virtual inertia and fast frequency control. The work in [98] summarizes the requirements of the capacity for the connection of DERs and ESSs to the grid. A comprehensive review of the technical aspects of the VPP, the active power control strategy applied in DERs, as well as the charging and discharging characteristics of ESS is also provided. In [19], an EMS strategy is presented to provide the load power demand in distinct operating status by means of achieving the active power regulation in a small-scale VPP. The paper also proposes a hybrid Alternating Current (AC)/DC connection scheme for VPPs. The devices are integrated in the VPP via a DC-bus to reduce the number of required interface power converters.

Two other aspects of VPPs and ESSs are very important: the actuation and allocation of ESSs. Research presented in [18] specifies that islanded and low-inertia systems are more sensitive to load-generation imbalances and suffer larger frequency swings at these occurrences. Fast acting storage systems are employed in this proposal as dynamic frequency control support assets. The study is focused on islanded power systems with high shares of renewable generation that cannot contribute with inertia. Similarly, in [88], the authors study how to allocate ESSs efficiently with the aim to minimize storage system sizes and, thus, their costs. Hence, frequency reserves service is procured at reduced social costs. As such minimum size designs might underperform in cases of frequency overshooting, dissipating emergency resistors are also proposed.

A relevant question is whether the frequency response provided by VPPs has both technical and economic feasibility. For example, the work in [101] describes the authors' experience with a large scale 1.6 MW/0.4 MWh lithium-ion battery ESS that provides primary frequency regulation in the framework of a 100 % renewable Danish energy market by 2050. Results indicate that the investment in the lithium-ion battery ESS can be profitable in the Danish market if it is committed to at least 10 years.

Among existing ESSs, EVs play a special role as they are expected to dramatically increase their capacity in the near future. EVs can, in effect, be used as a VPP, as discussed in [5], in which EVs are utilized to support primary reserve in smart grids. By using online information of EVs like the initial state of charge, arriving time, the required state of charge for the next trip, and the temperature time, the primary frequency reserve not only averts reduction in frequency, but also improved the frequency response of the modeled Great Britain's power system. A fixed droop coefficient for each EV is individually considered to keep frequency nadir above 49.85 Hz, thereby improving the primary frequency response and avoiding overshoots caused by adaptive droop controllers.

The study in [16] notes the impact of three different EV charging strategies, namely, proportional response, soft control, and aggressive control, on the frequency response of a system under a variety of wind generation scenarios. It is concluded that the participation of EVs in frequency control significantly improves the dynamic behavior of the system. The proposed EV control strategies have similar performance. In [106], EVs are used as storage for WGs in order to enable their participation to the day-ahead electricity markets. This is achieved through VPPs that aggregate many EVs and WGs. The paper shows through a realistic case study based on real data that this approach is profitable for both EVs and WGs.

EVs can be also included in MGs. The authors of [44] present a frequency control strategy of an MG supported by VPP coordination. The MG consists of various distributed generation and storage resources and loads. By applying the VPP concept control method, the active power balance is sustained, thereby controlling the frequency of the MG. Particle swarm optimization and firefly algorithm metaheuristic algorithms are used to tune the PID controllers of the MG for frequency control. The control of EVs and their communication are of vital importance for the effective integration of EVs into VPPs. The research in [36] focuses on the control architecture and communication requirements for EVs-VPP. The paper emphasizes the importance of a reliable, secure, and inexpensive communication infrastructure to effectively operate the distributed resources included in the EVs-VPP.

An efficient control of EVs considering charging rate issues is proposed in [30]. This work shows that an aggregator can effectively exploit the frequency regulation service that can be provided by EVs, while keeping in mind that these assets are also loads and seek to serve their primary purpose as mobility devices. The charging rates are thoroughly assessed to better perform the overall control. Similarly, in [50], it is aimed to balance the frequency regulation provision by EVs while ensuring that the EV battery is charged to the user's preferred level for mobility reasons. Adaptive frequency droop control and EV charging with frequency regulation are the two control strategies proposed in the context of this work. All control is proposed to be implemented in a decentralized manner abiding by aspirations for a more robust management strategy.

2.2 Taxonomy

In this section and in view of how they procure frequency control, VPPs are categorized according to different types of components, frameworks, control methods, frequency regulation stages, operators, and grid strength. For each category, a table with relevant references is given.

2.2.1 Components

A VPP is most typically composed of four parts, namely DERs, ESSs, ICTs, and controllable loads. Table 2.1 shows the VPP components and relevant references.

Table 2.1: VPP components

VPP components	References
DERs	[3,5,16,19,21,22,25,35,42–45,54,75,81,87,89,90,93,97,98,101,106,117,118,127]
ESSs	[3, 19, 21, 22, 35, 45, 54, 81, 87, 89, 93, 98, 101, 102, 117, 118,127]
ICT	[19, 22, 36, 81, 87, 89, 118, 127]
Controllable loads	[5,16,35,36,44,54,93,106, 117]

2.2.1.1 Distributed Energy Resources

DERs as VPP components can be categorized according to the type of the primary energy source, the capacity of DG, the ownership of DG, and the operational nature of DG.

(a) **Primary energy source type:** Primary energy sources are divided into RES based like wind-based generators, PV arrays, solar-thermal systems, and small hydro-plants, and non-RES based like combined heat and power, biomass, biogas, diesel generators, gas turbines, and fuel cells.

(b) **DG capacity:** The DERs can be classified as per the capacity of DG. The Small-scale capacity DGs that must be connected to the VPP to increase access to the electricity market or they could be connected with controllable loads to form MGs. Also, the medium- scale and large-scale capacity DGs that can independently take part in the electricity market. However, they may opt for being connected to VPP to gain optimal steady revenue.

(c) **DG ownership:** The ownership of DGs can be considered for the classification of DERs . Residential-owned, Commercial-owned, and Industrial-owned DGs, aka domestic DGs, that are utilized for supplying all/part of its load. Utility-owned DGs, aka public DGs, that are used to support the main grid supply shortage. Commercial company-owned DGs, aka independent power producers DGs, that are to generate profits from selling power production to the network.

(d) **DG operational nature:** When it comes to wind or PV systems as DG units, the output power is uncontrollable because it relies highly on a variable input resource. To address this, such DGs must be equipped with battery storage to control the output power. This operational nature of DGs is called stochastic nature. Other DG technologies such as fuel cells and micro-turbines have an operational dispatchable nature. They are able to alter their operation rapidly. Thus, VPP should incorporate controllable loads, energy storage elements, and dispatchable DGs to compensate for the vulnerability of the stochastic nature-DG type.

2.2.1.2 Energy Storage Systems

To narrow the gap between the generation and demand, ESSs have an important role as they can arbitrate energy. ESSs can be categorized according to their applications as either energy supply or power supply, as below:

(a) **For energy supply:** Hydraulic pumped energy storage, compressed air energy storage.

(b) **For power supply:** Flywheel energy storage, super conductor magnetic energy storage, super capacitors, battery.

2.2.1.3 Information and Communication Technologies

The heart of a VPP is an EMS that coordinates the power flows from the generators, controllable loads, and storages. So, EMS is the backbone of information and communication systems. Receiving information about the status of each element inside the VPP, forecasting RES primary sources and output power, loads forecasting and management, power flow coordination between the VPP elements, and also operation control of DGs, storage elements, and controllable loads are the most important duties of the EMS. The main aims and objectives of the EMS are generation cost minimization, energy losses minimization, greenhouse gases minimization, profit maximization, voltage profile improvement, and power quality enhancement.

2.2.1.4 Controllable Loads

The controllable loads can be vehicle-to-grid functionalities of EVs, refrigerators, freezers, air conditioners, water heaters, heat pumps, battery storage, heat storage, etc. Below, different types of the controllable loads are provided:

(a) **Type a:** including residential loads such as fridges, washing machines, air conditioners, space cooling/heating, water heating, etc. which are interrupted or shifted by the load's utilities monitor. These loads cannot inject power to the network at any time.

(b) **Type b:** including battery storage, vehicle-to-grid, the combined cooling heating and power, etc. As opposed to Type a of the controllable loads, these loads are able to inject power into the network. They can be charged from or discharged to the network. They have also more considerable flexibility to be scheduled and thus, they are tailored to network needs.

(c) **Type c:** including MG, VPP, etc. Although MG and VPP have DGs, battery storage, renewable energy, etc., the loads take a great proportion in these systems.

2.2.2 Frameworks

From the perspective of the nature of the entity and their topology, VPPs are classified into Commercial Virtual Power Plant (CVPP) and Technical Virtual Power Plant (TVPP). CVPPs operates just like a traditional generator, bidding in the electricity markets without considering the effect of its operation on the local grid. By contrast, TVPPs employ DERs to handle the local grid in terms of thermal and voltage congestions. The TVPPs are also able to provide ancillary services to help the security of the system. The operation and duties of CVPPs and TVPPs are explained below. Also, relevant references are indicated in Table 2.2.

Table 2.2: VPP frameworks

VPP frameworks	References
TVPP	[3,5,16,19,22,35,36,42–45, 54,81,87,89,90,98,101,102, 117,118,127]
CVPP	[21,42,54,75,89,90,93,101, 106,118]

2.2.2.1 Technical Virtual Power Plant

The primary responsibility of a TVPP is to properly dispatch the DERs and the ESSs to manage the energy flow inside the VPP cluster, and offer the ancillary services accordingly. A TVPP receives information from the CVPP about the contractual DGs and the controllable loads. The most important data that TVPP must consider are the maximum capacity and commitment of each DER unit, the prediction of production and consumption, the location of DER units and loads, the capacity and the locations of the ESSs, the available control strategy of the controllable loads at all times during the day as per the contractual obligations between the VPP and the loads. On the whole, some duties of TVPPs are as follows:

- Managing the local distribution network.
- Providing balancing, management of the network, and execution of ancillary services.
- Providing visibility of the DERs in the distribution grids to the TSO, thereby setting the stage for DG and demand to make contribution to the transmission system management activities.
- Monitoring the DER operation based on the requirements obtained by the CVPP (system status information).
- Constantly monitoring the status for the retrieval of equipment historical loadings.

2.2.2.2 Commercial Virtual Power Plant

A CVPP carries out bilateral contracts with the DG units and the customers. The data of these contracts is sent out to the TVPP to consider the amount of the contracted power all through the performance of technical research. The most important responsibilities of CVPP are:

- Production scheduling as per the predicted needs of consumers.
- Trading in the wholesale electricity market.
- Providing services to the system operator.
- Submitting characteristics, costs, and maintenance of DERs .
- Predicting production and consumption as per weather forecasting and demand profiles.
- Providing outage demand management.
- Selling DER power in the electricity market.

2.2.3 Control Methods

Table 2.3 shows VPP control methods and relevant references. For optimal operation of VPPs in terms of power loss minimization, cost reduction, profit maximization, and environmental emission reduction, a wide variety of numerical and heuristic control methods are used.

Table 2.3: VPP control methods

VPP control methods	References
Numerical methods	[36, 42, 54, 106, 118]
Metaheuristic methods	[14, 44, 75, 118]
Hybrid optimization algorithm based methods	[44, 118]

2.2.3.1 Numerical Methods

The most widely used numerical methods are linear programming that addresses optimization problems in terms of optimal DER power and DG energy extraction, where nonlinear programming is to determine the length of time of several DGs. Gradient search, sequential quadratic programming, dynamic programming, and exhaustive are searched for finding several purposes like optimal DG locations, optimal DG sizes, minimization of cost, and also loss minimization.

2.2.3.2 Heuristic Methods

Due to the potential and proven capabilities of metaheuristic methods for solving optimization problems, a wide variety of metaheuristic algorithms have been presented. The most common ones are genetic algorithm, particle swarm optimization, fuzzy logic controller, artificial neural network, tabu search, ant colony optimization, artificial bee colony, harmony search, cat swarm optimization, and firefly algorithm. The most important purposes that have been considered in objective functions of the above algorithms were optimal placement, size, and type of DG, power loss minimization, energy loss minimization, profit maximization, voltage profile improvement, maximization of DG penetrations, power quality improvement, reliability indices. It is worth pointing out that over the years, combination and hybrid metaheuristic algorithms have come to researchers' attention with the same purposes yet better performances.

2.2.4 Frequency Regulation

This service brings back the frequency to the nominal operating level after any deviation occurrence due to the physical unbalance between generation and demand. This is attainable by adjusting the active power reserves of the system through automatic and rapid responses. The TSOs need to plan, in advance, to make sure that the correct levels of active power reserves are available in real-time, as well as that the TSOs must take remedial actions, when it comes to a shortage. Active power reserves embrace generator units, storage, and sometimes demand response. The main ancillary services for frequency regulation are shown in Table 2.4.

Table 2.4: VPP frequency regulation

VPP frequency regulation	References
Inertia (& inertial emulation) & Primary response (load following)	[3,5,14,16,18,24,35,44,45, 50, 54, 72, 81, 84, 87–89, 91, 101, 102, 107, 118, 121, 122, 127]
Secondary & Tertiary	[3,19,24,25,42,89,91,107, 114,117,118,122]
Procurement/concerns for frequency reserves	[21,30,54,75,118]

2.2.4.1 Frequency Containment Reserve/Primary Frequency Control

Frequency Containment Reserve (FCR) is the first control action to be activated, usually within 30 s, in a decentralized fashion over the synchronous area. In the European Union Internal Electricity Balancing Market, FCR means operating reserves necessary for constant containment of frequency deviations (fluctuations) from the nominal value to constantly maintain the power balance in the whole synchronously interconnected system.

2.2.4.2 Frequency Restoration Reserve/Secondary Frequency Control

Frequency restoration reserve is the centralized automated control, enabled from the TSO in the time interval between 30 s and 15 min from the unbalance occurrence. Frequency restoration reserve can be categorized according to reserves with both automatic and manual activation.

2.2.4.3 Replacement Reserves/Tertiary Frequency Control

Replacement reserves is a manual control. The typical activation time for the replacement reserves is from 15 min after the unbalance occurrence up to hours.

2.2.4.4 Procurement/Concerns for Frequency Reserves

The procurement methods are compulsory provision, bilateral contracts, tendering, and spot markets. In the first method, a class of generators is involved to provide specific reserves of ancillary services. This engagement can be market-based or rises through the national regulations and network codes. In the second method, the TSO negotiates with each provider the quantity and price of the offered ancillary service. This permits the TSO to purchase only a specific ancillary services amount and to deal with sellers to minimize the overall expense. The last two methods refer to an ancillary service exchange process characterized by increased competition. Although the tendering market is usually composed of long-duration services, the spot market involves shorter and less standardized products.

2.2.5 Operation

The owner or operator of the VPP may be controlling the VPP assets either as an actual entity, like system operator control room personnel, or as a software framework, similar to distribution management systems or EMS. Regardless of this detail, the VPP operator will need to abide by the level of the electric grid to which the size of the VPP and its assets are operating. The classification of the VPP operation and relevant references are listed in Table 2.5.

Table 2.5: VPP operation

VPP operation	References
Distribution level	[3, 19, 21, 22, 43, 44, 87, 90, 93, 98, 118, 127]
Transmission level	[3, 5, 36, 42, 43, 45, 75, 81, 90,93,101,102,106,117,118, 127]

2.2.5.1 Distribution Level

At the distribution network level, VPPs are not expected to contribute directly to frequency regulation services as the aggregated power of their assets cannot easily justify the procurement of reserves and their release upon disturbances. Furthermore, for any single generating or storage asset, no standardized code/regulation explicitly required them to contribute to the frequency regulation until recently that a framework was discussed [IEEE 1547- 2018]. Nevertheless, aggregators of assets or collectives of VPP operators may coordinate and bid their reserves for services to the market operator, provided a proper regulatory framework exists.

2.2.5.2 Transmission Level

Most of the resources connected at the transmission network level are expected to contribute with frequency regulation services to support the grid stability. Except for renewables, all other generators have been typically designed with governors that respond to frequency deviations at either the primary or secondary level. In terms of market involvement, generating assets at the transmission level submit bids for up and down reserves (i.e. to increase their active power output or decrease it, according to the frequency deviations, respectively) and the operator clears and assigns them. In this sense, VPP operators are expected to handle both the market and technical aspect of frequency regulation and the procurement of reserves in cases the VPP assets are connected at the transmission network level.

2.2.6 Grid Strength (Inertia and/or Sensitivity to Load Changes)

An important aspect of frequency regulation (of any service not just VPPs) is whether this service is offered in strong or weak grids. This distinction affects how frequently this service is activated and whether higher reserves are required to implement it. Relevant references on this topic can be found in Table 2.6.

Table 2.6: Grid strength (inertia and/or sensitivity to load changes)

Grid strength (inertia and/or sensitivity to load changes)	References
Strong/interconnected	[3, 5, 19, 21, 22, 24, 25, 30, 36, 42–45, 50, 72, 81, 84, 87–89, 91, 93, 101, 102, 106, 107, 117–119, 121, 127]
Weak/islanded or high inverter share	[14, 16, 18, 43, 54, 75, 89, 114, 121, 122]

2.2.6.1 Strong Grids

Strong grids, with considerably high number of rotating masses (conventional generators and motors) connected tend to be less affected by typical load-generation imbalances, hence, frequency in such systems changes less sharply and in tighter deviations intervals. This implies that a VPP connected to a strong grid will not be required to procure considerable reserves or activate them as much. As a by-product this VPP might not have to be involved in primary frequency control, as other rotating generators may be assigned this role.

2.2.6.2 Weak Grids

Contrary to strong grids, weak grids have few rotating machines (generators and motors) and, in some cases inverter-interfaced DGs and storage systems. In these grids, frequency deviations are more frequent and more severe and VPP assets might be expected to respond more frequently and in broader operating ranges causing added wear and tear. This implies that the frequency regulation provided by VPPs connected to weak grids has a higher cost than that of VPPs included in strong grids. Additionally, the VPP assets need to be clearly and more thoroughly accounted for in stability studies of weak grids.

2.3 Conclusions

VPPs are expected to participate actively in the procurement and offer of ancillary services. Most typical and crucial of the ancillary services is frequency control, as it expresses the effort to retain generation-demand equilibrium at any given moment. This chapter reviews the roles that researchers and policy makers have proposed for the involvement of VPPs in frequency control. The chapter introduces first a background on conventional frequency control of power systems and why VPP is a paradigm that can and should contribute substantially to frequency regulation. Then the chapter provides a comprehensive review with respect to VPP frequency regulation. Next, the chapter defines various classifications for VPPs in the context of frequency control procurement and realization. For each category, relevant works are reviewed in the chapter. The classification of these works shows that most of the literature focuses on how DERs are integrated into a VPP so as to offer PFC. This is not surprising. As large conventional power plants are decommissioned, in fact, the services they provided have to be covered by DERs .

The literature review provided in this chapter suggests that there needs to be a shift of focus on the subject of frequency control by VPPs. Much effort has been focused on the individual actions of DER and ESSs, and less attention has been paid on VPP-level frequency control in light, also, of broader system dynamics. There are numerous indications that as the inertia from conventional resources is displaced by inverter-interfaced DERs and ESSs, the matter of frequency control of non-synchronous resources as a potential cause for system instability and a source of low-frequency oscillations will become a growing concern [56]. VPPs are uniquely positioned to actively aggregate, control and manage the effects of DERs and ESSs at the highest level of coordination that ensures grid stability. VPP control has to handle the matter of system stability from a disadvantaged position as it lacks grid visibility (e.g., does not have information about the topology of the grid). In this sense, data-heavy models, sensing and novel state estimation techniques are needed to enable VPPs in this complicated role in modern power systems. Information and communication infrastructure and innovations are also needed to support VPP operation. VPPs, in fact, need to respond to frequency variations and fast acting inverter-driven controls that may lead to negative and undesired grid dynamics.

Chapter 3

Coordinated Frequency Control of Virtual Power Plants

In recent years, the efficient utilization of the DERs in VPPs has become an ongoing and relevant research topic. Most studies on VPPs, however, focus exclusively on the operation and economic aspects [15, 26, 57, 93]. The transient behavior of VPPs as well as their impact on the overall power system dynamic response, on the other hand, have not been thoroughly studied. Other aspects that have not been fully addressed so far are the impact of the VPP topology on the dynamic performance of the system, as well as the impact on the dynamic performance of VPPs of communication delays due to communication networks and the stochastic variations of loads, wind speed and solar irradiance. This chapter presents simple yet effective coordinated control approaches of VPPs and addresses the aspects above through a comprehensive case study.

3.1 Introduction

As mentioned in Chapter 2, VPPs comprise multiple resources that are dispersed over potentially vast areas. If properly coordinated, VPPs can provide regulating reserve and frequency support services. Similar to conventional SM, the VPP primary frequency control aims to improve the recovery of the frequency to its reference value in short-term transients following a power unbalance [71]. To this aim, DERs and ESSs are integrated and coordinated to provide the frequency containment service.

DERs are the main component of a VPP as they define the capacity of the VPP and allow its participation to the electricity market. With this regard, control strategies for the multiple DERs in a VPP have been proposed in the literature for both centralized [2, 97, 108, 112] and decentralized [47, 53, 74, 115]. In particular, a coordinated control method for SPVGs and controllable loads that aggregates the power output of the VPP to improve the stability and security of power grids is proposed in [54]. On the other hand, in [106], the EV is used as a storage for WG to overcome its uncertainty of generation. Regarding the aggregation of DERs in VPP, reference [3] explores an algorithm to integrate SPVG and WG that smooths the VPP output fluctuation.

The ability of the VPP to provide regulation, in particular frequency containment, relies also on other resources, the most important of which are ESSs. ESS is a crucial element of the fast frequency control in the low-inertial system and, in turn, of VPPs. Reference [98] summarizes the requirements for the connection of ESSs as well as their charging and discharging characteristics. The control and allocation of ESSs are also important. Reference [88] proposes a novel control algorithm based on historic frequency measurements to allocate ESSs efficiently. The algorithm extends the SoC limitation of ESS and the application of emergency resistors. Similarly, in [18], it is specified that the islanded and low-inertia systems are more sensitive to power imbalances and suffer greater frequency excursions at such occurrences. In this vein, in [18], fast-acting ESSs enable the provision of synthetic inertia to mitigate the impact of SPVG and WG on the stability of the grid.

Another crucial element of each VPP is the EMS, which heavily relies on ICT [53, 116]. For different VPPs structures, the centralized approach consists in collecting the information from ESSs and DGs in a single control center, whereas in a cooperative (distributed) control, each DER shares its information only with neighboring DERs [46]. When a control such as the FFR relies on communication networks, latency and communication delays have to be taken into account as they can have an impact on the dynamic behavior of the VPP as well as of the overall system [4, 41, 95, 99, 116]. This aspect is particularly relevant if the VPP is scattered across the transmission system and the DERs are significantly far away from each other. Reference [22] presents the ICT requirements of VPPs to procure, offer and realize ancillary services. The VPP requirements are then mapped against the services of the extended IEC 61850 standard to enhance the coordination between the VPP service center and DERs. The set up of the communication network in this thesis (see Appendix D.3) also follows these requirements.

The remainder of the chapter is organized as follows. Section 3.2 outlines the proposed coordinated control schemes of VPP. Section 3.3 presents the two types of VPP topologies considered in this work. Section 3.4 discusses in detail the case studies. Finally, Section 3.5 draws conclusions.

3.2 Coordinated Control Schemes

This section describes the proposed coordinated frequency control for the purpose of VPPs control in two ways: (i) by coordinating only ESS with the VPP active power output to provide fast frequency regulation to the grid; (ii) by coordinating all the RESs within VPP to improve power system short-term dynamics. The description of the controllers of ESS, WG, SPVG and PLL that utilized in this work, as well as their control diagrams are given in Appendix B.

3.2.1 Coordinated Frequency Control Scheme for ESS

Considering exclusively the primary frequency control of the VPP, the main objective of the coordination is to guarantee a FFR of the VPP by means of the active power control of ESSs. A centralized control strategy is proposed in this section to ensure a consistent response from all the resources in the VPP. This centralized strategy is illustrated in Figure 3.1. The frequency is measured through, say, a Phasor Measurement Unit (PMU) at the PoC of the VPP with the rest of the transmission grid. All DER regulators use the same input frequency signal in their local control loop. Then the information of each DER, i.e. the active power output, is sent and collected by a Data Management System (DMS) located within the VPP. The communication system enables the VPP operator to transmit measurements and data from the PMU to the DERs, or/and from the DERs to the DMS.

The power generated by the VPP is obtained by summing up the production of each DER devices included in the VPP. The coordinated control of DERs and ESSs is achieved through the primary frequency control support provided by the ESS, based on the information shared from the DERs included in the VPP. With this aim, a feedback

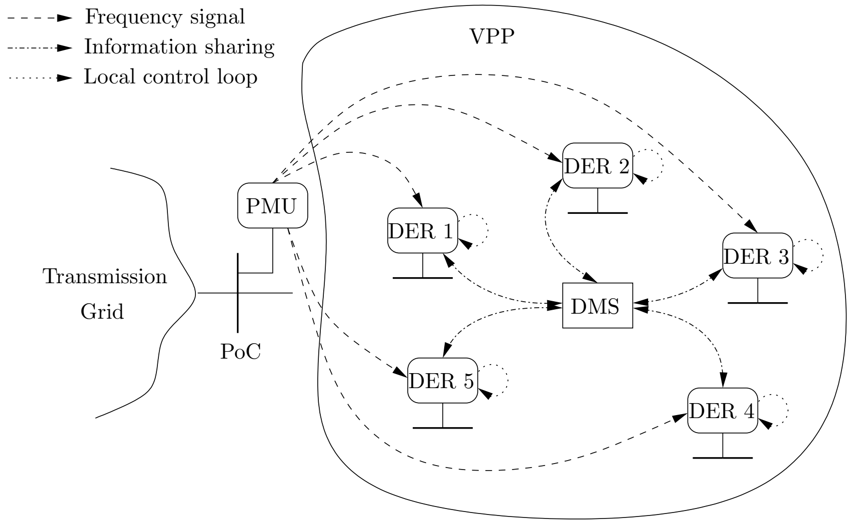

Figure 3.1: Illustration of a VPP with centralized control strategy.

signal is added to the local control loop of ESS to consider the active power outputs from WG and SPVGs. Fugure 3.2 illustrates the control scheme of the ESS with a coordinated signal from the DERs of the VPP.

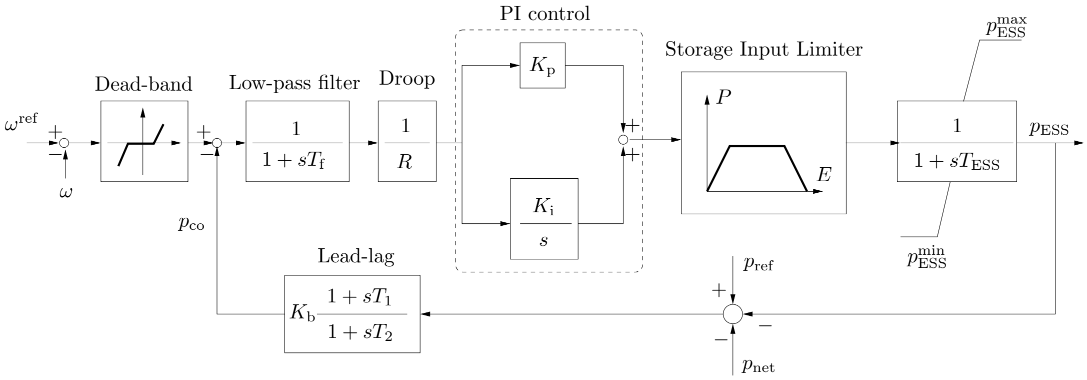

Figure 3.2: Primary frequency controller of an ESS belonging to a VPP with inclusion of a coordinated control signal.

The process of the control scheme can be expressed as:

$$\begin{cases} p_{\text{CO}} & = K_{\text{b}} \dfrac{1+sT_1}{1+sT_2} * (p_{\text{ESS}} + p_{\text{net}} - p_{\text{ref}}), \\ p_{\text{net}} & = \sum\limits_{i=1}^{l} p_{\text{ESS}}^{i} + \sum\limits_{j=1}^{m} p_{\text{wind}}^{j} + \sum\limits_{k=1}^{n} p_{\text{solar}}^{k} \\ & -p_{\text{loss}}^{\text{TOT}} - p_{\text{load}}^{\text{TOT}} - p_{\text{inj}}^{\text{TOT}}, \\ & i = 1,2,...,l; j = 1,2,...,m; k = 1,2,...,n \end{cases} \tag{3.1}$$

where p_{CO} is the feedback signal through a lead-lag controller, p_{ESS} is the active power output from the local ESS, p_{net} is the net active power of the VPP, which is sending from the control center, $\sum_{i=1}^{l} p_{\text{ESS}}^{i}$ is the total active power output from all the ESSs except the local ESS, p_{ref} is the initial reference set-point equal to the p_{net}, $\sum_{j=1}^{m} p_{\text{wind}}^{j}$ and $\sum_{k=1}^{n} p_{\text{solar}}^{k}$ are the sum output of the active power from the DERs in VPP. Finally $p_{\text{loss}}^{\text{TOT}}$, $p_{\text{load}}^{\text{TOT}}$ and $p_{\text{inj}}^{\text{TOT}}$ are the total active power losses and load in VPP, and the injection from/to the transmission grid, respectively.

3.2.2 Coordinated Frequency Control Scheme for VPP

The ability of ESSs to provide frequency control is limited by their capacity and SoC of any given time. As a consequence, ESS might not always be effective and improve the dynamic performance and stability of the grid [65, 127]. To address this problem, apart from ESSs, other RESs within a VPP, such as WGs and SPVGs, can be coordinated to provide FCR.

Figure 3.3 shows the proposed coordinated control of the resources that compose a VPP. This control is similar to a conventional secondary frequency control. However, it is aimed at improving the FFR of the VPP and, thus, it operates in the same time scale as the primary frequency control.

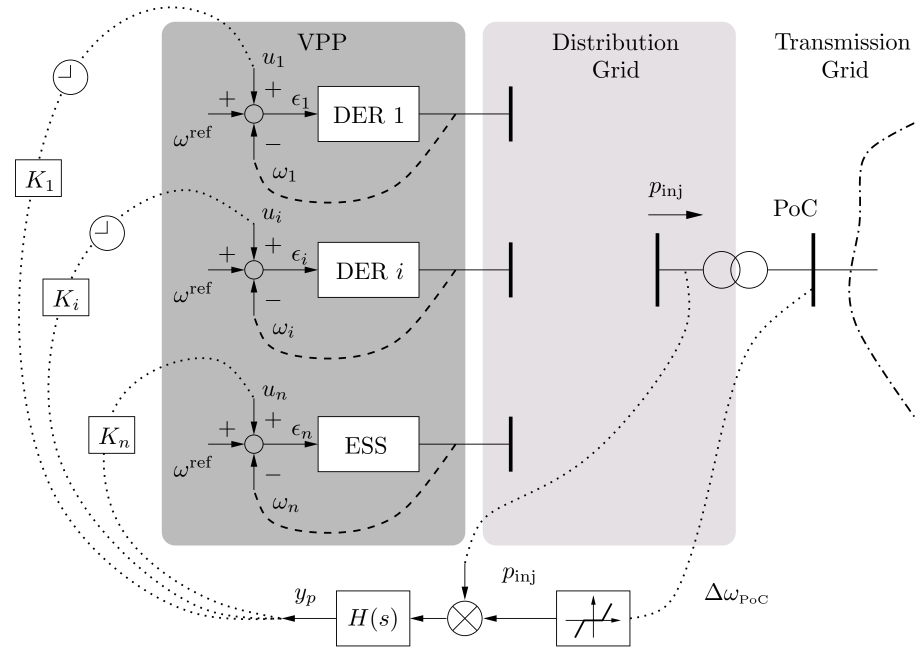

Figure 3.3: Control diagram of the proposed coordinated control of VPPs.

It is assumed that, in normal operating conditions and in a given period, the VPP power set-point is defined by the TSO based on the solution of an electricity market problem such as the unit commitment. Hence, before the occurrence of any contingency, p_{inj} is the set-point of the VPP as scheduled by the TSO in a given period.

The proposed approach consists in measuring the total active power injected (p_{inj}) into the transmission grid by the VPP as well as the frequency variation ($\Delta\omega_{\text{PoC}}$) and then transmitting the following signal:

$$y_p = H(s)\,\Delta\omega_{\text{PoC}}\,p_{\text{inj}} \tag{3.2}$$

to the DERs and ESSs that compose the VPP. In (3.2), $H(s)$ is the transfer function of the coordinated control. $H(s)$ includes a proper gain that adjusts the magnitude of y_p and makes it consistent and compatible with the primary frequency controllers of the resources of the VPP. Apart from the proportional controller considered in (3.2), other controllers such as PI and lead-lag can also be utilized. The case study in Section 3.4.1 compares and discusses the performance of different controllers.

The rationale of the proposed coordinated controller is as follows. In steady-state conditions, $\Delta\omega_{\text{PoC}} = 0$ and hence the primary controllers of the resources that form the VPP are decoupled. For practical implementation issues, a small Deadband (DB) is then included on the signal $\Delta\omega_{\text{PoC}}$, to avoid unnecessary communications of the signal y_p when the frequency deviations are negligible. The DB is utilized only to make the coordinated control insensitive to noise.

After the occurrence of a major contingency in the transmission grid, e.g. a fault or the outage of a large load/generator, the frequency of the system varies. This events leads to $\Delta\omega_{\text{PoC}} \neq 0$ and thus triggers the coordinated feedback control.

The effect of y_p is, in turn, to "amplify" the sensitivity of the primary control with respect to the local frequency deviation by a coefficient that is proportional to the power generated by the VPP. In fact, assuming that $\Delta\omega_{\text{PoC}}$ measured at the PoC is the same as the local frequency deviation measured by the DERs, one has that the overall signal entering into the primary frequency controllers is:

$$\begin{aligned} \epsilon_i &= (\omega^{\text{ref}} - \omega_i) + u_i \\ &\approx [1 + K_i H(s)\,p_{\text{inj}}]\,\Delta\omega_{\text{PoC}}\,, \end{aligned} \tag{3.3}$$

where $\omega^{\text{ref}} - \omega_i$ is the local frequency error as measured by the ESS or DER controller; and $u_i = K_i y_p$.

Figure 3.3 shows that timers are included in the signals sent to the DERs. These timers are triggered by a threshold value of u_i and allows improving the coordination of the DERs and ESSs. This point is duly discussed and illustrated in the case study.

3.2.3 VPP Control Modes

In this section, different coordinated control methods for ESS and DERs in VPP are introduced.

- **Mode 1**: DERs and ESSs regulate the frequency but are fully independent ($y_p = 0$).
- **Mode 2**: Only ESSs regulate the frequency. DERs do not include a frequency controller.
- **Mode 3**: DERs do not include a frequency control. The ESS is regulated in order to keep a given power injection p_{inj} of the VPP into the PoC. This is a typical VPP operation mode, where TSO schedules the VPP output every 15 minutes.
- **Mode 4**: In [71], the weather-driven DERs such as WGs and SPVGs are considered as non-dispatchable resources due to the stochastic nature of the wind and clouds. The ESS is the only device that regulates frequency. Therefore, in this mode, only the ESS is fed with the signal y_p.
- **Mode 5**: In [8], it is proposed that wind farms and VPPs can be used for emergency frequency control in smart super grids. Hence, in this mode, both ESS and DERs are coordinated with the signal y_p.
- **Mode 6**: Similarly to Mode 5, both the ESS and DERs are coordinated in this mode. However, the feedback signal y_p is utilized differently for ESSs and DERs. ESSs are always fed with y_p and, thus, their primary frequency regulation acts immediately after the contingency. On the other hand, DERs are included in the coordinated control and receive the signal y_p after a given time after the occurrence of the contingency, e.g. 15 s. The timer that activates the feedback signal for the DERs is triggered by the magnitude of the variation of the frequency $\Delta\omega_{\text{PoC}}$.

3.3 VPP Topologies

At the system level, two main types of VPP topologies are relevant: (i) Transmission System Virtual Power Plant (TS-VPP), where the ESS and DERs are connected directly to the high-voltage transmission grid; and (ii) Distribution System Virtual Power Plant (DS-VPP), for which the devices are connected to the transmission grid via a PoC. The TS-VPP topology is widely adopted to combine geographically dispersed and/or high-capacity DERs, whereas the DS-VPP is suitable for the geographically close and small/medium capacity DERs [126]. Figures 3.4 and 3.5 illustrate these two topologies.

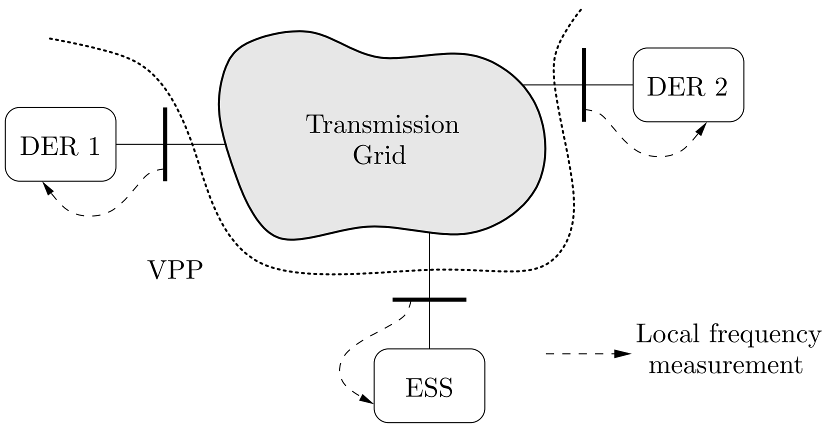

Figure 3.4: Illustration of the TS-VPP topology.

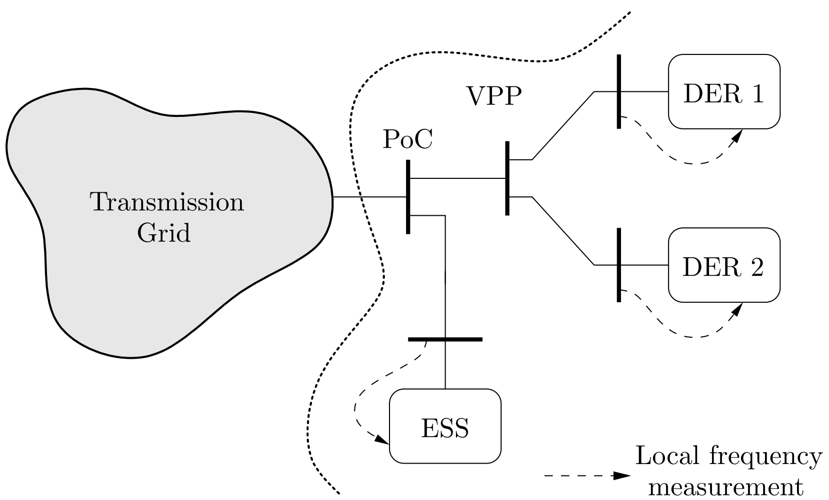

Figure 3.5: Illustration of the DS-VPP topology.

3.4 Case Study

The power system model considered in this work includes stochastic processes, which take into account wind and solar generation as well as load variations. Since the proposed coordinated control requires the transmission of remote signals, time delays are also considered to model the communication system. The resulting overall model of the system is given in Appendix A. In particular, the communication delay model is presented in Appendix C.1.3.

3.4.1 Case Study I: Coordinated ESS

This case study considers a modified version of the well-known WSCC 9-bus, 3-machine test system, where the load at bus 6 is replaced with a 8-bus, 38 kV distribution system that includes a VPP [78, 94]. Note that the parameters of the SMs have been adjusted to adapt the distribution system. The topology and data of the overall system is given in Appendix D.2.

Two scenarios have been studied in this section. First, Section 3.4.1.1 studies the impact of VPP on power system transient response considering four types of VPPs: (i) without DERs frequency control but with the ESS controlling the frequency; (ii) without ESS but with DERs controlling the frequency; (iii) with non-coordinated DERs and ESS and (iv) with coordinated ESS and DERs, considering both deterministic and stochastic simulations. On the other hand, Section 3.4.1.2 focuses on the impact of communication delay of the remote control signal transmitted in different levels of communication networks.

For all scenarios, the contingency is a three-phase fault at bus 7 at $t = 1$ s, cleared after 100 ms by opening the line connecting buses 5 and 7.

3.4.1.1 Impact of Coordinated Control

The performance of the system for the different control schemes is studied by comparing the frequency at bus 6. Fugure 3.6 shows the frequency response following the disturbance for the four scenarios. If the ESS is installed in the VPP, the steady-state frequency error is lower compared to the case without the ESS, however not zero due to limited capabilities of the ESS and the fact that the AGC is not considered in the simulation. On the other hand, the frequency shows the maximum deviation for the case where DERs do not participate to the frequency control. The best dynamic response is achieved through a coordinated control of DERs and ESS.

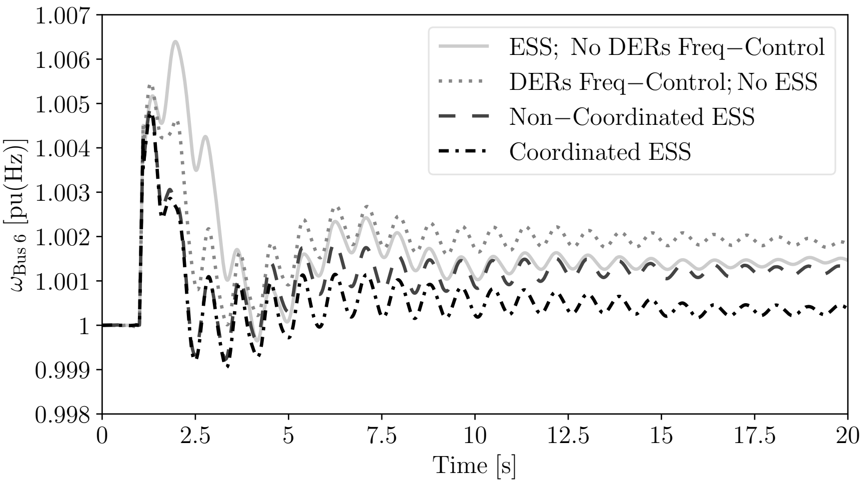

Figure 3.6: Frequency response at bus 6 following the contingency.

The active power output of DERs and the active power absorption of the ESS are shown in Fugure 3.7 with non-coordinated and coordinated ESS control. Due to the coordination of the DERs outputs, the ESS reaches its maximum power output limit after the contingency.

The impact of the limit of the energy capacity of the ESS is studied next by performing a simulation with a longer time scale and assuming that the ESS is at a 70% state of charge before the contingency. Fugure 3.8 shows the frequency at bus 6 for the scenarios without ESS and with ESS with coordinated control and with small (9 pu(MJ)) energy capacity. Note that, in the case with small energy capacity, the ESS stops regulating the frequency at about $t = 35$ s and, as a consequence, the frequency deviation is even larger than in the case without ESS. This happens because, if the ESS is close to its maximum/minimum stored energy, the energy saturation/deficiency causes an abrupt transient oscillation [83]. This indicates that the size of the ESS is critical for the proper control of the VPP and its interaction with the rest of the system.

Moreover, stochastic variations of the wind speeds of 10% of the loads in the VPP is taken into account. 500 Monte Carlo simulations are carried out for each of the four scenarios considered in this case study. The capacity of the ESS included in the VPP is assumed to be small. The histogram and the best-fit PDFs are calculated at $t = 15$ s, as illustrated in Fugure 3.9, where σ is the standard deviation.

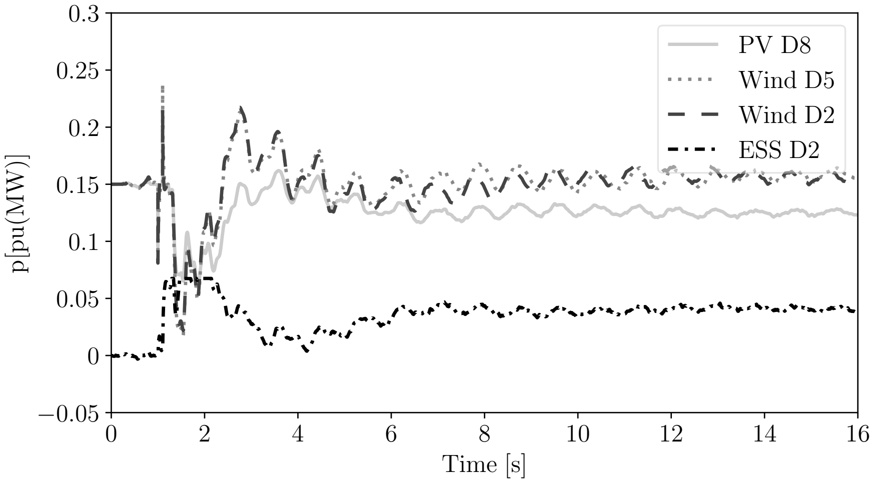

(a)

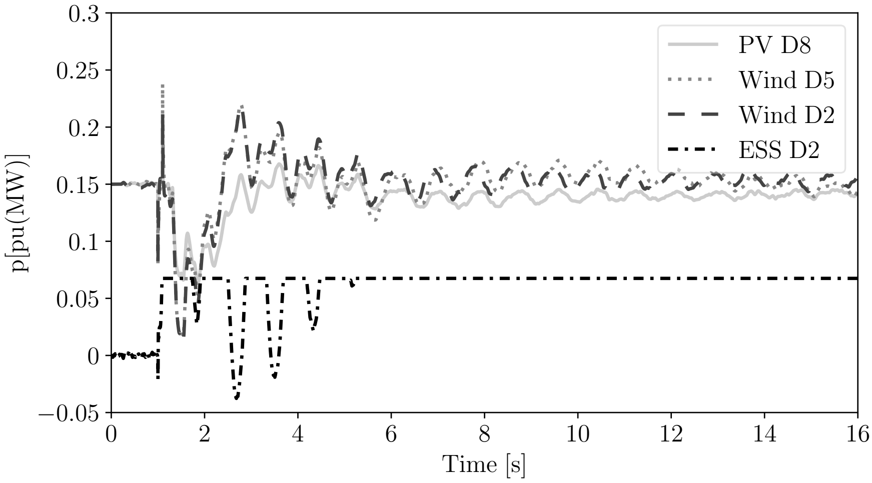

(b)

Figure 3.7: Active power output of the DERs in VPP: (a) with non-coordinated ESS (b) with coordinated ESS.

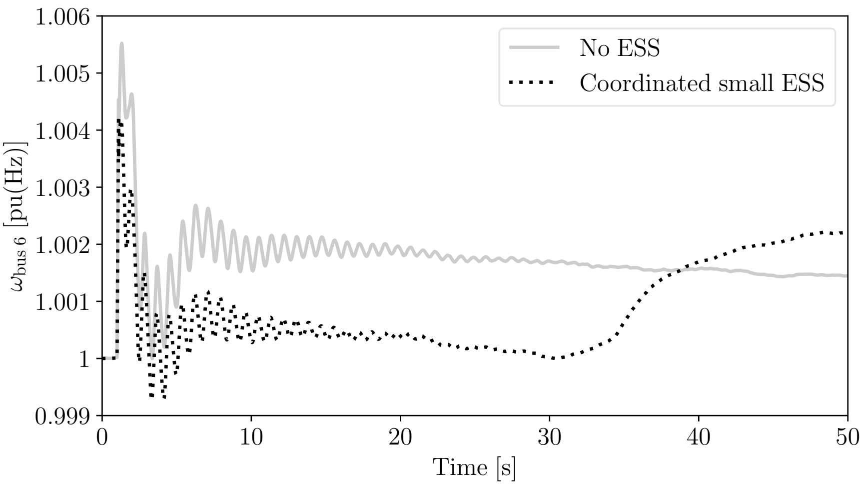

Figure 3.8: Frequency response at bus 6 following the contingency with VPP after a mid-term.

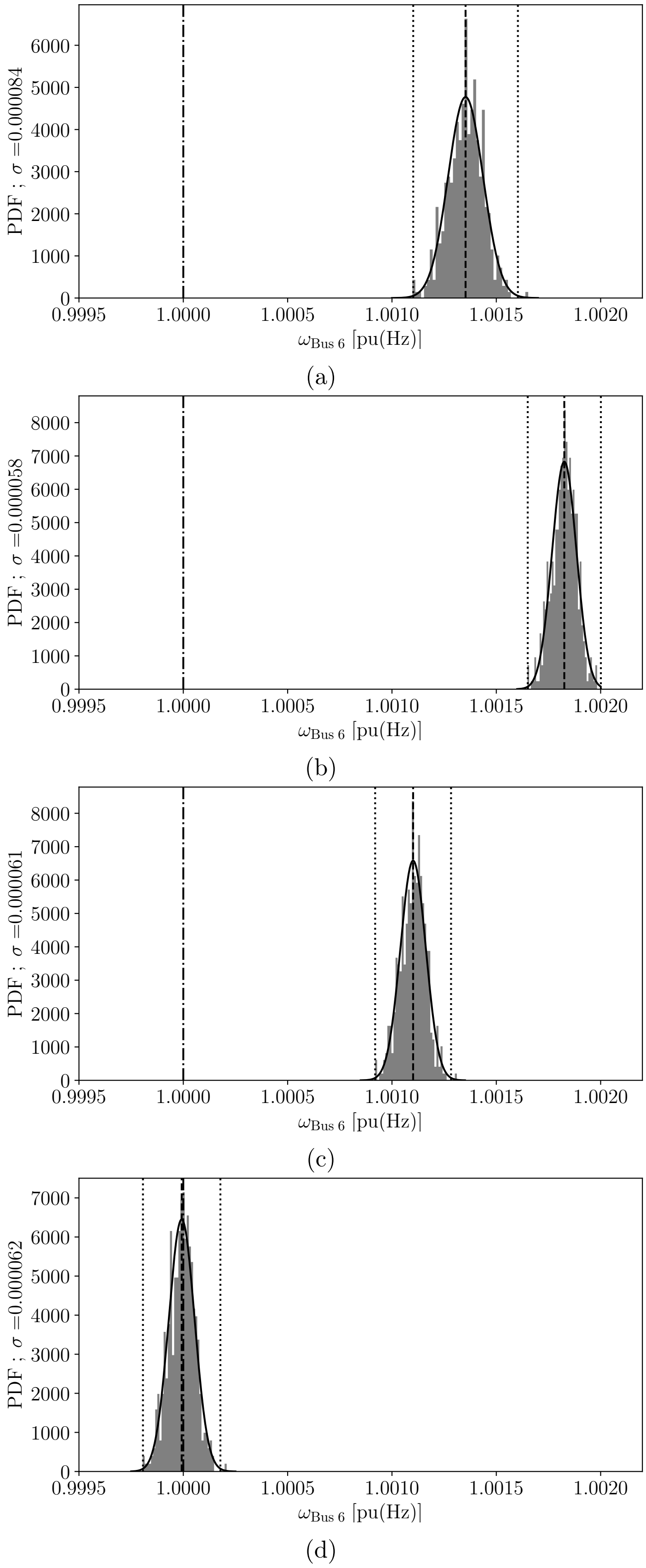

Figure 3.9: Histogram and PDF-fit of the trajectories at $t = 15$ s: (a) no frequency control on DERs; (b) no ESS (c) non-coordinated ESS; (d) coordinated ESS.

Comparing the standard deviation of $\omega_{\mathrm{Bus\,6}}$, σ, the VPP without frequency control on DERs shows a worse performance, where other three control schemes do not have significant differences. However, the coordinated ESS control scheme manages to recover the frequency closer to the reference value.

3.4.1.2 Impact of Communication Delays

The communication delays of the remote signal transmitted are taken into account in this section. Three levels of communication networks, namely high-speed, middle-speed, and low-speed communication network are considered. The settings of the communication networks are as presented in Appendix D.3.

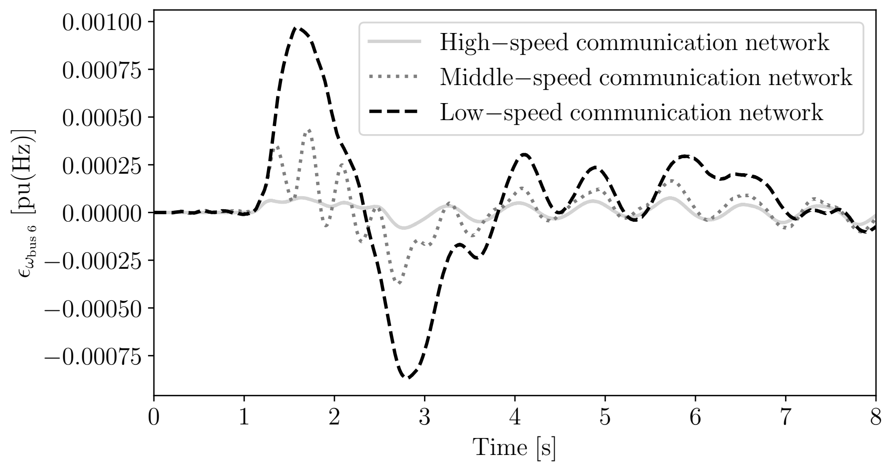

Figure 3.10: Errors of the frequency at bus 6, the signal are transmitted in a different level communication network and compared with the non-delayed signal.

The simulation results, in this case, are shown in Fugure 3.10. The responses with inclusion of communication delays are compared with the non-delay trajectory of Fugure 3.6. Fugure 3.10 also shows the impact of communication delays of the different communication network. The high-speed communication network has a better response compared to the other two.

The signal transmitted through a low-speed communication network has a more significant delay, which leads to a larger frequency deviation, even if the background traffic in such a network is ignored. Observe that the impact of communication networks in frequency response is nonlinear. The frequency deviation between the high-speed (40 Mbps) communication network and the middle-speed (4 Mbps) network is smaller than the deviation between the middle-speed network and the low-speed (0.4 Mbps) network, which means there exists a critical range of the bandwidth, over which increases the bandwidth can only slightly reduce communication delay. It is expected to find a suitable bandwidth of the communication network that the impact of delay on the system response is acceptable, and the cost of establishing a communication network is economical.

3.4.2 Case Study II: Coordinated VPP

In this case study, the same test system with Section 3.4.1 is utilized. In this case, the power injected by the VPP into the grid, namely p_{inj}, is the power flow from Bus D1 to Bus 6 (see Figure D.2). The stochastic processes of the wind speeds, load consumption and solar irradiance described in the previous section are included in all scenarios of the case study.

3.4.2.1 Monte Carlo Analysis

This section discusses the robustness of the proposed control approach concerning the perturbations such as a three-phase fault at bus 7 occurring at $t = 1$ s and cleared after 100 ms. The stochastic perturbations are the power variations of wind and solar power plants with respect to the forecast of wind speed/solar irradiance, and 15% of the loads in the whole system. For each scenario, 500 Monte Carlo time domain simulations are solved. Figure 3.11 shows the frequency trajectories for the system that VPP without frequency control on DERs and without ESS. The trajectories of the frequencies for Modes 1 to 3 are shown in Fugure 3.12, whereas the trajectories of the frequency for Modes 4 to 6 with three different transfer functions $H(s)$ are shown in Fugure 3.13. The considered transfer functions are the most commonly used controllers such as proportional gain, PI controller and lead-lag controller. For all controllers, the parameters the lead to the best dynamic performance are selected through a trial-and-error approach. For simplicity, and since the size of all DERs and the ESS is similar, $K_i = 1$, $\forall i = 1, \ldots, n$. Finally, Table 3.1 shows the mean frequency, μ_{CoI}, as well as the standard deviation of the frequency σ_{CoI}, calculated at $t = 50$ s, for the six control modes and the three transfer functions $H(s)$ considered in this case study.

The comparison of Figs. 3.11, 3.12 and 3.13 indicates that the VPP without DER frequency control and without ESSs leads to the largest frequency deviation in the

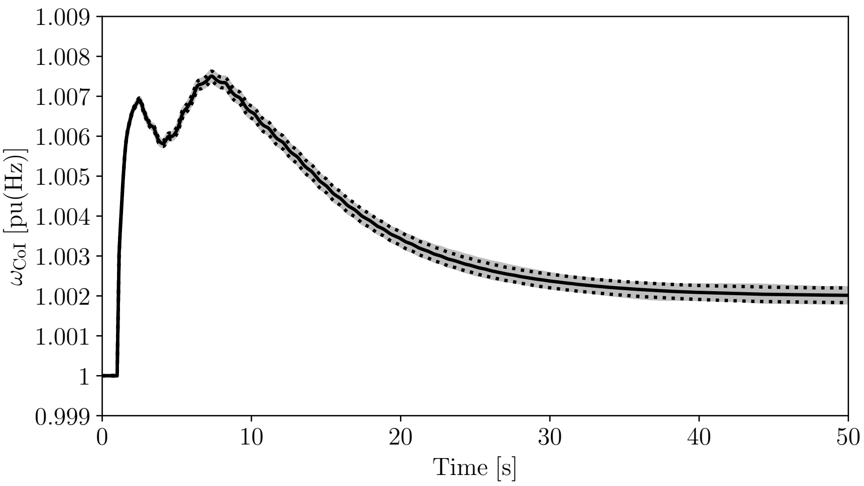

Figure 3.11: Trajectories of the frequency of the CoI without VPP frequency control and without ESS. The mean and the standard deviation of the frequency at $t = 50$ s are $\mu_{\mathrm{CoI}} = 1.002$ pu(Hz) and $\sigma_{\mathrm{CoI}} = 6.16 \cdot 10^{-5}$ pu(Hz), respectively.

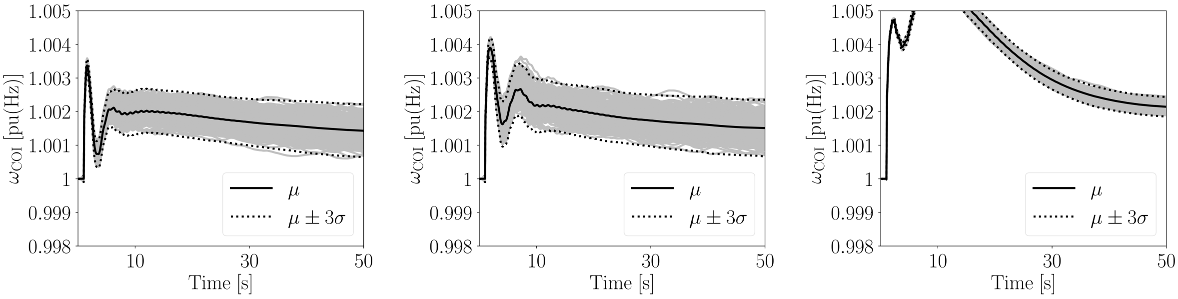

(a) Mode 1 (b) Mode 2 (c) Mode 3

Figure 3.12: Trajectories of the frequency of the CoI without the proposed coordinated control.

Table 3.1: Mean frequency μ_{CoI} and standard deviation σ_{CoI} for different VPP control modes.

	Statistics	Mode 1	Mode 2	Mode 3
	μ_{CoI}	1.001431	1.001511	1.002144
	$\sigma_{\mathrm{CoI}} \times 10^{-5}$ [pu(Hz)]	23.6	28.1	9.73
Control Type	**Statistics**	**Mode 4**	**Mode 5**	**Mode 6**
Prop. Control	μ_{CoI} [pu(Hz)]	1.000328	1.000323	1.000321
	$\sigma_{\mathrm{CoI}} \times 10^{-5}$ [pu(Hz)]	1.83	1.58	1.43
Lead-Lag	μ_{CoI} [pu(Hz)]	1.000198	1.000155	1.000135
	$\sigma_{\mathrm{CoI}} \times 10^{-5}$ [pu(Hz)]	8.62	2.24	3.27
PI	μ_{CoI} [pu(Hz)]	1.000267	1.000020	1.000023
	$\sigma_{\mathrm{CoI}} \times 10^{-5}$ [pu(Hz)]	12.4	1.37	1.60

system. Note that the results shown in Fugure 3.11 can be also viewed as the worst-case scenario representing the complete outage of the communication network in the

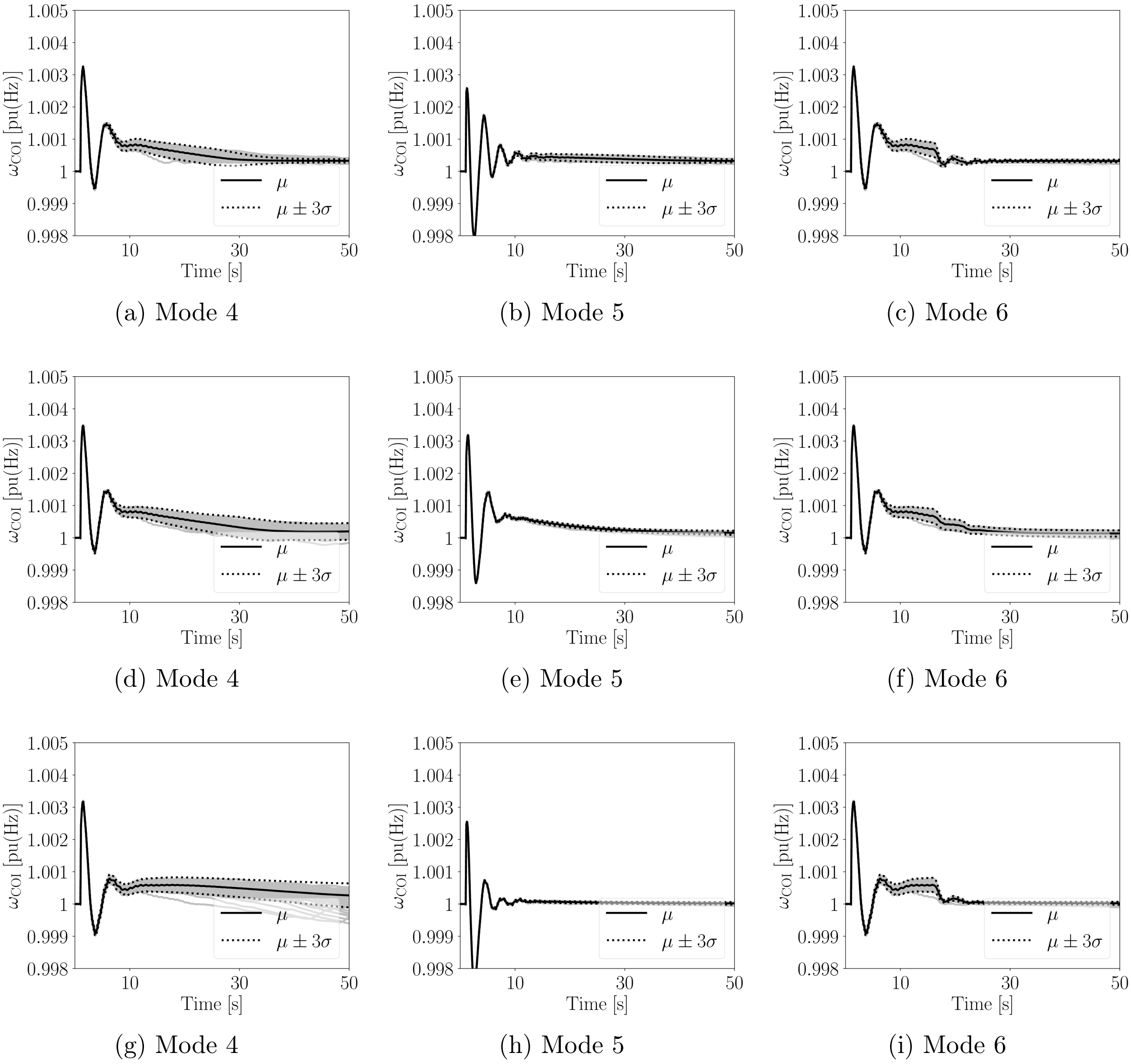

(a) Mode 4 (b) Mode 5 (c) Mode 6

(d) Mode 4 (e) Mode 5 (f) Mode 6

(g) Mode 4 (h) Mode 5 (i) Mode 6

Figure 3.13: Trajectories of the frequency of the CoI using: (a)-(c) proportional gain; (d)-(f) lead-lag controller; and (g)-(i) PI controller.

VPP. The comparison of the trajectories shown in Figs. 3.12 and 3.13 as well as of the results given in Table 3.1 indicates that the VPP control modes that include the proposed coordinated approach control (Modes 4-6) have an overall better performance than the strategies with no coordination (Modes 1-3).

It is interesting to note that, for Mode 4 (see Figs. 3.13a, 3.13d and 3.13g), the standard deviation slightly increases for $10 < t < 30$ s because the ESS is running at its maximum output that loses its capability to regulate the frequency. Coordinating the DERs, i.e. Mode 5, to provide extra frequency support can help to solve this problem as shown in Figs. 3.13b, 3.13e and 3.13h. However, this leads to a larger frequency deviation during the initial transients ($0 < t < 10$ s). Finally, Mode 6, where a timer is utilized to delay the action of DERs, shows the best dynamic performance (see Figs. 3.13c, 3.13f and 3.13i).

The results shown in Fugure 3.13 are obtained with the best set of parameters for each controller, namely proportional gain, lead-lag controller, and PI controller. For the PI controller, a small dead-band on the frequency deviation $\Delta\omega_{\mathrm{PoC}}$. While all controllers performs well, they have different performances depending on the mode. The PI controller performs best if both ESS and DERs regulate the frequency. However, if only the ESS is utilized to regulate the frequency, the PI controller leads more often the ESS to its maximum power output, thus making the control less efficient as with the proportional controller and lead-lag. All controllers perform well for Mode 6, i.e. when a timer shifts the action of the DERs. The timer in fact exploits the ability of the ESS to regulate the frequency in the first seconds but avoids ESS saturations in the longer term.

3.4.2.2 Impact of Communication Delays

As mentioned in Section 3.2, there exists a delay when the frequency signal $\Delta\omega_{\mathrm{PoC}}$ and active power p_{inj} transmitted through the communication network. In this section, the communication delay with respect to three levels of communication networks, namely, high-speed, middle-speed, and low-speed communication networks are considered the same as Section 3.4.1 (see also Appendix D.3).

Most real-world communication networks utilized in power system applications are somewhere in between the high-speed and medium-speed communication networks. However, low-bandwidth communication networks are cheaper and, thus, the low-speed communication network is also considered here. Clearly, the lower the speed (bandwidth) of the communication network, the higher the delays of the control signals.

Figure 3.14 shows the impact on the frequency of the CoI of communication delays as obtained with the three communication networks. The system undergoes the same three-phase fault considered in Section 3.4.2.1. Only Modes 4, 5 and 6 are compared as these are the modes that require a communication network. Simulation results, which were obtained using the proportional controller, indicate that the proposed coordinated control approach, especially Modes 5 and 6 are particularly impacted by communication delays.

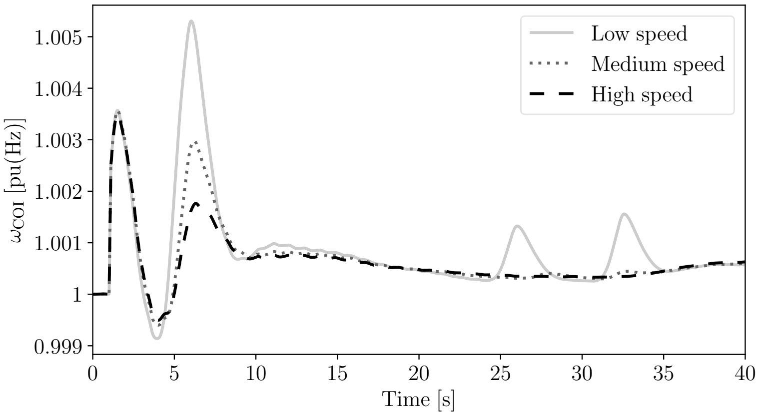

(a) Mode 4

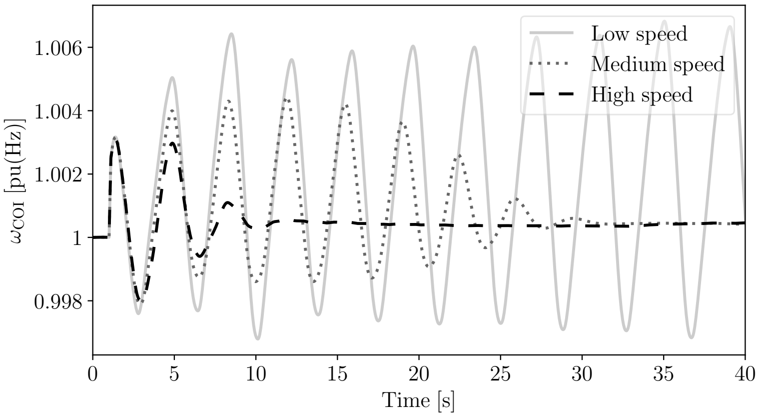

(b) Mode 5

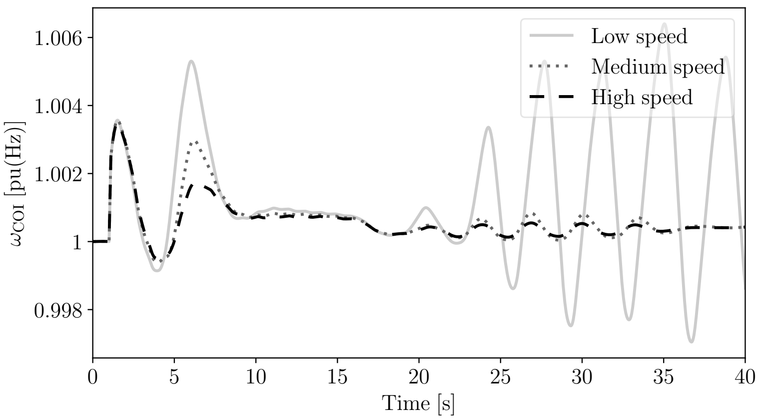

(c) Mode 6.

Figure 3.14: Frequency of the CoI following a three-phase fault occurs in the transmission grid, where the measurements $\Delta\omega_{\text{PoC}}$ and p_{inj} are transmitted through high/medium/low speed communication networks, respectively.

When the communication network has a low bandwidth with a large time-varying delay of around 200 ms, the approach that only coordinates the ESS gives raise to an oscillation on the system frequency (see the interval between 25 and 35 s in Fugure 3.14a). Mode 6 sharply increases this oscillation. Then in the medium-speed communication network with a medium time-varying delay of around 100 ms, the performances for Modes 4 and 6 are acceptable, however, for Mode 5, the frequency oscillation are still significant. Finally, the delays of the high-speed communication network are around 55 ms. These delay has only a slight impact on the overall frequency behavior. Based on the simulation results, it appears, thus, that communication delays should be kept below 100 ms when the proposed coordinated control approach is adopted.

It is important to note that, due to the nonlinearity of the model of the power systems, it is not possible to draw general conclusions on the impact of delays. However, based on our knowledge and experience with several systems and scenarios, communication delays in control loops can be expected to worsen the dynamic response of the system and reduce its stability margin (see for example [64] and [52]).

3.4.3 Case Study III: VPP Topologies

In this case study, a feedback signal, $p_{\rm co}$, that takes into account the difference between the total net active power outputs of DERs ($p_{\rm net}$) and the VPP active power scheduled for a given period ($p_{\rm ref}$) is included in the frequency control of the ESS through a lead-lag controller (see Figure 3.2). The case study considers the scenario where the signal $p_{\rm co}$ is also included in the frequency controllers of the DERs [125]. That is, the input signal in the schemes of Figures. B.3 and B.2 is assumed to be $\omega^{\rm ref} - \omega + p_{\rm co}$.

The TS-VPP and DS-VPP topologies considered in this chapter are both based on a modified version of the well-known WSCC 9-bus, 3-machine system [94].

The test system of the DS-VPP in this case study is the same as Section 3.4.1 (see Fugure D.2). The setup of the grid for the TS-VPP is shown in Fugure 3.15. In this scenario, the active and reactive powers of the original load at bus 6 are reduced to 57.8 MW and 11.7 Mvar, respectively. Then, one SPVG, two WGs and one ESS are connected at buses D8, D6, D7, and 9, respectively. The WGs and the SPVG both generate 15 MW at $t = 0$. Finally, the power rate of the ESS is 10 MW.

3.4.3.1 Monte Carlo Analysis

This section studies the statistical behavior of the frequency control provided by the TS-VPP and DS-VPP. The study considers both un-coordinated ($K_{\rm b} = 0$) and coordinated ($K_{\rm b} \neq 0$) frequency controllers as introduced in Section 3.4.3, as well as

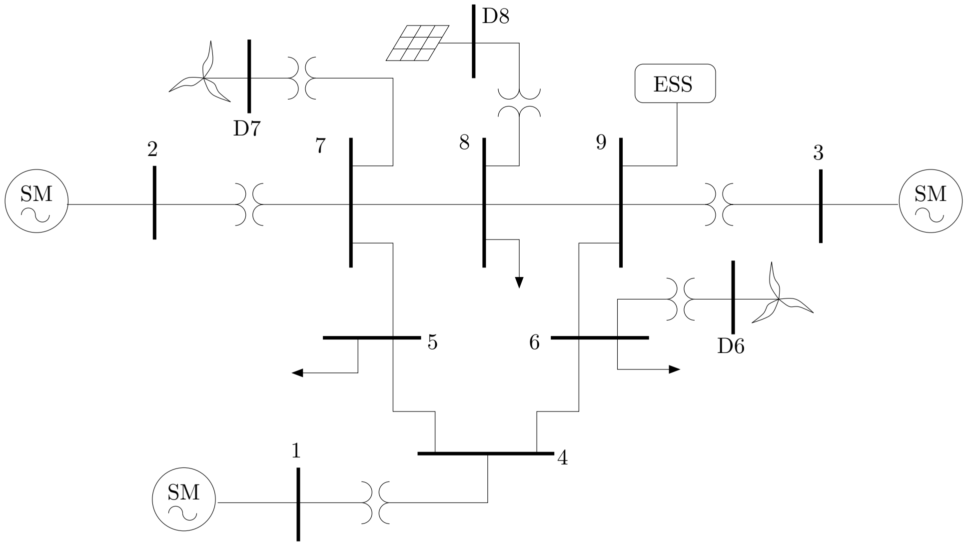

Figure 3.15: Modified WSCC 9-bus, 3-machine system with a TS-VPP topology.

the case of VPP without frequency control on DERs and without ESS. The stochastic fluctuations affect 10% of the power consumption of all loads as well as of the wind/solar generated power variations with respect to the forecast of wind speed/solar irradiance. 500 Monte Carlo simulations are carried out for each scenario.

The case study considers both the situations of over and under frequency. With this aim, the following two contingencies are considered: (i) a three-phase fault occurring at bus 5 at $t = 1$ s and cleared after 100 ms by opening the line that connects buses 5 and 7; and (ii) a load step increase occurring at $t = 1$ s and corresponding to the 3% of the total loading level of the system. The trajectories of the CoI are shown in Figs. 3.16, 3.17 and 3.18, where σ_{CoI} is the standard frequency deviation and μ_{CoI} is the mean frequency. Specifically, Fugure 3.16 shows the transient behavior of the WSCC system with the VPP but without ESS and frequency control on DERs. Whereas Figs. 3.17 and 3.18 show the behavior of the system with inclusion of a VPP with non-coordinated and coordinated, respectively, frequency control of its resources.

It is interesting to observe, from Fugure 3.16, that the cases when the DERs are aggregated into a distribution network, i.e. cases (b) and (d), lead to a better dynamic behavior compared to the cases when DERs are directly connected to the transmission grid, i.e. cases (a) and (c). Furthermore, as expected, the cases with the VPP and without ESS and frequency control on DERs (Fugure 3.16), leads to higher frequency deviations

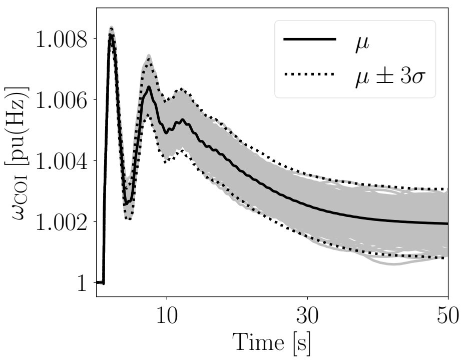

(a) DERs connected to transmission grid.

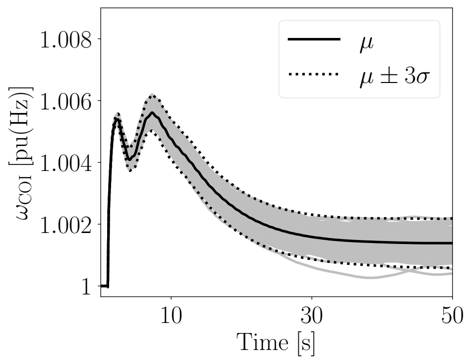

(b) DERs connected to distribution grid.

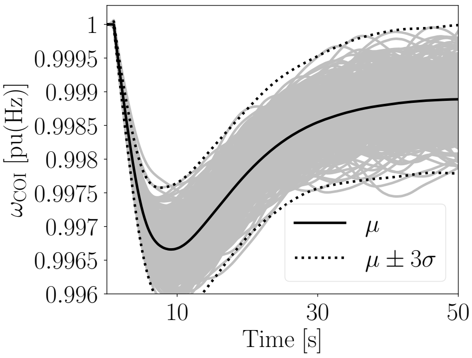

(c) DERs connected to transmission grid.

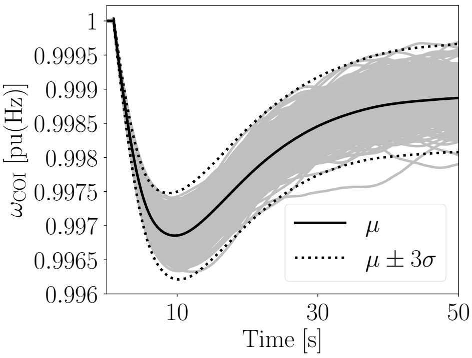

(d) DERs connected to distribution grid.

Figure 3.16: Trajectories of the frequency CoI with 500 Monte Carlo simulations for the WSCC 9-bus system with inclusion of DERs without frequency control and without ESS: (a) and (b) three-phase fault; (c) and (d) load increase.

compared to the cases with inclusion of a VPP with non-coordinated and coordinated frequency control of its resources (Figs. 3.17 and 3.18).

With respect to the considered VPP control strategies, the VPP that coordinates the control of DERs and ESSs shows a better frequency transient behavior than the VPP composed of independent devices. With regard to VPP topologies, geographically dispersed DERs and ESSs provide better frequency support to the whole system. In fact, the TS-VPP leads to lower frequency oscillations in the first seconds after the contingency ($0 < t < 10$ s) and a statistically lower spread of the frequency with respect to the DS-VPP (see Table 3.2).

Table 3.2: Standard deviation of the frequency CoI, σ_{CoI}. The scenarios corresponds to those indicated in Figs. 3.16, 3.17 and 3.18.

Topology	DERs – no freq. control				TS-VPP				DS-VPP			
Scenario	(a)	(b)	(c)	(d)	(a)	(b)	(c)	(d)	(a)	(b)	(c)	(d)
$\sigma_{\mathrm{CoI}} \times 10^{-5}$ [pu(Hz)]	37.8	26.6	36.7	26.5	13.8	13.9	5.93	8.19	14.2	14.3	6.41	8.86

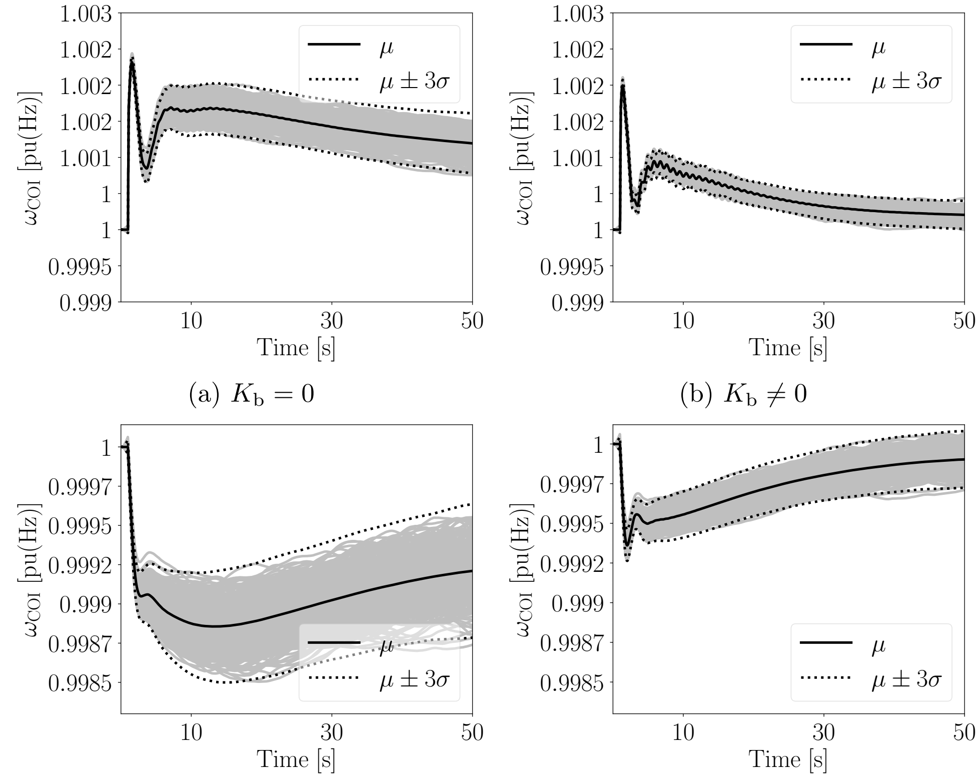

(a) $K_{\mathrm{b}} = 0$ (b) $K_{\mathrm{b}} \neq 0$

(c) $K_{\mathrm{b}} = 0$ (d) $K_{\mathrm{b}} \neq 0$

Figure 3.17: Trajectories of the frequency CoI with 500 Monte Carlo simulations for the WSCC 9-bus system with inclusion of a TS-VPP: (a) and (b) three-phase fault; (c) and (d) load increase.

3.4.3.2 Impact of Communication Delays

The impact of communication delays is studied next. To this aim, the communication delay with respect to three levels of communication networks, namely, high-speed, medium-speed, and low-speed communication networks, are introduced. The detailed setup and parameters of the communication networks can be found in Appendix D.3. Table 3.3 shows the approximate value of the mean delays in different communication networks. The contingency is the same three-phase fault as Section 3.4.3.1, and the control approaches of DERs and ESS are coordinated ($K_{\mathrm{b}} \neq 0$) in both TS-VPP and DS-VPP.

Table 3.3: Mean delays of the communication networks.

Levels	High-speed	Medium-speed	Low-speed
TS-VPP	0.1 s	0.5 s	1.0 s
DS-VPP	0.05 s	0.1 s	0.2 s

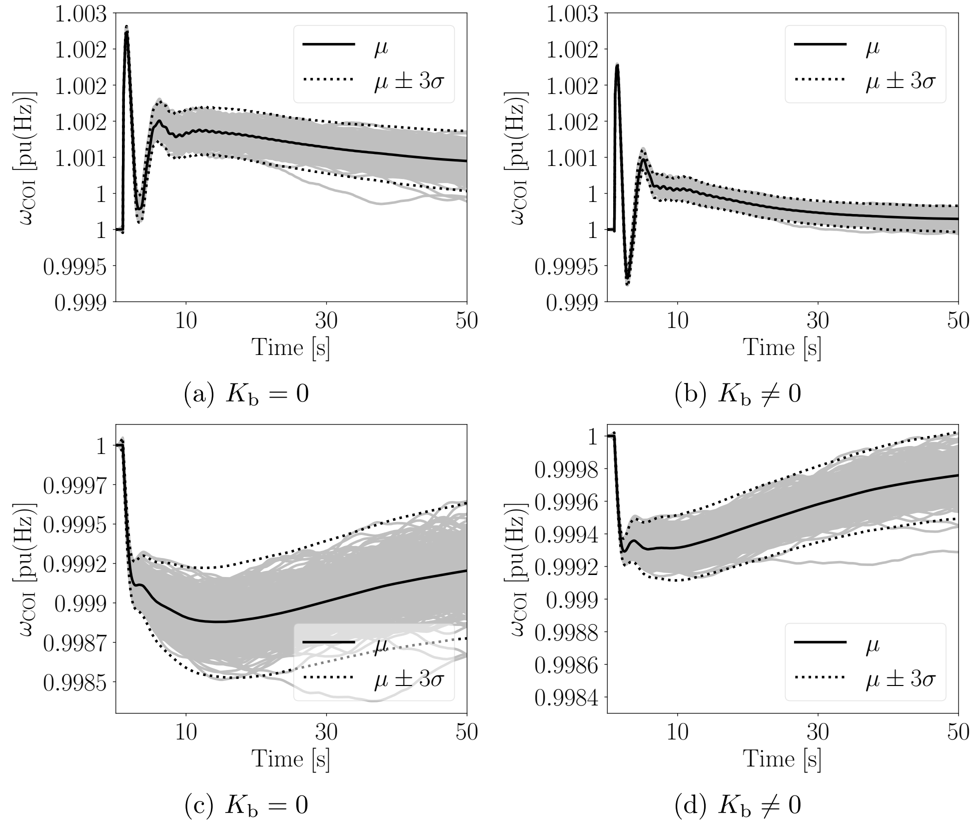

(a) $K_\mathrm{b} = 0$ (b) $K_\mathrm{b} \neq 0$

(c) $K_\mathrm{b} = 0$ (d) $K_\mathrm{b} \neq 0$

Figure 3.18: Trajectories of the frequency CoI with 500 Monte Carlo simulations for the WSCC 9-bus system with inclusion of a DS-VPP: (a) and (b) three-phase fault; (c) and (d) load increase.

Figure 3.19 shows the trajectories of the impact of communication delays with respect to communication networks with different bandwidths on the system frequency CoI. For the TS-VPP, the data transmitted through the geographically dispersed devices give rise to bigger communication delays than for the DS-VPP (see Table 3.3). Simulation results, however, indicate that the DS-VPP is more sensitive to the communication delays than the TS-VPP even if these delays have a smaller magnitude. On the other hand, it is interesting to note that, even if delays are larger, the TS-VPP has a better dynamic performance than the DS-VPP even for the scenario with low-bandwidth communication network. These results indicate that a uniform geographical distribution of the resources of the VPP is beneficial for the regulation of the overall grid and can overcome the deterioration due to the latency of the communication network.

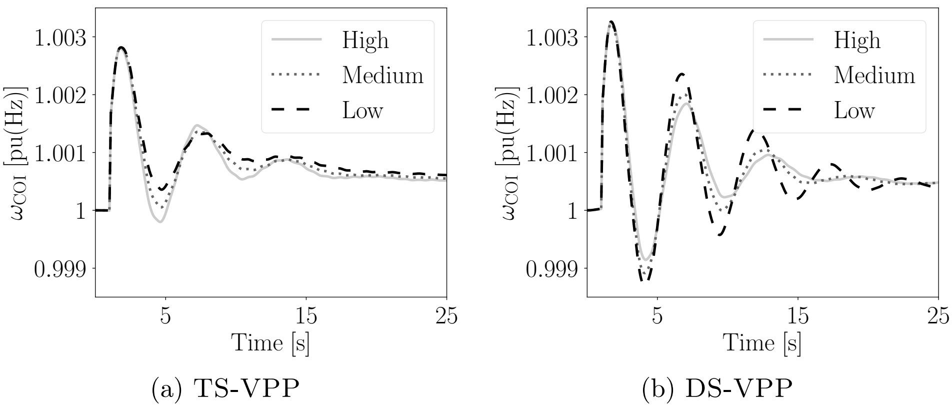

Figure 3.19: Frequency of the CoI following a three-phase fault for the 9-bus system with VPP and coordinated resources. The signal $p_{\rm co}$ is transmitted through high/medium/low-bandwidth communication networks, respectively.

3.5 Conclusions

This chapter presents a coordinated control method of VPP to improve power system short-term transient frequency response. The strategy is based on a coordinated control of (i) only ESS and, (ii) DERs and ESSs, in the VPP. A variety of control modes are compared and validated through Monte Carlo simulations. The impact of communication delays, stochastic processes as well as of the capacity of ESS on the overall transient behavior are also outlined. Based on the simulation results, the following conclusions can be drawn.

1. The proposed coordinated control approach for ESS and DERs in VPP can significantly improve the dynamic performance of the power system. The proposed control approach performs better than either conventional VPPs that do not regulate the frequency, i.e. utilize a constant power set-point, and VPPs that regulate the frequency through the independent controllers of ESSs and DERs.

2. Communication delays have a more significant impact on DERs than ESSs in the proposed coordinated control approach. This had to be expected, as the proposed strategy works as a sort of *fast* secondary frequency control. To reduce the negative impact of communication networks without increasing the bandwidth, a two-phase coordinated control is proposed. In this operating mode, the ESS acts first whereas DERs are included in the coordinated control in a second phase. This reduces the impact of the limited capacity of the ESS and, in turn, improves the transient stability.

Moreover, this chapter compares the performance of VPP primary frequency regulation considering different topologies as well as different frequency control approaches of DERs and ESSs. The impact of communication delays and stochastic disturbances of wind, load, and solar irradiance are also taken into account. Simulation results indicate that, without proper control, DERs deteriorate the dynamic response of the grid, in particular if they are distributed all-over the transmission grid. Interestingly, the averaging effect of stochastic processes helps reducing the negative impact of DERs if they are located at the distribution and connected to the transmission system through a single point of common coupling. On the other hand, as expected, the frequency control of VPPs can effectively contribute to improve the frequency response of the system. The TS-VPP with coordinated control of DERs and ESSs has, in general, a better performance than the DS-VPP. Moreover, the geographical scattering of the resources of the TS-VPP makes the TS-VPPs outperform the DS-VPPs with respect to the reduction of the dynamic impact of communication delays.

Chapter 4

Combined Voltage-Frequency Control of Distributed Energy Resources

Environmental and sustainability concerns drive the gradual replacement of fossil fuel-based power plants by non-synchronous DERs, including renewable sources and storage systems [65]. As the share of DERs to the energy mix increases, their contribution to the frequency and voltage regulation are considered essential services to maintain the stability and performance of the grid [31]. DERs are typically connected to the grid via power electronic converters, which provide high flexibility in their control design as well as the ability to act faster than the controllers of conventional generators [7, 82]. This chapter introduces a general control strategy that improves the overall dynamic response of power systems by efficiently exploiting the active and reactive control capabilities of converter-based DERs [128].

4.1 Introduction

As the penetration of converter-based resources to the grid increases, the total amount of rotational inertia decreases. This leads to high frequency variations which, in case of a severe power imbalance, may trigger a system-level collapse [65]. The capability of DERs to regulate the frequency through the available power reserve is limited because (i) they are typically designed to achieve a (near) maximum power extraction; and (ii) the availability of a certain power reserve is hard to be ensured, since a large portion of DER generation is stochastic, e.g. wind and solar PV [58].

Frequency regulation in power systems is traditionally provided through the active power, while the reactive power is employed to regulate the voltage. This is an intuitive choice for conventional large-scale systems, where the active (P) and reactive (Q) power flows are largely decoupled due to the highly inductive nature of transmission lines [48]. On the other hand, DERs are often integrated within distribution networks, where the resistance/inductance (R/X) ratio of feeders is large, thus leading to a strong interaction of P and Q with voltage and frequency, respectively. In this vein, a solution that has been proposed is to artificially impose the P-Q decoupling through the control of power converters, e.g. with the application of a virtual impedance control [27, 49]. Instead, this chapter effectively exploits the P-Q coupling with scope to improve the frequency and voltage regulation provided by DERs.

In this vein, the authors in [23] study the ability of converter-based resources to regulate the frequency through voltage control, taking advantage of load sensitivity to voltage variations in MGs. The concept of voltage-based frequency control has been also recently applied to improve the frequency response of large power systems through Static Var Compensators (SVCs) connected to load buses [77, 111]. In addition, a multi-band PSS to improve the primary frequency response of SMs is proposed in [70]. In this work, the problem of frequency regulation is translated into the one of damping the so-called system frequency regulation mode, see [113]. A reactive power-based frequency control for solar PV is presented in [76], while a voltage-based feedback to mitigate the part of DER active power injection that does not contribute to the frequency regulation thus improving the system dynamic response is proposed in [105]. Finally, the authors in [104] study the effect of combined active and reactive power control to the frequency response of DFIGs.

The references above indicate that voltage and reactive power regulation can contribute to the improvement of the frequency response both in small and large scale systems. On the other hand, recent research results show that active power regulation can also be utilized to improve the voltage response of the system. For example, reference [29] proposes a voltage controller through active power management for hybrid fuel-cell/energy-storage distributed generation systems, while an active power-voltage control scheme for islanded MGs is presented in [37]. Moreover, the authors in [120] propose a voltage regulation strategy that combines the battery management of EVs and the active power curtailment of PV, to address voltage variations in distribution networks.

The remainder of the chapter is organized as follows. Section 4.2 provides the theoretical framework of the chapter starting from the well-known power flow equations, and presents a metric to assess the joint voltage/frequency response at any bus of a power network. Section 4.3 introduces the proposed DER control strategy for primary frequency and voltage regulation. The case study is discussed in Section 4.4, based on a modified version of the IEEE 39-bus system. Finally, conclusions are drawn in Section 4.5.

4.2 Theoretical Background

The complex power injection at the network buses of a power system can be described as:

$$\begin{aligned}\bar{\boldsymbol{S}}(t) &= \boldsymbol{P}(t) + \jmath \boldsymbol{Q}(t) \\ &= \bar{\boldsymbol{v}}(t) \circ \bar{\boldsymbol{\imath}}^*(t) \\ &= \bar{\boldsymbol{v}}(t) \circ \left(\bar{\mathbf{Y}}\, \bar{\boldsymbol{v}}(t)\right)^*,\end{aligned} \tag{4.1}$$

where $\boldsymbol{P}, \boldsymbol{Q} \in \mathbb{R}^{n\times 1}$ are the column vectors of bus active and reactive power injections, respectively; n is the number of network buses; $\bar{\mathbf{Y}} \in \mathbb{C}^{n\times n}$ is the network admittance matrix; $\bar{\boldsymbol{v}}, \bar{\boldsymbol{\imath}} \in \mathbb{C}^{n\times 1}$ are the vectors of bus voltages and current injections, respectively; $\circ$ denotes the element-wise multiplication; and $*$ indicates the conjugate. The h-th elements of $\boldsymbol{P}$ and $\boldsymbol{Q}$ can be written as:

$$\begin{aligned}P_h &= \sum_{k=1}^{n} P_{hk} = \sum_{k=1}^{n} v_h v_k \big(G_{hk}\cos\theta_{hk} + B_{hk}\sin\theta_{hk}\big)\,, \\ Q_h &= \sum_{k=1}^{n} Q_{hk} = \sum_{k=1}^{n} v_h v_k \big(G_{hk}\sin\theta_{hk} - B_{hk}\cos\theta_{hk}\big)\,,\end{aligned} \tag{4.2}$$

where the time dependency is omitted for simplicity; P_{hk}, Q_{hk} are the active and reactive power flows, respectively, from bus h to bus k; G_{hk} and B_{hk} are the real and imaginary parts of the (h,k) element of $\bar{\mathbf{Y}}$, i.e. $\bar{Y}^{hk} = G_{hk} + \jmath B_{hk}$; v_k is the voltage magnitude at bus k, $k = 1, 2, \dots, n$; and $\theta_{hk} = \theta_h - \theta_k$, where θ_h and θ_k are the voltage phase angles at buses h and k, respectively. Differentiation of (4.2) gives:

$$\begin{aligned} dP_h &= \sum_{k=1}^{n} \frac{\partial P_h}{\partial \theta_{hk}} d\theta_{hk} + \sum_{k=1}^{n} \frac{\partial P_h}{\partial v_k} dv_k \equiv dP_{\theta,h} + dP_{v,h} \, , \\ dQ_h &= \sum_{k=1}^{n} \frac{\partial Q_h}{\partial \theta_{hk}} d\theta_{hk} + \sum_{k=1}^{n} \frac{\partial Q_h}{\partial v_k} dv_k \equiv dQ_{\theta,h} + dQ_{v,h} \, , \end{aligned} \tag{4.3}$$

where $dP_{\theta,h}$, $dQ_{\theta,h}$ are the quota of dP_h and dQ_h that depend on the voltage angles and consequently, the components of the active and reactive power that can be effectively used to regulate the frequency in the system; and $dP_{v,h}$, $dQ_{v,h}$ are the quota of dP_h and dQ_h that depend on the voltage magnitudes and thus the components that can be used to modify the voltage response [63, 67].

Consider equations (4.3). Then, the parts of $dP_{\theta,h}$, $dQ_{\theta,h}$ and $dP_{v,h}$, $dQ_{v,h}$ that are due to local variations of the frequency and the voltage at bus h, respectively, are given by the following expressions [10]:

$$\begin{aligned} dP_{\theta,h}^{\rm loc} &= -Q_h d\theta_h \, , \quad & dQ_{\theta,h}^{\rm loc} &= P_h d\theta_h \, , \\ dP_{v,h}^{\rm loc} &= \frac{P_h}{v_h} dv_h \, , \quad & dQ_{v,h}^{\rm loc} &= \frac{Q_h}{v_h} dv_h \, . \end{aligned} \tag{4.4}$$

Then rewriting equations (4.4) using time derivatives, one has:

$$\frac{dP_{\theta,h}^{\rm loc}}{dt} = -Q_h \theta_h' \, , \qquad \frac{dQ_{\theta,h}^{\rm loc}}{dt} = P_h \theta_h' \, , \tag{4.5}$$

$$\frac{dP_{v,h}^{\rm loc}}{dt} = P_h u_h' \, , \qquad \frac{dQ_{v,h}^{\rm loc}}{dt} = Q_h u_h' \, , \tag{4.6}$$

where

$$\theta_h' = \frac{d\theta_h}{dt} \, , \qquad u_h' = \frac{1}{v_h} \frac{dv_h}{dt} \, . \tag{4.7}$$

The first term, namely θ_h', is the deviation of the bus frequency with respect to the synchronous frequency; whereas u_h' represents the transient rate of change of the voltage normalized with respect to the bus voltage magnitude. The latter quantity has the same unit as a frequency and is thus comparable with the frequency deviation θ_h' [63].

4.2.1 Metric to Evaluate the Effectiveness of Voltage/Frequency Controllers

In the remainder of this chapter, a quantity is utilized to assess the combined active/reactive injection effect on the voltage/frequency response provided at bus h, as follows:

$$\mu'_h = \sqrt{(\theta'_h)^2 + (u'_h)^2}\,. \tag{4.8}$$

The particular interest is in assessing the cumulative effect of μ'_h for a given time interval $[t_0, t]$. This interval is determined based on the time scale of the primary response of generators, which typically lasts from few seconds to few tens of seconds.

Finally, the following quantity is proposed as a metric to assess the joint frequency/voltage response at a given bus h of a power network:

$$\mu_h = \int_{t_0}^{t} \mu'_h \; dt\,. \tag{4.9}$$

The metric in (4.9) possesses the property that the two components corresponding to the frequency and voltage are considered with the same weights, while having the same units, thus being summable and directly comparable. In this chapter, the metric is used in the case study of Section 4.4 to compare the effectiveness of different DER active/reactive control configurations. With this regard, note that smaller values of μ_h are in general obtained for smaller frequency and voltage variations, which in turn, indicate a better dynamic response at bus h.

4.3 Proposed Control Scheme

This section describes the structure of the proposed DER control scheme. Since the focus is on utilising the active/reactive controllers and on which control signal is dedicated to which control objective, the standard filters and controllers widely used in industrial applications are chosen to keep each control loop simple yet practical.

Considering a simplified DER model, the block diagram of the control scheme is depicted in Figure 4.1. The control scheme consists of an inner current control loop and two outer loops for frequency and voltage regulation, respectively. The current control loop regulates the d and q axis components of the current (i_{d}, i_{q}) in the dq reference

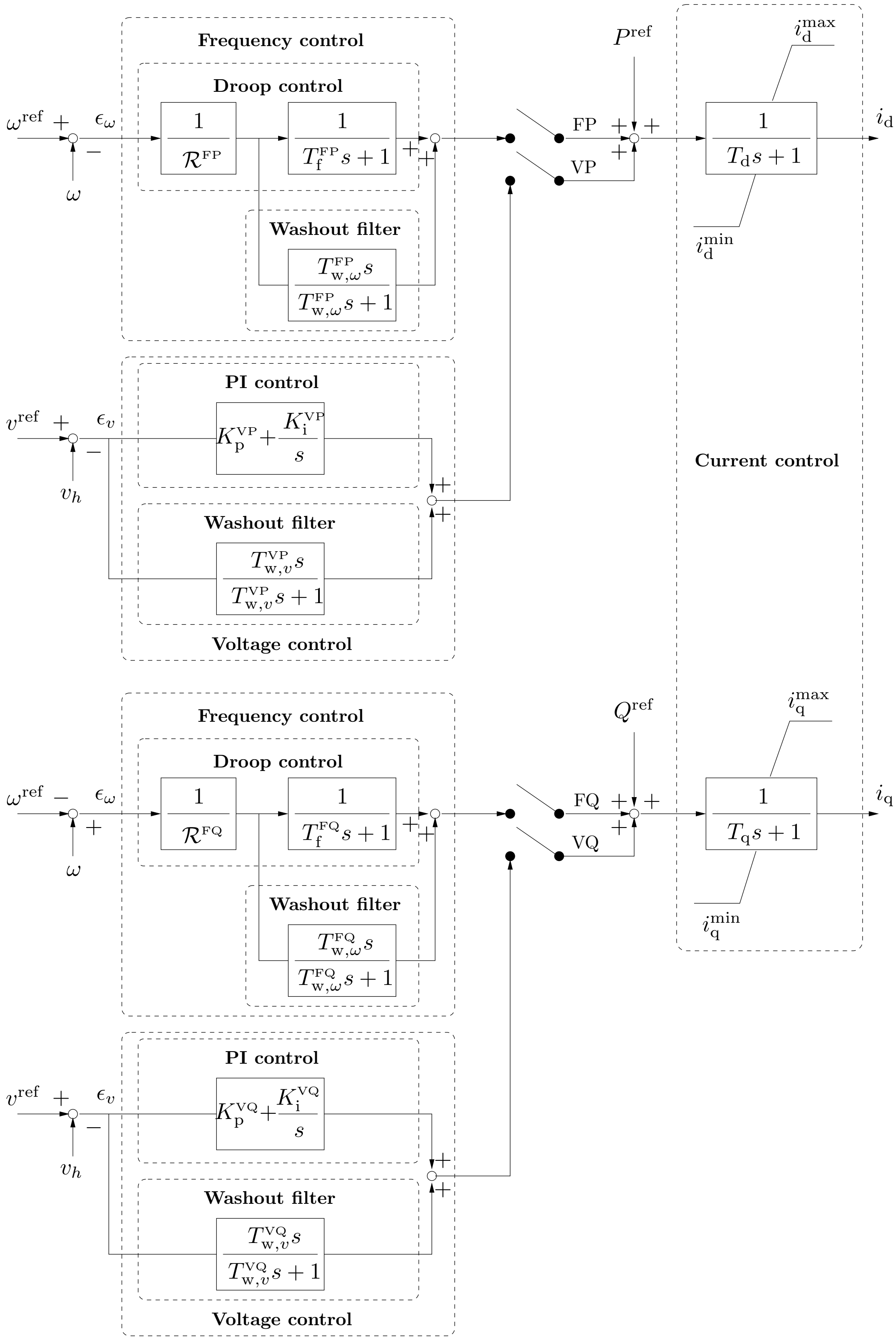

Figure 4.1: Proposed DER control scheme.

frame. These components are limited between their minimum and maximum values through an anti-windup limiter. The frequency control loop receives the frequency error ϵ_ω and applies a droop control and a washout filter acting in parallel. On the other hand, the voltage control loop adjusts the bus voltage error ϵ_v by means of a PI controller and a washout filter also connected in parallel. The outputs of the frequency and voltage controllers are then added to the DER's active and reactive power references. It is worth observing that the adoption of simple conventional controllers is on purpose, as these are the most commonly implemented in practice and to allow easily reproducing the results presented in the case study. As a matter of fact, the main objective of this work is to show how combining the effect of different control channels impact on the performance of the overall system.

The proposed DER control scheme includes four channels that can be combined to formulate different active and reactive power control modes. A summary of the available control modes for the active power of the DER is as follows:

- FP: The active power is employed to regulate the frequency. The FP mode is the standard way to regulate the frequency in conventional power systems.

- VP: The active power is employed to regulate the voltage. In this mode, a voltage control channel acts by modifying the DER active power reference.

- FVP: The active power reference is modified to control both the frequency and the voltage. In this case, both FP and VP in Figure 4.1 are switched on.

Similarly, the available modes for the control of the DER reactive power can be summarized as follows:

- VQ: The reactive power is utilized to regulate the voltage. This is the classic approach, since voltage regulation is conventionally realized by means of the VQ mode.

- FQ: The reactive power reference of the DER is modified to provide frequency regulation.

- FVQ: Both VQ and FQ are switched on in a combined control of the reactive power.

In this work, the effectiveness of frequency and voltage regulation provision through both the active and reactive power of DERs is studied, which leads to the combined scheme FVP+FVQ. In the case study of Section 4.4, the dynamic performance of this configuration is compared to other configurations, including the the conventional approach to frequency-voltage control, i.e. FP+VQ.

4.4 Case Study

This section presents simulation results based on the IEEE 39-bus benchmark system [33]. The system comprises 10 SMs (SM 1-10), totaling 6354.1 MW and 1357.1 MVAr of active and reactive power generation. SMs are represented by 4-th order (two-axis) models and are equipped with Automatic Voltage Regulators (AVRs), TGs, and PSSs. In this chapter, SMs are also assumed to participate to secondary frequency regulation through an AGC scheme. The AGC is modeled as an integrator (with gain $k_{\text{AGC}} = 0.2$), the output of which is used to update the active power set-points of the machines every 5 s.

Table 4.1: Parameters of DER controller.

Controller	Parameters
Current	$T_{\text{d}} = 0.04$ s, $T_{\text{q}} = 0.04$ s
Frequency	$\mathcal{R}^{\text{FP}} = \mathcal{R}^{\text{FQ}} = 0.075$,
	$T_{\text{f}}^{\text{FP}} = T_{\text{f}}^{\text{FQ}} = 0.12$ s, $T_{\text{w},\omega}^{\text{FP}} = T_{\text{w},\omega}^{\text{FQ}} = 0.05$ s
Voltage	$K_{\text{p}}^{\text{VP}} = 1.5$, $K_{\text{p}}^{\text{VQ}} = 5$,
	$K_{\text{i}}^{\text{VP}} = K_{\text{i}}^{\text{VQ}} = 10$, $T_{\text{w},v}^{\text{VP}} = T_{\text{w},v}^{\text{VQ}} = 0.1$ s

Loads are modeled using the ZIP model, the active and reactive power consumption of which, $P_{\text{L},h}$, $Q_{\text{L},h}$, are quadratic expressions of the bus voltage, as follows [59]:

$$
\begin{aligned}
P_{\text{L},h} &= P_{zo}\left(\frac{v_h}{v_o}\right)^2 + P_{io}\frac{v_h}{v_o} + P_{po}\,, \\
Q_{\text{L},h} &= Q_{zo}\left(\frac{v_h}{v_o}\right)^2 + Q_{io}\frac{v_h}{v_o} + Q_{qo}\,,
\end{aligned}
\tag{4.10}
$$

where v_o is the nominal voltage at the load bus; v_h is the measured load bus voltage; P_{zo}/Q_{zo}, P_{io}/Q_{io}, P_{po}/Q_{qo} are the corresponding quota of constant impedance, constant current and constant power consumption, respectively. The ZIP loads in this section consist of 20% constant power (e.g., milling machines), 10% constant current (e.g., electric vehicle chargers), and 70% constant impedance (e.g., heating systems) consumption [69].

For the purpose of this case study, the system is modified to include a 30% penetration of non-synchronous generation. To this aim, the SMs 5, 6 and 8 that connected to buses 34, 35 and 37, are substituted by converter-based DERs. Considering the practical capacity of a single DER, the DERs connected at each bus here are not single generation sources but modeled as a combination of several DERs. The single-line diagram of the modified IEEE 39-bus system is shown in Figure 4.2. DERs and their controls are modeled as described in Section 4.3.

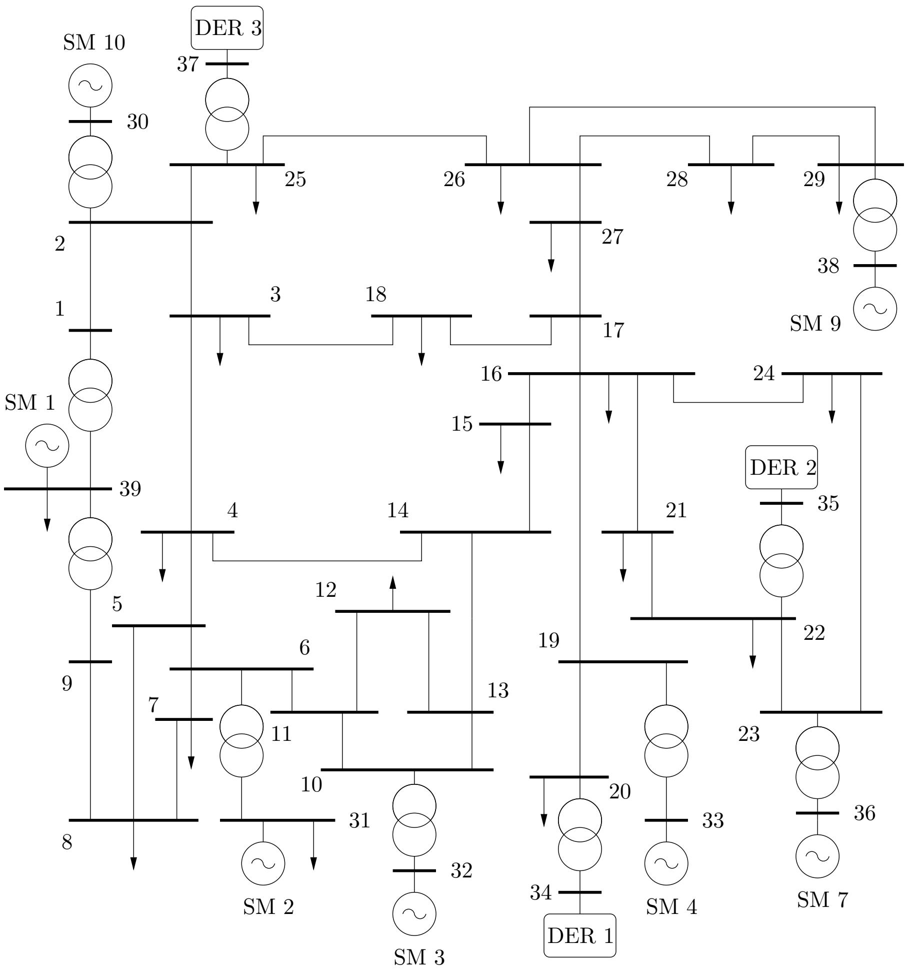

Figure 4.2: Single-line diagram of the modified IEEE 39-bus system.

The parameters of the frequency, voltage, and inner current controllers of the DERs are given in Table 4.1. The first estimation of the control parameters of each filter has been obtained by setting the time constants of the corresponding differential equations based on the requirements for the time scale of their action, which leads most of the parameters to lie in a certain range. Then the final values of the parameters have been determined through a trial-and-error procedure. It is also relevant to note that the controllers employed in the chapter provide an acceptable response for a wide range of operating conditions. For example, for the droop constants of the PFC, good results are obtained in the range $\mathcal{R} \in [10^{-2}, 10^{-1}]$.

To guarantee a fair comparison, different control modes in the chapter are compared keeping constant control parameter settings. Note that different approaches are also tried in the case study. For example, each control mode has been separately tuned with an aim to achieve the best dynamic response. However, since, as discussed above, the controllers perform well for a relatively large range of their parameters, their setup does not modify the main conclusions that are drawn in this section.

4.4.1 Evaluation of FQ and VP Control Modes

This section considers the FQ and VP controls, which are the components that differentiate the proposed FVP+FVQ control strategy from the classical approach, where frequency and voltage regulation are provided only by means of FP and VQ, respectively (see mode definitions in Section 4.3).

The FQ mode is firstly examined, i.e. the ability of DERs 1-3 to improve the dynamic response of the system by controlling the frequency through the reactive power. To this aim, the system is simulated for both positive/negative signs of the input control error assuming the tripping of SM 10 at $t = 1$ s. Results are shown in Figure 4.3 where, for the sake of comparison, the response of the system when DERs (i) do not provide any control and (ii) act based on the classic FP control are included. Figure 4.3 indicates that the FQ control improves the CoI frequency response of the system if utilized with input error $\epsilon_\omega = \omega - \omega^{\rm ref}$. The main reason for FQ's effectiveness in this case is that the DERs respond to the under-frequency by reducing their reactive power injection and thus the voltage levels at the network. Due to the voltage dependency of loads, see (4.10), the power demand level decreases, thus reducing the imbalance and helping the recovery of the frequency. Note, finally, that the improvement provided by the FQ mode is lower than the one of the classic FP. This result is as expected. Yet, as it will be seen in Section 4.4.5, the benefits of using FQ are more apparent when applied at the distribution network level.

The effect of regulating the voltage at the DER terminal bus through its active power injection, i.e. the VP mode, is shown. A simulation is carried out considering the outage of line 15-16 and results are shown in Figure 4.4. The VP mode improves the transient behavior of the voltage when the control input error is $\epsilon_v = v^{\rm ref} - v_h$. However, this mode also introduces large deviations in the power sharing among the DERs connected to the system and thus, using it individually is not suggested. The VP can still contribute to improve the overall system dynamic response if utilized with a relatively small gain and

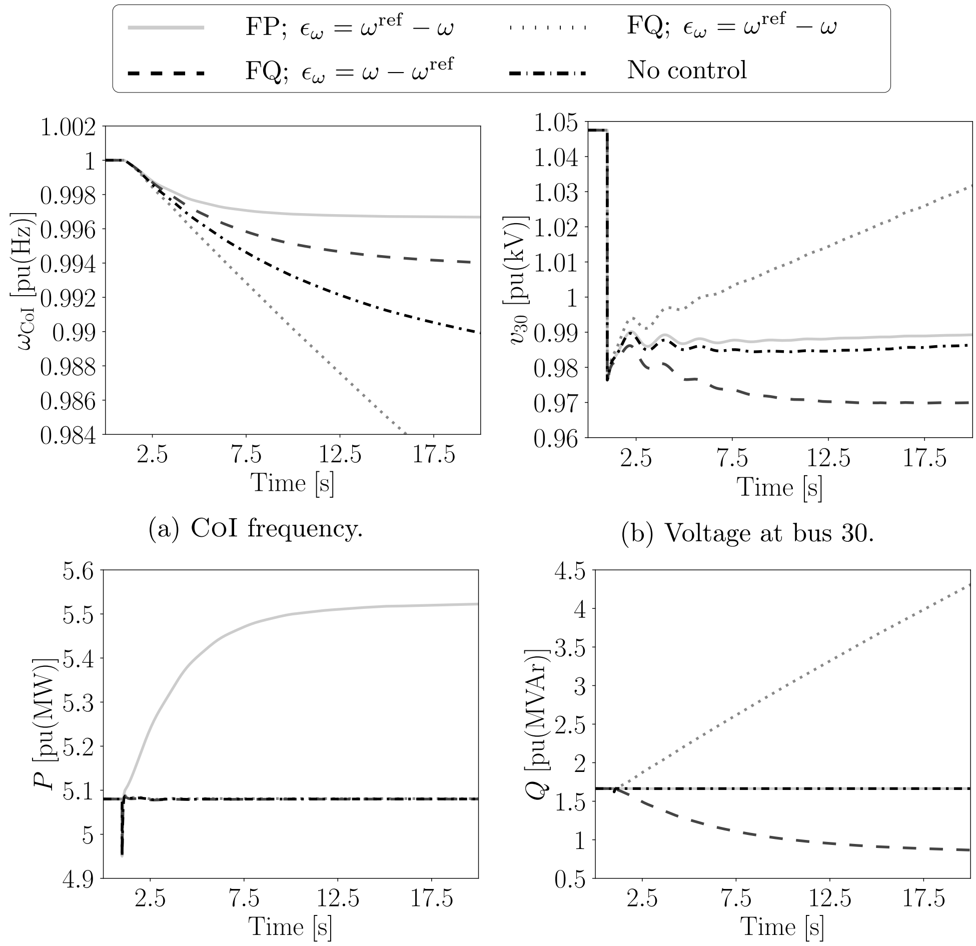

(a) CoI frequency.

(b) Voltage at bus 30.

(c) DER 1 active power injection.

(d) DER 1 reactive power injection.

Figure 4.3: Transient response following the loss of SM 10.

as an auxiliary control that coordinates with other modes. This point is further discussed in the remainder of this case study.

The following remark on the signs of the control input errors ϵ_ω, ϵ_v is relevant. For the frequency response of the system to improve, ϵ_ω in FQ has to be the opposite from the one utilized in FP. In terms of the theoretical derivations of Section 4.2, the need for opposite actions when regulating the frequency through the active and reactive power, respectively, can be observed in the structure of (4.5). On the other hand, to improve the voltage regulation, ϵ_v needs to be implemented with the same sign for both VP and VQ modes. This is consistent with the derivations of Section 4.2, and in particular with (4.6), which suggests that regulating the voltage variations requires actions in the same direction for both active and reactive power. Hence, $\epsilon_\omega = \omega - \omega^{\rm ref}$ and $\epsilon_v = v^{\rm ref} - v_h$ are chosen for FQ and VP in the remainder of the case study.

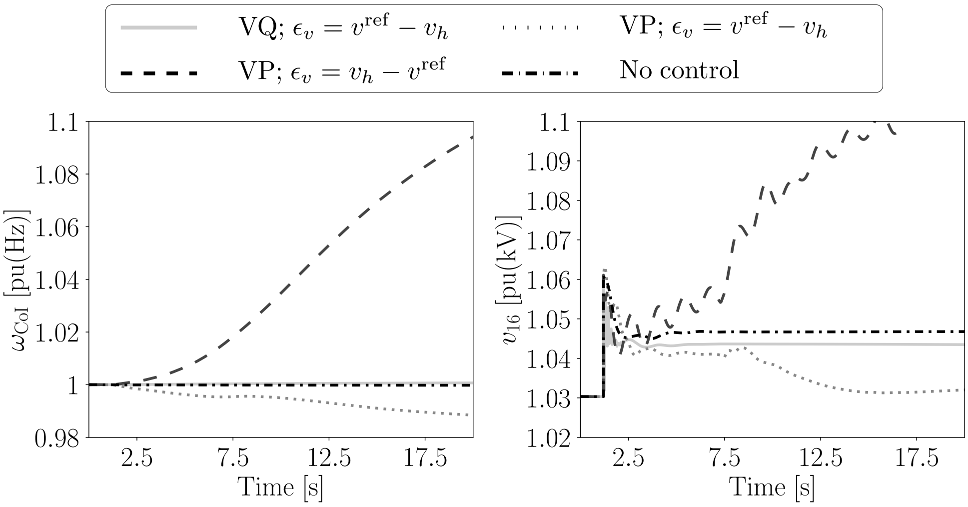

(a) CoI frequency.

(b) Voltage at bus 16.

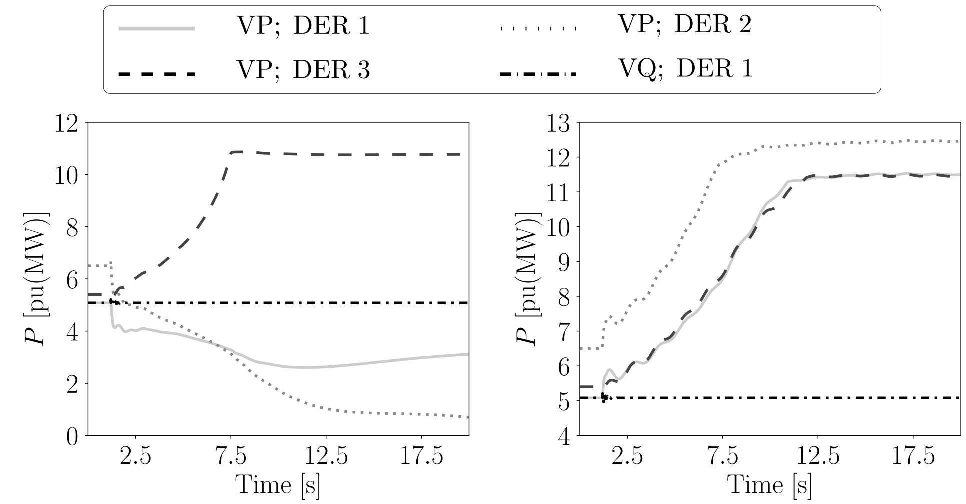

(c) DERs active power injection. Modes VP and VQ ($\epsilon_v = v^{\mathrm{ref}} - v_h$).

(d) DERs active power injection. VP: $\epsilon_v = v_h - v^{\mathrm{ref}}$; VQ: $\epsilon_v = v^{\mathrm{ref}} - v_h$.

Figure 4.4: Transient response following the outage of line 15-16.

4.4.2 Performance of FVP+FVQ Control

In this section, the performance of the proposed FVP+FVQ control scheme is studied. This scheme is compared to the classic FP+VQ control, as well as to FP+FQ, VP+VQ, and FP+FVQ. A simulation is carried out considering the disconnection of the load at bus 3 ($P_{\mathrm{L},3} = 3.22$ pu, $Q_{\mathrm{L},3} = 0.024$ pu). The transient behavior of the system following the disturbance is presented in Figure 4.5 where, the response of the system with all DER controls disconnected as well as that of the original IEEE 39-bus system serve as references for comparison.

The following remarks are relevant.

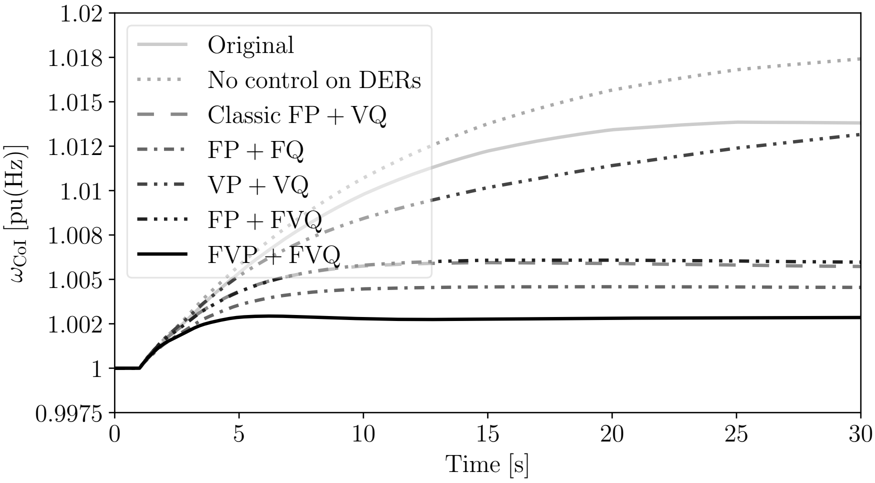

(a) CoI frequency.

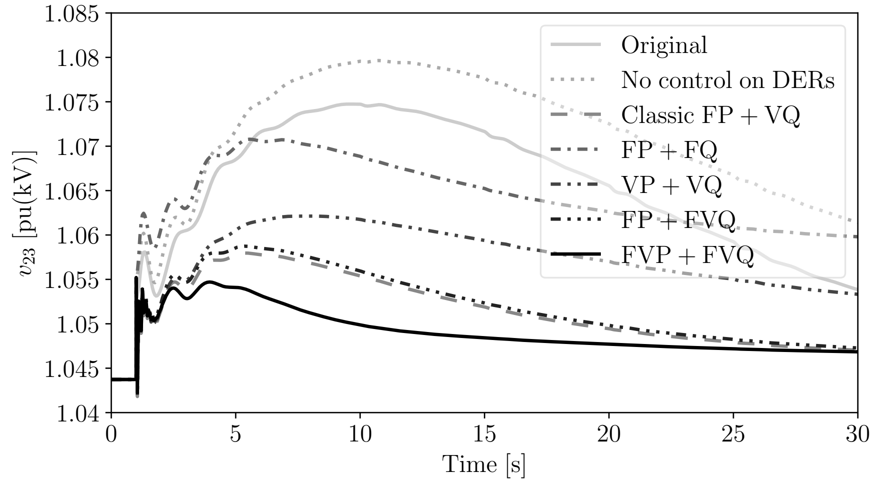

(b) Voltage at bus 23.

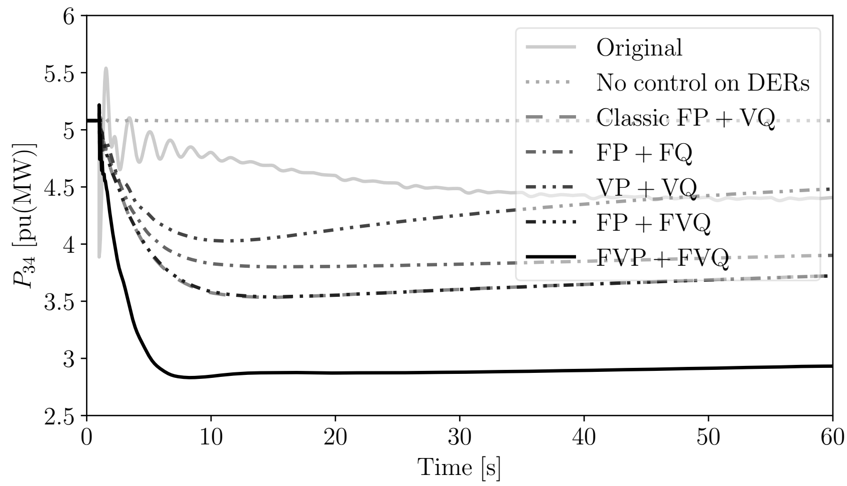

(c) Active power injection at bus 34 (DER 1).

Figure 4.5: Transient response after disconnection of load at bus 3.

- Compared to the original system, a 30% penetration of DERs worsens the overall dynamic behavior of the system, when these resources provide no restorative control actions. This result is as expected.

- The FP+FQ control shows a better frequency response than the classic FP+VQ, yet, it leads to a poor voltage behavior (see Figure 4.5b).

- Although the VP+VQ scheme shows a very good voltage response, it leads to a poor frequency response.

- Combining the FP+FQ and VP+VQ modes in a single scheme leads to the proposed FVP+FVQ which provides the best frequency and voltage dynamic response among the schemes compared.

To validate the tuning of the parameters of the controllers and build the trust of the adequateness of this tuning for the stability of the overall system, we have assessed the transient behavior of the system for a wide range of operating conditions and disturbance scenarios. With this aim, the proposed control has been tested for a variety of disturbances, including generator tripping, line outages, short circuits, and load disconnections. Moreover, the impact of varying the voltage dependency of loads by considering a constant impedance load model are also considered. A summary of the results obtained is presented in Table 4.2, where $\Delta\omega$ refers to the relative variation of the frequency of the CoI and Δv refers to the relative variation of a bus voltage magnitude that is local to the disturbance. For each scenario, the table provides the maximum relative variations, as well as the variations few seconds for primary frequency and voltage responses after the disturbance, i.e. at t = 20 s of the simulation for the frequency and at t = 10 s for the voltage. The smallest frequency/voltage variations obtained for each scenario are marked in bold.

Simulation results suggest that, overall, the proposed FVP+FVQ control leads to an improvement of both primary frequency and voltage regulation of the system. This improvement is significant in case of an outage of synchronous generation, a load switching, or a line trip, while for short circuits, FVP+FVQ performs as the conventional FP+VQ. Finally, note that in contrast to commonly proposed solutions, the performance enhancement provided by FVP+FVQ comes in an inexpensive way, i.e. without the need to install any extra equipment, e.g. storage devices.

Table 4.2: Frequency/voltage deviations for different contingencies, control modes and load models.

Load model	ZIP						Constant impedance					
Control	Classic FP+VQ		FP+FQ		FVP+FVQ		Classic FP+VQ		FP+FQ		FVP+FVQ	
$\Delta\omega$ (%)	max	at 20 s	max	at 20 s	max	at 20 s	max	at 20 s	max	at 20 s	max	at 20 s
Load 3 out.	0.5814	0.5946	0.4593	0.4593	**0.2934**	**0.2817**	0.5518	0.5516	0.4082	0.4075	**0.2717**	**0.2637**
Load 20 out.	1.1452	1.1318	0.9476	0.9456	**0.5533**	**0.5202**	1.1378	1.1355	0.8986	0.8985	**0.5501**	**0.5246**
SM 4 out.	−1.1478	−1.1404	−0.7056	−0.7050	**−0.5141**	**−0.4727**	−1.1029	−1.1028	−0.6199	−0.6158	**−0.4946**	**−0.4644**
SM 7 out.	−1.0663	−1.0495	−0.7422	−0.7348	**−0.5393**	**−0.4826**	−1.0408	−1.0325	−0.6711	−0.6685	**−0.5331**	**−0.4852**
Line 8-9 out.	0.0231	0.0229	0.0180	0.0180	**0.0121**	**0.0118**	0.0804	0.0804	0.0657	0.0655	**0.0537**	**0.0526**
Line 21-22 out.	0.1610	0.1598	0.1544	0.1544	**0.1390**	**0.1354**	0.1994	0.1993	0.1840	0.1837	**0.1612**	**0.1564**
Fault at bus 4	**0.3066**	**−0.0201**	0.3970	−0.0217	0.3505	−0.0238	**0.3543**	0.0294	0.4585	**0.0133**	0.4245	−0.0294
Fault at bus 8	**0.2527**	**0.0042**	0.3182	0.0049	0.2989	0.0059	**0.2865**	0.0276	0.3590	0.0211	0.3257	**0.0150**
Δv (%)	max	at 10 s	max	at 10 s	max	at 10 s	max	at 10 s	max	at 10 s	max	at 10 s
Load 3 out.	1.2867	0.7845	1.7309	1.5417	**1.2533**	**0.6042**	1.2126	0.8275	1.5831	1.4612	**1.1632**	**0.6719**
Load 20 out.	2.6464	1.5891	6.7898	6.7588	**2.6464**	**1.4299**	2.5097	1.5937	6.4399	6.4291	**2.5097**	**1.4550**
SM 4 out.	−7.4634	−3.5033	−10.319	−10.264	**−7.4634**	**−3.2346**	−6.0130	−3.3522	−8.7384	−8.7016	**−6.0130**	**−3.1234**
SM 7 out.	−4.8425	−2.9453	−8.0907	−8.0907	**−4.8425**	**−2.8840**	−3.6201	−2.7031	−6.9113	−6.9113	**−3.6201**	**−2.6622**
Line 8-9 out.	−2.8946	−1.9047	−2.8946	−1.9217	**−2.8946**	**−1.9044**	**2.3011**	1.7715	2.3376	1.7594	2.3220	**1.7590**
Line 21-22 out.	−6.2882	−4.2634	−6.6219	**−4.1781**	**−6.2882**	−4.2203	−5.5680	−4.0392	−6.1302	**−3.9151**	**−5.5680**	−4.0117
Fault at bus 4	−100	−2.1525	−100	**−2.1329**	−100	−2.1749	−100	−2.0802	−100	**−2.0603**	−100	−2.1052
Fault at bus 8	−100	−1.3188	−100	**−1.3138**	−100	−1.3244	−100	−1.2711	−100	**−1.2645**	−100	−1.2762

4.4.3 Performance of the Proposed Metric μ_h

This section studies the accuracy of metric μ_h to assess the joint voltage/frequency response of DERs. In particular, Table 4.3 shows the value of the metric at bus 34, where DER 1 is connected, at $t = 15$ s and for the same disturbances considered in Table 4.2. The value of μ_{34} for each scenario is calculated using the local voltage and its time derivative (v_{34}, dv_{34}/dt) and the variation of the frequency of the CoI ($\Delta\omega_{\mathrm{CoI}}$). Moreover, the results for all control modes are normalized so that the metric for FP+VQ at $t = 15$ s equals to 1. Comparison between Table 4.3 and Table 4.2 indicates that the proposed metric can capture the combined voltage/frequency response with good accuracy. With this regard, recall from Section 4.2 that smaller values of μ_h imply a better overall dynamic response. It is also worth noting that in the occurrence of a fault at bus 4 and for constant impedance loads, the FP+FQ control shows the worst dynamic response from the metric point of view, although its $\Delta\omega$ and Δv (Table 4.2) are not the worst. In fact, the voltage response for FP+PQ control in this scenario is worse than the other controllers at the first 4 s of the simulation, which is not shown in Table 4.2 and it is not observable unless the researchers check the full time domain response of both the frequency and the voltage. μ_h captures these effects and hence, provides an accurate and convenient way to evaluate the joint frequency and voltage response of DERs. μ_h is utilized as a tool to assess the performance of DER control modes in the remainder of this case study.

Table 4.3: Metric μ_{34} (DER 1) for different contingencies, control modes and load models.

Load model	ZIP			Constant impedance		
Control	FP+VQ	FP+FQ	FVP+FVQ	FP+VQ	FP+FQ	FVP+FVQ
μ_{34}	at 15 s	at 15 s	at 15 s	at 15 s	at 15 s	at 15 s
Load 3 out.	1	0.7891	**0.5467**	1	0.7543	**0.5528**
Load 20 out.	1	0.8283	**0.5327**	1	0.8029	**0.5384**
SM 4 out.	1	0.6278	**0.4953**	1	0.5816	**0.5187**
SM 7 out.	1	0.7171	**0.5511**	1	0.6857	**0.5665**
Line 8-9 out.	1	0.8671	**0.7708**	1	0.8192	**0.7315**
Line 21-22 out.	1	0.9544	**0.9101**	1	0.9155	**0.8602**
Fault at bus 4	**1**	1.5189	1.1792	**1**	3.4706	1.5001
Fault at bus 8	**1**	1.5611	1.2027	**1**	1.9155	1.0742

4.4.4 Application to Aggregated Power Generation

This scenario assumes that the converter-based resources connected to buses 34, 35, 37 consist of several smaller DERs, the power generation and control modes of which are coordinated through a power aggregation mechanism. This mechanism can be implemented in practice as a VPP [125, 127]. For the purpose of this study, a varying percentage of the DERs that compose the VPP utilize the proposed FVP+FVQ scheme, and the rest act based on the classic FP+VQ control.

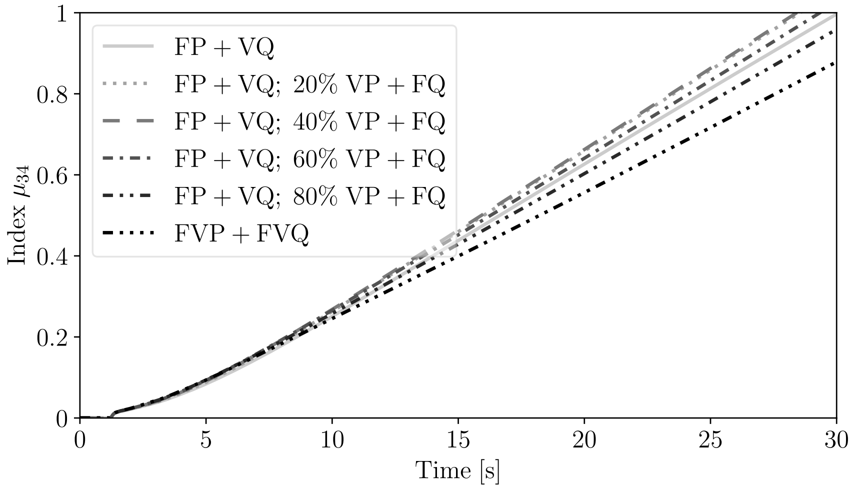

(a) Transient response following the outage of line 21-22.

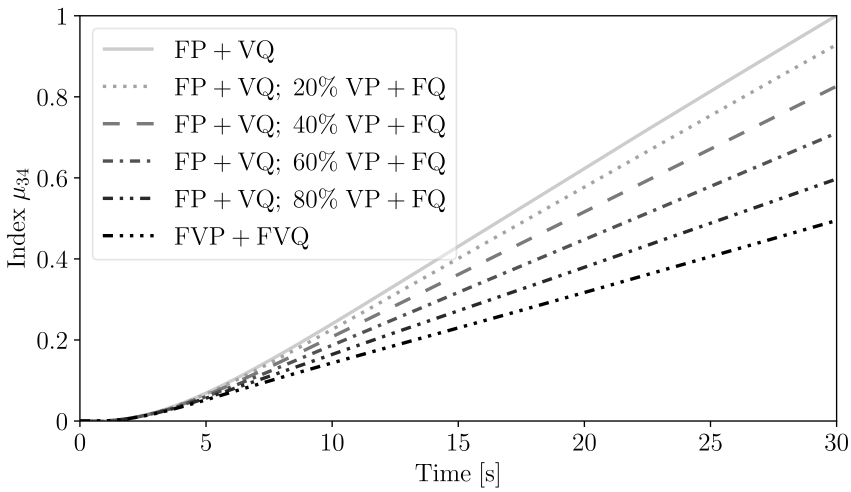

(b) Transient response following the load disconnection at bus 20.

Figure 4.6: μ_{34} (DER 1) for FVP+FVQ applied to a portion of VPP assets.

Figure 4.6 shows the results for two disturbances, (a) outage of the line 21-22, and (b) disconnection of the load connected to bus 20 (P_{20} = 6.28 pu, Q_{20} = 1.03 pu). The results are compared by means of the joint frequency/voltage response metric at bus 34 (μ_{34}), where DER 1 is connected. The metric is calculated as discussed in

Section 4.4.3. As expected, the proposed FVP+FVQ mode has the best performance for both disturbances, which confirms the results shown in Table 4.2. Interestingly, the classic FP+VQ mode combined with 20%-40% FVP+FVQ control worsens the transient response for disturbance (a). In conclusion, depending on practical requirements, the VPP operator can design its assets to apply and/or switch between different control modes.

4.4.5 Impact of R/X Line Ratio

In this section, the performance of the proposed control when applied to DERs integrated within distribution networks are concerned. To study the distribution network effect, the R/X ratios of the feeders that connect the DERs to the rest of the system are altered so that $R/X \approx 1$.

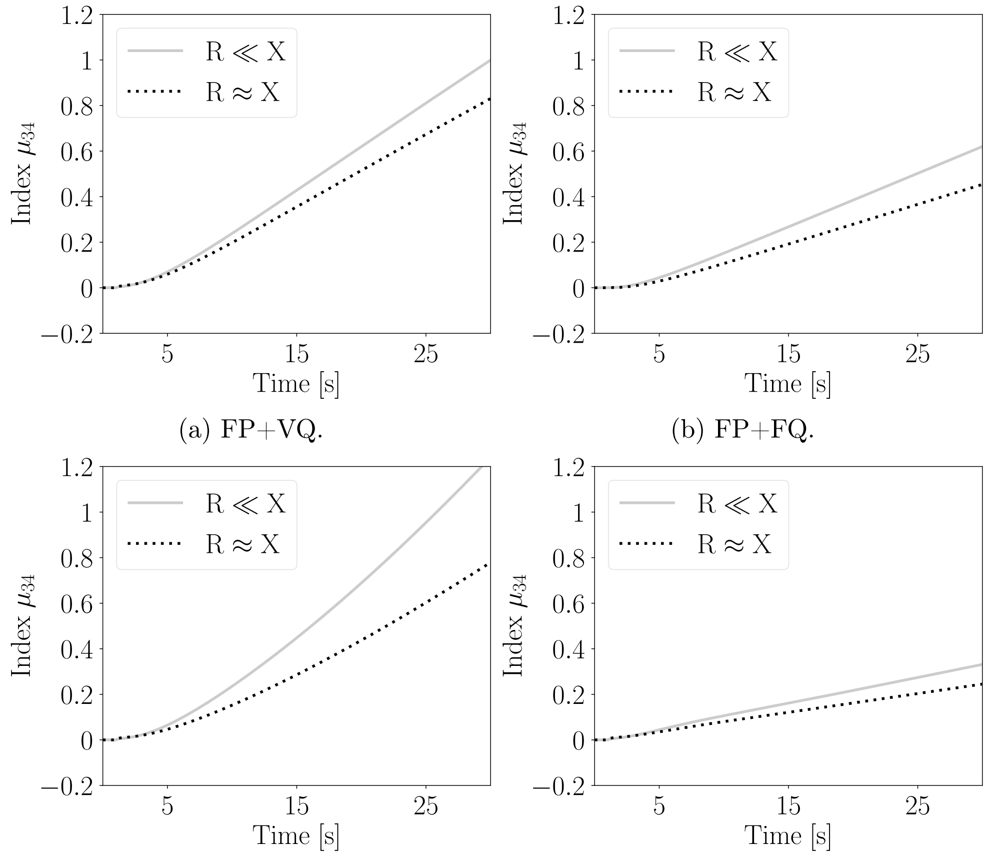

(a) FP+VQ. (b) FP+FQ.

(c) VP+VQ. (d) FVP+FVQ.

Figure 4.7: Transient response following the loss of SM 10.

The evolution of μ_{34} for different control modes is presented in Figure 4.7, where we have considered the loss of SM 10 at $t = 1$ s. Moreover, the results are normalized so that for FP+VQ μ_{34} equals to 1 at $t = 30$ s when $R/X \ll 1$. As it can be seen, when $R \approx X$, all DER control modes have a better performance. It is interesting to observe that for $R \approx X$, VP+VQ has the most significant improvement among the examined modes. The same effect can also be observed under different disturbance scenarios in this test system. Finally, the proposed FVP+FVQ control shows the best overall dynamic response among the modes compared.

4.4.6 Impact of DER Penetration Level

This scenario studies the impact of the share of DERs to the total generation mix of the system on the performance of the proposed control scheme. To this aim, and in addition to the DERs at buses 34, 35, 37, DERs are also connected to buses 36 and 38, by replacing the local SMs. As a consequence, the penetration of DERs to the modified IEEE 39 bus system increases to 50%.

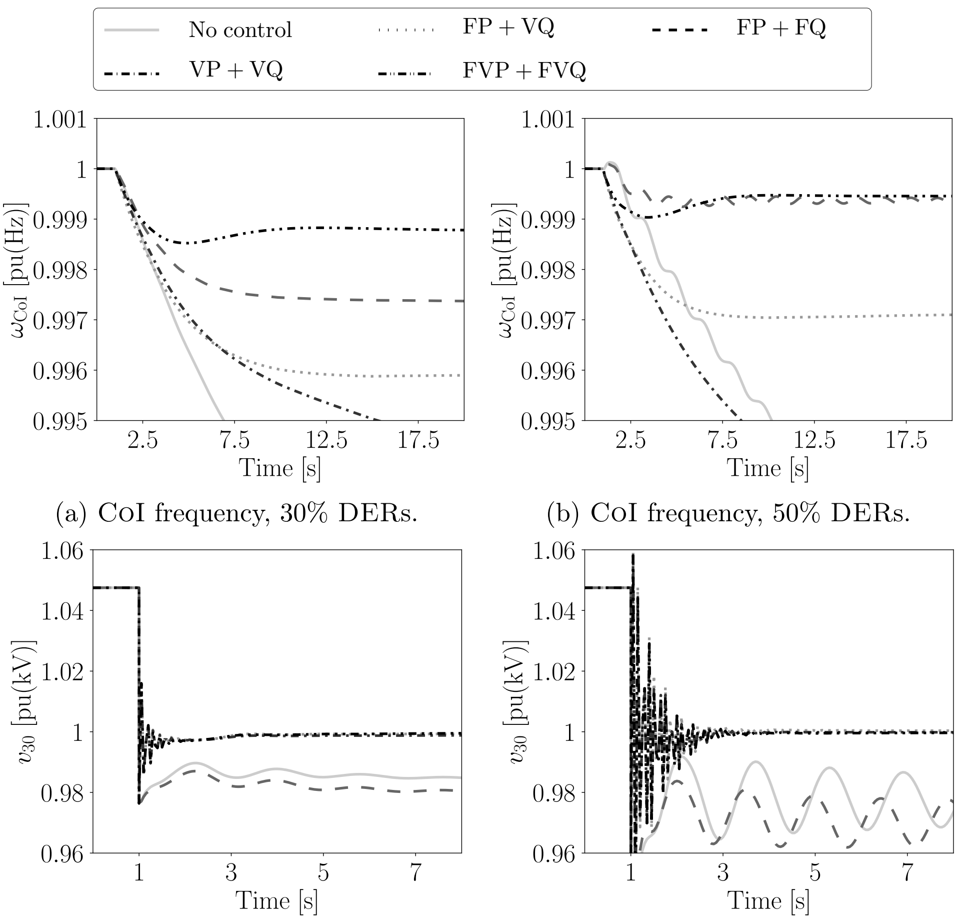

(a) CoI frequency, 30% DERs. (b) CoI frequency, 50% DERs.

(c) bus 30 voltage, 30% DERs. (d) bus 30 voltage, 50% DERs.

Figure 4.8: Transient response following the loss of SM 10.

A time domain simulation of the system is carried out by applying the loss of SM 10 at $t = 1$ s and results are presented in Figure 4.8. As it can be seen, increasing the DER penetration from 30% to 50%, although it leads to a worse voltage response, it does not deteriorate the frequency regulation of the system, which interestingly, slightly improves. Compared to the classic FP+VQ, the FP+FQ outperforms in terms of frequency, but leads to a poor voltage response. As expected, the dual effect holds when the VP+VQ scheme is applied. Most importantly, the FVP+FVQ control leads to the best dynamic behavior among the examined control modes.

4.4.7 Impact of System Granularity

This section emphasises the effect of the system's granularity and further evaluates the proposed control when employed for resources connected to the distribution level. To this aim, a more detailed modeling of the distribution network and loads is considered. In particular, each of the SMs at buses 32-38 and loads at neighbor buses is substituted with the 8-bus, 38 kV distribution system shown in Figure 4.9 [78] (note that, for illustration, in Figure 4.9, only one distribution network is shown). As a byproduct, the instantaneous

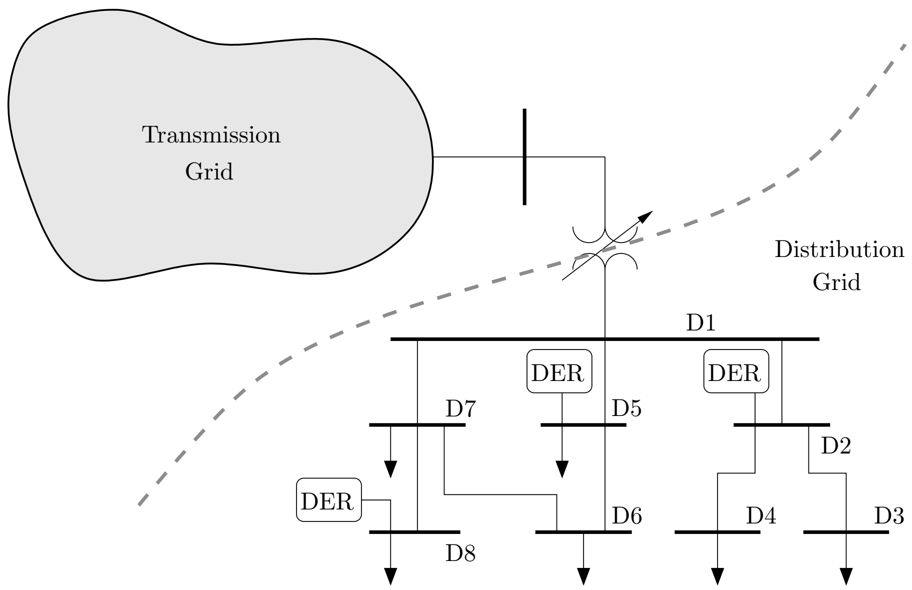

Figure 4.9: Topology of distribution network model used in Section 4.4.7.

power generation by DERs is increased to 70%. The behavior of loads in this example is represented using the dynamic load model proposed in [38]. Moreover, to account for the proximity of loads, for potential imbalances, as well as for possible harmonics of the power converters, noise has been added on the voltage angle at every bus of the distribution network. Noise is modeled as an Ornstein-Uhlenbeck's process with Gaussian distribution [62].

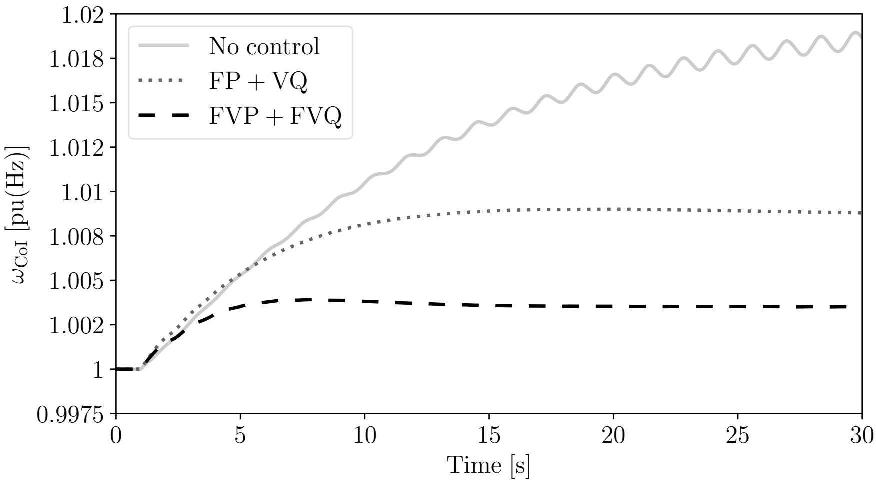

(a) CoI frequency.

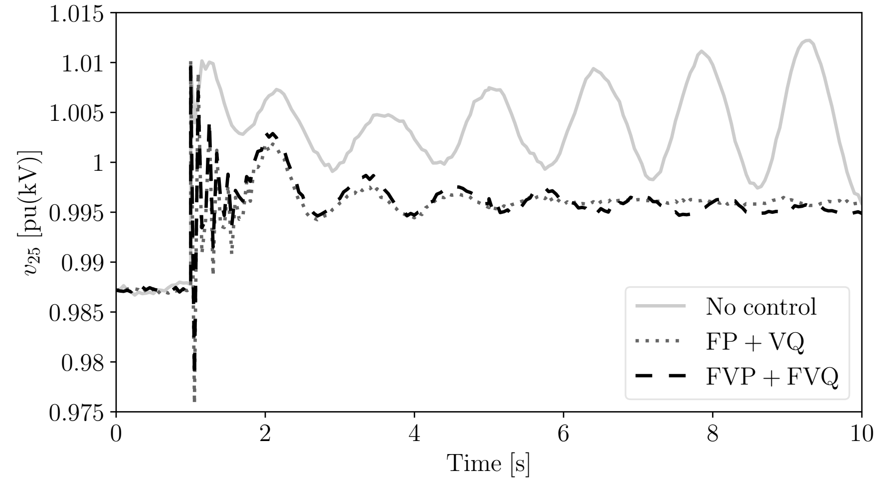

(b) Voltage at bus 25.

Figure 4.10: Transient response after disconnection of load at bus 3.

A time domain simulation is carried out, considering the disconnection of the load at bus 3 at $t = 1$ s. A comparison of the FP+VQ and FVP+FVQ modes is presented in Figure 4.10, which indicates that FVP+FVQ leads to an overall better dynamic behavior. Note that the proposed control is in general expected to be more effective and thus lead to larger improvement of the system's response, the higher is the coupling between the active and reactive power flows, i.e. at lower voltage levels and distribution network applications. This is confirmed by Figure 4.10, when compared to results discussed in previous sections of this case study, for example with Figure 4.5.

4.5 Conclusions

This chapter presents a control scheme to improve power system stability through the active and reactive control channels of power electronic converter-based DERs. This scheme is a combined controller in which both active and reactive power injections are modified to compensate both for frequency and voltage variations.

The controller is evaluated in terms of local voltage variations and system CoI frequency dynamic response, as well as in terms of a properly defined joint voltage/frequency response metric. In particular, the proposed metric complements and completes the information provided by the conventional frequency and voltage deviation metrics. Time domain simulations are carried out considering the effects of load voltage sensitivity, resistance of network lines, and level of DER penetration, and results indicate that, overall, the proposed scheme outperforms other possible active/reactive power control modes and provides a significant improvement to the dynamic response of the system.

Chapter 5

Inertia and Fast Frequency Control Estimation of Virtual Power Plants

A VPP aggregates the capacities of several devices, e.g. DERs, ESSs and dispatchable loads, which are controlled to operate like one grid-connected generator [90]. The devices that compose a VPP are typically connected to the grid through power converters and thus, in contrast to SMs, they do not provide mechanical inertia to the system. However, these devices can be designed to emulate the inertial response of SMs, as well as to regulate the frequency, thus enhancing the system's overall stability and performance. How to estimate on-line and accurately the equivalent inertia and the equivalent FFR of a VPP is the topic discussed in this chapter.

5.1 Introduction

In a conventional power system, inertia is naturally provided by SMs, as a consequence of the kinetic energy stored in the masses of their rotors. The rotational inertia of SMs plays a crucial role in maintaining the frequency during the first instants that follow the occurrence of a contingency or of a large power imbalance in the network. However, this inertia is reducing as a result of the gradual substitution of SMs by non-synchronous devices. In general, systems with lower inertia show larger frequency and Rate of Change of Frequency (RoCoF) variations and hence are more prone to instability and blackouts [65]. Hence, during the last decade there has been a growing interest on the stability and control of low-inertia systems as well as on establishing methods to estimate the system's inertia in a precise and fast way [11, 34, 110]. With this regard, measurement-based methods have been proposed in the literature for both off-line [11,34] and on-line [109,110] estimation of the available mechanical inertia at a given time. If properly controlled, non-synchronous devices can provide inertial response and frequency regulation services that are similar to the ones provided by SMs. Recent studies propose control schemes that tackle this problem, with some of them focusing on the coordination of devices that comprise VPPs, see [17, 55, 57, 90, 125].

Non-synchronous devices do not provide mechanical inertia to the system. In contrast, the inertial response of non-synchronous devices results from control and is not generally based on actual rotational inertia. It is thus relevant to evaluate how this control compares with rotational inertia. In this vein, [67] presents a formula to estimate, in transient conditions, the equivalent inertia of both synchronous and non-synchronous devices. Based on [67], the authors in [51] propose an inertia estimator with improved numerical stability and provide, as a byproduct, a formula to track the FFR droop gain of non-synchronous devices.

The estimators presented in [67] and [51] track the inertia of a single device connected to a bus of the network and under the assumption that the device's internal reactance is known. However, a VPP typically consists of many resources that are dispersed in multiple buses of the network and thus, defining the total equivalent reactance of a VPP is not straightforward. In this vein, a technique to estimate the equivalent internal reactance and then the inertia of a VPP is proposed in [123]. The method in [123] imposes for the estimation a simplified SM model without damping which does not allow an estimation of the equivalent FFR droop gain of the VPP [124].

The remainder of the chapter is organized as follows. Section 5.2 briefly provides the theoretical background behind our approach to inertia estimation in this chapter. Section 5.3 reviews the inertia estimation method developed in [51] and extends it to formulate the proposed equivalent inertia and FFR droop gain estimation for VPPs. Section 5.4 presents a case study based on the WSCC 9-bus system. Finally, conclusions are drawn in Section 5.5.

5.2 Background

The starting point of the theoretical background is the well-known power flow equations. The concepts described in this section are utilized in Section 5.3.2 for the estimation of the VPP equivalent inertia and FFR droop gain. The expressions of the complex power injections at a network with n buses, namely $\bar{\boldsymbol{S}}$, the h-th element-wise notations of $\bar{\boldsymbol{S}}$, namely P_h, Q_h and their differentiation, namely dp_h, dq_h, are given in Chapter 4 but are reported here for clarity:

$$
\begin{aligned}
\bar{\boldsymbol{S}}(t) &= \boldsymbol{P}(t) + \jmath\boldsymbol{Q}(t) = \bar{\boldsymbol{v}}(t) \circ \left(\bar{\mathbf{Y}}\,\bar{\boldsymbol{v}}(t)\right)^* , \\
P_h &= \sum_{k=1}^{n} v_h v_k \big(G_{h,k}\cos\theta_{h,k} + B_{h,k}\sin\theta_{h,k}\big) , \\
Q_h &= \sum_{k=1}^{n} v_h v_k \big(G_{h,k}\sin\theta_{h,k} - B_{h,k}\cos\theta_{h,k}\big) , \\
dp_h &= \sum_{k=1}^{n} \frac{\partial p_h}{\partial \theta_{h,k}} d\theta_{h,k} + \sum_{k}^{n} \frac{\partial p_h}{\partial v_k} dv_k \equiv dp'_h + dp''_h , \\
dq_h &= \sum_{k=1}^{n} \frac{\partial q_h}{\partial \theta_{h,k}} d\theta_{h,k} + \sum_{k=1}^{n} \frac{\partial q_h}{\partial v_k} dv_k \equiv dq'_h + dq''_h .
\end{aligned}
\tag{5.1}
$$

Based on the *complex frequency* concept presented in [63], and using a matrix form, the quotas dp'_h, dq''_h (denoted in matrix form as $\dot{\boldsymbol{p}}'$, $\dot{\boldsymbol{q}}''$) can be approximately expressed as:

$$\dot{\boldsymbol{p}}' \approx \boldsymbol{B}'\boldsymbol{\omega} , \tag{5.2}$$

$$\dot{\boldsymbol{q}}'' \approx \boldsymbol{B}''\boldsymbol{\varrho} , \tag{5.3}$$

where $B'_{h,k} = -B_{h,k}$, $B'_{h,h} = \sum_{h\neq k}^{n} B_{h,k}$ are the elements of $\boldsymbol{B}'$ and $B''_{h,k} = -B_{h,k}$, $B''_{h,h} = -2B_{h,h}$ are the elements of $\boldsymbol{B}''$; $\boldsymbol{\omega}$ is the vector of bus frequencies; and the vector $\boldsymbol{\varrho} \equiv \dot{\boldsymbol{v}}/\boldsymbol{v}$ represents the transient rate of change of the bus voltages normalized with respect to their magnitude.

Equations (5.2) and (5.3) exploit the fact that dp'_h is the component of the active power that can effectively modify the frequency in the grid, whereas the impact of dp''_h on the frequency is negligible. Similarly, dq''_h is the component of the reactive power that varies the most when the voltage at bus h is regulated, whereas the contribution of dq'_h

to the voltage regulation is negligible. Equations (5.2) and (5.3) are duly utilized in the next section for the inertia and FFR droop gain estimation of VPPs.

5.3 Inertia and Fast Frequency Response Gain Estimation

In this section, the method developed in [51] is firstly recalled for the inertia estimation of a single device connected to a bus of a power network. Then the descriptions of the proposed equivalent inertia and FFR droop gain estimator for VPPs are provided.

5.3.1 Inertia Estimation of Synchronous Machines

The effect of the inertia constant M_{G} of a SM on its dynamics is described through the swing equation:

$$M_{\mathrm{G}}\dot{\omega}_{\mathrm{G}} = p_{\mathrm{m}} - p_{\mathrm{G}} - D_{\mathrm{G}}(\omega_{\mathrm{G}} - \omega_o)\,, \tag{5.4}$$

where ω_o is the SM's rated rotor speed; ω_{G} is the SM's rotor speed and $\dot{\omega}_{\mathrm{G}}$ its time derivative; p_{m} is the mechanical power provided by the turbine; p_{G} is the electrical power that the SM injects to the grid; and D_{G} is the damping coefficient.

The mechanical power, p_{m}, can be decomposed into the following three terms:

$$p_{\mathrm{m}} = p_{\mathrm{PFC}} + p_{\mathrm{SFC}} + p_{\mathrm{UC}}\,, \tag{5.5}$$

where p_{PFC} is the active power regulated by the PFC; p_{SFC} is the active power regulated by the SFC; and p_{UC} is the power set point determined by solving the Unit Commitment (UC) problem. The PFC and SFC for a SM are typically achieved through the TG and AGC, respectively.

Merging (5.4) and (5.5) and differentiating with respect to time:

$$M_{\mathrm{G}}\ddot{\omega}_{\mathrm{G}} = \dot{p}_{\mathrm{PFC}} + \dot{p}_{\mathrm{SFC}} + \dot{p}_{\mathrm{UC}} - \dot{p}_{\mathrm{G}} - D_{\mathrm{G}}\dot{\omega}_{\mathrm{G}}\,. \tag{5.6}$$

Considering the time scale of inertial response of the SM, in the very first instants after a contingency, one can assume that $\dot{p}_{\mathrm{UC}} \approx 0$, $\dot{p}_{\mathrm{SFC}} \approx 0$, and $|\dot{p}_{\mathrm{PFC}}| \ll |\dot{p}_{\mathrm{G}}|$. Then, one has:

$$M_{\mathrm{G}} \approx -\frac{\dot{p}_{\mathrm{G}} + D_{\mathrm{G}}\dot{\omega}_{\mathrm{G}}}{\ddot{\omega}_{\mathrm{G}}} \,. \tag{5.7}$$

Note that when $\ddot{\omega}_{\mathrm{G}}$ crosses zero following a contingency, a singularity occurs in (5.7). This singularity can be avoided if, instead of (5.7), the following equation is used to compute M_{G}:

$$T_M \dot{M}_{\mathrm{G}} = \gamma\big(\ddot{\omega}_{\mathrm{G}}\big)\big(\dot{p}_{\mathrm{G}} + M_{\mathrm{G}}\ddot{\omega}_{\mathrm{G}} + D_{\mathrm{G}}\dot{\omega}_{\mathrm{G}}\big) \,, \tag{5.8}$$

while the following equation allows estimating D_{G} [51]:

$$T_D \dot{D}_{\mathrm{G}} = \gamma\big(\Delta\omega_{\mathrm{G}}\big)\big(\Delta p_{\mathrm{G}} + M_{\mathrm{G}}\dot{\omega}_{\mathrm{G}} + D_{\mathrm{G}}\Delta\omega_{\mathrm{G}}\big) \,, \tag{5.9}$$

where

$$\Delta\omega_{\mathrm{G}} = \int \dot{\omega}_{\mathrm{G}} dt \,, \quad \Delta p_{\mathrm{G}} = \int \dot{p}_{\mathrm{G}} dt \,, \tag{5.10}$$

and $\gamma(y)$ is defined as:

$$\gamma(y) = \begin{cases} -1 \,, & y \geq \epsilon_y \,, \\ 0 \,, & -\epsilon_y < y < \epsilon_y \,, \\ 1 \,, & y \leq -\epsilon_y \,, \end{cases} \tag{5.11}$$

where ϵ_y is a small positive threshold that helps reduce the impact of noise and improve the accuracy of $\gamma(y)$. A good choice for ϵ_y is in the range $[10^{-7}, 10^{-5}]$.

The term $\dot{p}_{\mathrm{G}} + M_{\mathrm{G}}\ddot{\omega}_{\mathrm{G}} + D_{\mathrm{G}}\dot{\omega}_{\mathrm{G}}$ is zero at the equilibrium and non-zero during transients. Consider an example for which $\dot{p}_{\mathrm{G}} + M_{\mathrm{G}}\ddot{\omega}_{\mathrm{G}} + D_{\mathrm{G}}\dot{\omega}_{\mathrm{G}} > 0$. The sign of $\ddot{\omega}_{\mathrm{G}}$ decides the sign of $\gamma(\ddot{\omega}_{\mathrm{G}})$. If $\ddot{\omega}_{\mathrm{G}} > 0$, M_{G} has to decrease, to also reduce $\dot{p}_{\mathrm{G}} + M_{\mathrm{G}}\ddot{\omega}_{\mathrm{G}} + D_{\mathrm{G}}\dot{\omega}_{\mathrm{G}}$ and converge to the equilibrium. In this case, $\dot{M}_{\mathrm{G}} < 0$ and thus $\gamma(\ddot{\omega}_{\mathrm{G}}) = -1$. Vice versa, if $\ddot{\omega}_{\mathrm{G}} < 0$, M_{G} has to increase and thus $\gamma(\ddot{\omega}_{\mathrm{G}}) = 1$. The rate of change of M_{G} is defined by the time constant T_M. A small T_M tracks M_{G} faster, although it might generate numerical oscillations. Hence, T_M, T_D are considered in the time scale of the inertial response, i.e. $T_M, T_D \in [10^{-3}, 10^{-2}]$ s. The rationale behind (5.9) can be described in a similar way.

5.3.2 Proposed VPP Inertia Estimation

The expressions (5.8) and (5.9) can be extended to any non-synchronous device that is controlled to provide a similar dynamic response with a SM in the inertial response time scale. For a non-synchronous device, one has [51]:

$$\begin{aligned} T_M \dot{M}_{\mathrm{D},h} &= \gamma\big(\ddot{\omega}_{\mathrm{D},h}\big)\big(\dot{p}'_h + M_{\mathrm{D},h}\ddot{\omega}_{\mathrm{D},h} + D_{\mathrm{D},h}\dot{\omega}_{\mathrm{D},h}\big)\,, \\ T_D \dot{D}_{\mathrm{D},h} &= \gamma\big(\Delta\omega_{\mathrm{D},h}\big)\big(\Delta p'_h + M_{\mathrm{D},h}\dot{\omega}_{\mathrm{D},h} + D_{\mathrm{D},h}\Delta\omega_{\mathrm{D},h}\big)\,, \end{aligned} \tag{5.12}$$

where the index $_{\mathrm{D},h}$ represents the device connected to bus h; and $\dot{p}'_h$ is the derivative of the quota of the active power that varies the frequency at bus h (see also Section 5.2). The presence of $D_{\mathrm{D},h}$ in (5.12) can enhance the accuracy of the estimator while being meaningful, since it can be understood as the equivalent droop gain of the FFR that the device provides [51]. The internal frequency of the device $\omega_{\mathrm{D},h}$ is obtained based on (5.2):

$$\omega_{\mathrm{D},h} = \Delta\omega_h - x_{\mathrm{D},h}\dot{p}'_h\,, \tag{5.13}$$

where $\Delta\omega_h$ is the frequency deviation at bus h; and $x_{\mathrm{D},h}$ is the equivalent internal reactance of the device.

A poor choice of $x_{\mathrm{D},h}$ in (5.13) can significantly affect the accuracy of (5.12). Most importantly, how to define the equivalent reactance of a VPP is not straightforward, since VPPs aggregate several resources that span multiple buses and thus they may have significant complexity and granularity. In the remainder of this section, a technique is developed to estimate $x_{\mathrm{D},h}$ based on the voltage and reactive power variations at the point of connection with the rest of the grid [123].

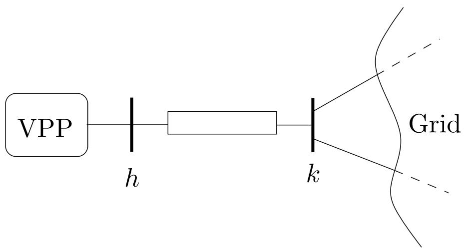

Figure 5.1: VPP connected in antenna to the grid.

Assume that a subnetwork comprising possibly several devices (e.g. a VPP) is connected to bus h of the network. An example is shown in Figure 5.1, where a VPP is connected in antenna to the grid. Applying (5.3) to bus h, we have:

$$\dot{q}''_h \approx B''_h \varrho_h + \sum_{k=1}^{n} B''_{h,k}\varrho_k\,, \tag{5.14}$$

where ϱ_h, is the h-th element of $\boldsymbol{\varrho}$. In this chapter, a low-pass filter is applied to ϱ_h to reduce the reactive power fluctuations and noise. B''_h can be obtained from:

$$B''_h = B''_{\mathrm{D},h} + B''_{h,h} + \sum_{k=1}^{n} B''_{h,k} \,, \tag{5.15}$$

where $B''_{\mathrm{D},h}$ is the equivalent internal susceptance of the device at bus h. From (5.14), (5.15), one has:

$$B''_{\mathrm{D},h} = \frac{\dot{q}''_h - \sum_{k=1}^{n} B''_{h,k}\varrho_k}{\varrho_h} - \sum_{k=1}^{n} B''_{h,k} - B''_{h,h} \,. \tag{5.16}$$

The equivalent reactance $x_{\mathrm{D},h}$ can be obtained from the reciprocal of $B_{\mathrm{D},h}$, as follows:

$$x_{\mathrm{D},h} = \frac{\varrho_h}{\alpha} \,, \tag{5.17}$$

where

$$\alpha = \dot{q}''_h - \sum_{k=1}^{n} B''_{h,k}\varrho_k - \left(\sum_{k=1}^{n} B''_{h,k} + B''_{h,h} \right) \varrho_h \,. \tag{5.18}$$

Equation (5.17) suffers from the same numerical issue as (5.7). To overcome the problem, $x_{\mathrm{D},h}$ is processed with the following differential equation:

$$T_x \dot{x}_{\mathrm{D},h} = \gamma\big(\alpha\big)\big(x_{\mathrm{D},h}\alpha - \varrho_h\big) \,, \tag{5.19}$$

where $\gamma(\alpha)$ is defined by (5.11), and $T_x \in [10^{-2}, 10^{-1}]$ s.

The equivalent inertia $M_{\mathrm{D},h}$, FFR droop gain $D_{\mathrm{D},h}$ and the equivalent reactance $x_{\mathrm{D},h}$, of the VPP, can finally be estimated through the set of equations (5.11)-(5.13) and

(5.18)-(5.19), as follows:

$$
\begin{aligned}
T_M \dot{M}_{\mathrm{D},h} &= \gamma\big(\ddot{\omega}_{\mathrm{D},h}\big)\big(\dot{p}'_h + M_{\mathrm{D},h}\ddot{\omega}_{\mathrm{D},h} + D_{\mathrm{D},h}\dot{\omega}_{\mathrm{D},h}\big)\,, \\
T_D \dot{D}_{\mathrm{D},h} &= \gamma\big(\Delta\omega_{\mathrm{D},h}\big)\big(\Delta p'_h + M_{\mathrm{D},h}\dot{\omega}_{\mathrm{D},h} + D_{\mathrm{D},h}\Delta\omega_{\mathrm{D},h}\big)\,, \\
\omega_{\mathrm{D},h} &= \Delta\omega_h - x_{\mathrm{D},h}\dot{p}'_h\,, \\
T_x \dot{x}_{\mathrm{D},h} &= \gamma\big(\alpha\big)\big(x_{\mathrm{D},h}\alpha - \varrho_h\big)\,, \\
\alpha &= \dot{q}''_h - \sum_{k=1}^{n} B''_{h,k}\varrho_k - \left(\sum_{k=1}^{n} B''_{h,k} + B''_{h,h}\right)\varrho_h\,, \\
\gamma(y) &= \begin{cases} -1\,, & y \geq \epsilon_y\,, \\ 0\,, & -\epsilon_y < y < \epsilon_y\,, \\ 1\,, & y \leq -\epsilon_y\,. \end{cases}
\end{aligned}
\tag{5.20}
$$

The real-time loop for the proposed inertia and FFR droop gain estimator based on (5.20) is shown in Figure 5.2.

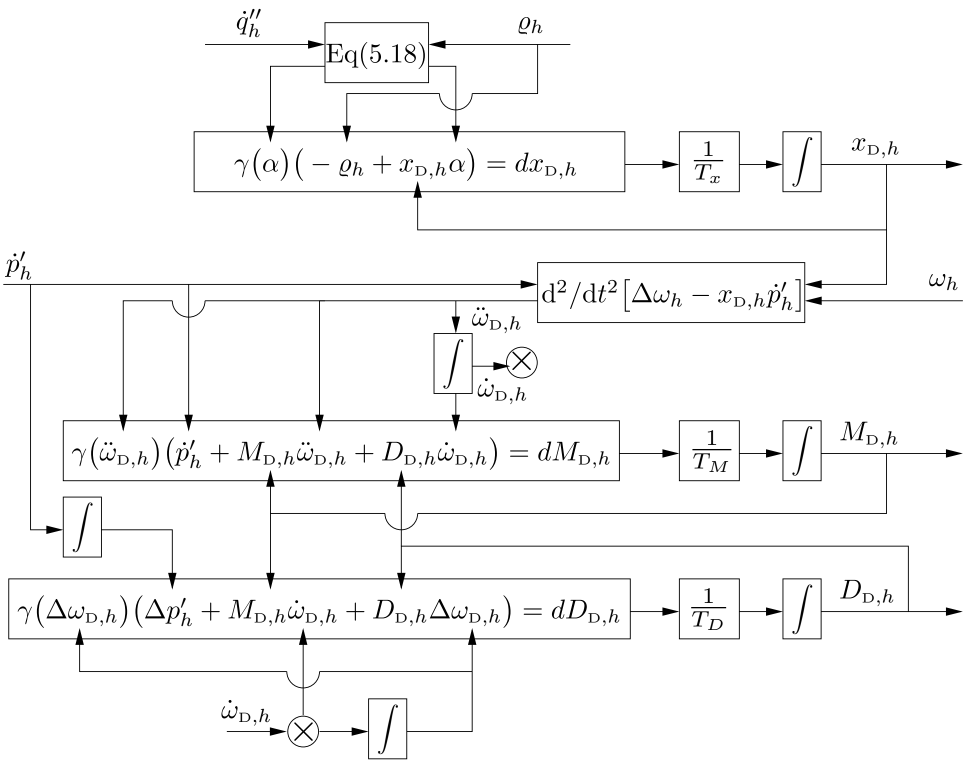

Figure 5.2: Real-time loop for the proposed inertia and FFR droop gain estimator.

5.4 Case Study

This section investigates the performance and accuracy of the proposed real-time inertia and FFR droop gain estimation technique, through simulations conducted on the well-known WSCC 9-bus system [94]. The single-line diagram and description of the test system is given in Appendix D. A SVC is also installed at bus 8 of the system. The accuracy of the estimator is first checked for SMs, and then applied to a DER and a VPP.

Loads are modeled using the same ZIP model that is utilized in Chapter 4, where the active and reactive power consumption, say $P_{\mathrm{L},h}$, $Q_{\mathrm{L},h}$, are quadratic expressions of the bus voltage [59]. Bus frequency estimations in this study are obtained using a PLL. In particular, SRF-PLL, which is one of the simplest and most commonly utilized schemes, are employed in the case study [32]. The single-line diagram and description of SRF-PLL is given in Appendix D. The parameters of the SRF-PLL and of the inertia estimator are listed in Table 5.1.

Table 5.1: PLL and estimator parameters.

Device	Parameters
SRF-PLL	$K_{\mathrm{p}} = 0.2$, $K_{\mathrm{i}} = 0.01$
Estimator	$T_q = 0.05$ s, $T_\varrho = 0.001$ s,
	$T_x = 0.01$ s, $T_M = 0.004$ s,
	$T_D = 0.001$ s

5.4.1 Single Synchronous Machine

This section provides a validation of the accuracy of the proposed method in estimating the inertia of a single SM, in particular of the machine connected to bus 2 of the WSCC 9-bus system (denoted as G2). The actual mechanical starting time and damping of G2 are $M_{\mathrm{G2}} = 12.8$ s and $D_{\mathrm{G2}} = 2.0$, respectively.

A time domain simulation of the system is carried out twice, considering a 20% variation of the load connected to bus 6 at $t = 1$ s. In the first simulation the load is decreased and in the second increased. Figure 5.3a shows how the estimated inertia compares to the actual mechanical starting time of G2. The proposed estimator can accurately capture the inertia of the SM. Note that the inertia estimator is initialized to zero, and thus the first 1-2 s following the disturbance basically represents the training period of the estimator. In the plots, the training period of the estimator is shaded. The values of the estimated quantities in the shaded regions have no physical meaning and have to be discarded. Moreover, the estimated equivalent reactance x_{G2} of G2 obtained with the proposed method is shown in Figure 5.3b, which indicates that the variation of the load has an impact on the estimation of x_{G2}. This in turn, slightly impacts on the final estimation of M_{G2}.

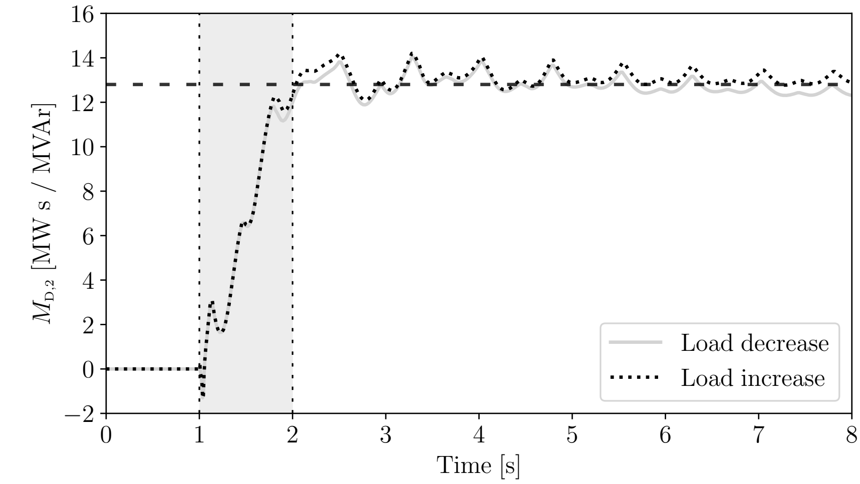

(a) Estimated inertia for G2.

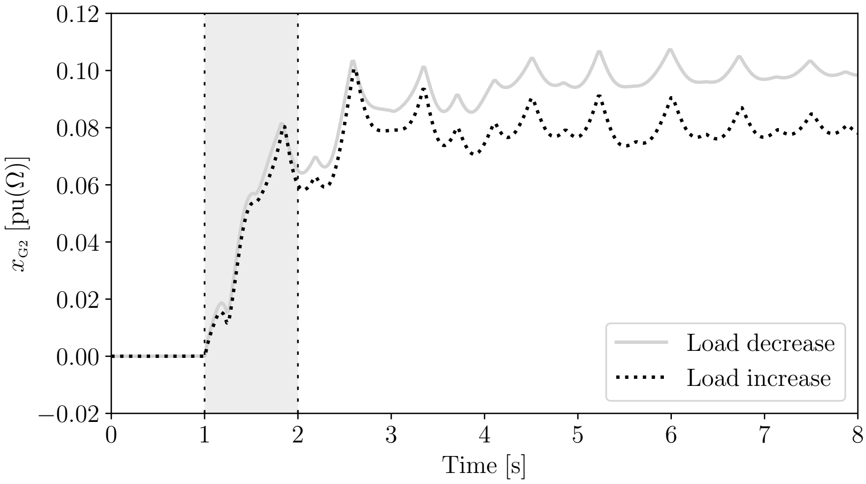

(b) Estimated reactance for G2.

Figure 5.3: 20% variation of load connected to bus 6.

For completeness, it is necessary to mention that for a single SM, the estimator in [51] is slightly more accurate than the one proposed in this chapter. This result is to be expected as proposed method involves the estimation of two quantities, x_{G2} and M_{G2}, where the estimation of M_{G2} depends on that of x_{G2}. In [51], instead, the value of x_{G2}

is assigned and assumed to be known accurately. On the other hand, if the value of x_{G2} is not correct, the method presented in [51] returns estimations with a systematic bias. The method proposed in this work is free from this potential bias as illustrated in Section 5.4.1.

Figure 5.4a shows how the proposed estimator compares to the estimator presented in [123]. Note that [123] adopts a simplified expression of (5.12), as follows:

$$T_M \dot{M}_{\mathrm{D},h} = \gamma\big(\ddot{\omega}_{\mathrm{D},h}\big)\big(\dot{p}'_h + M_{\mathrm{D},h}\ddot{\omega}_{\mathrm{D},h}\big)\,. \tag{5.21}$$

Simulation results indicate that including the damping in the SM model imposed for the estimation leads to more accurate results. Moreover, the damping estimation requires more training time than the inertia, since $\Delta\omega_{\mathrm{G}}$ varies more slowly than $\ddot{\omega}_{\mathrm{G}}$ in the first instants after the contingency (see (5.8), (5.9)).

Figure 5.4b shows that, if the SMs of the system are assumed not to have TGs, the estimator closely tracks the damping coefficient of G2. If TGs are included, the estimator captures the combined effect of the SM's damping plus the droop gain of the PFC. Note that lower TG droop constants R_{TG} lead to higher slopes in the estimated value.

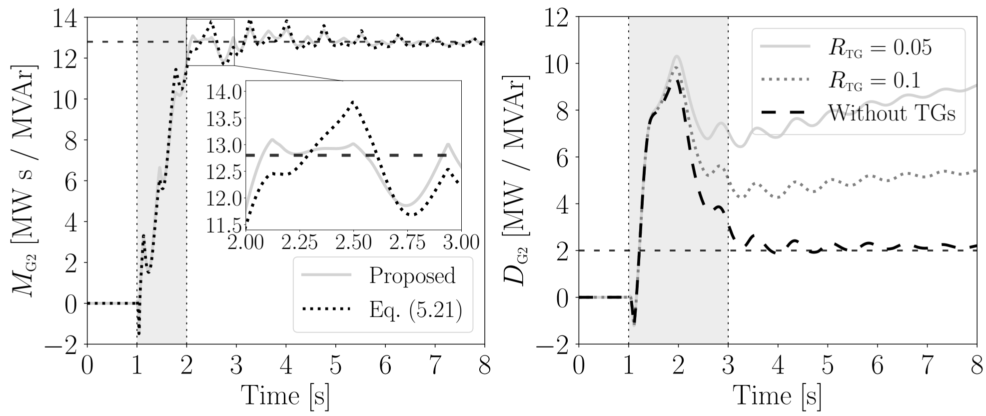

(a) Estimated inertia for G2. (b) Estimated damping for G2.

Figure 5.4: 20% increase of load connected to bus 6 at $t = 1$ s.

Next, the impact of load models and TGs on the accuracy of the proposed estimator is studied. In particular, the estimation using the ZIP load model is compared to the estimation when loads are represented using constant power (denoted as Constant PQ) and constant impedance (denoted as Constant Z) models. For each of these scenarios, two cases are assumed: (i) all machines are equipped with TGs; and (ii) no machine is

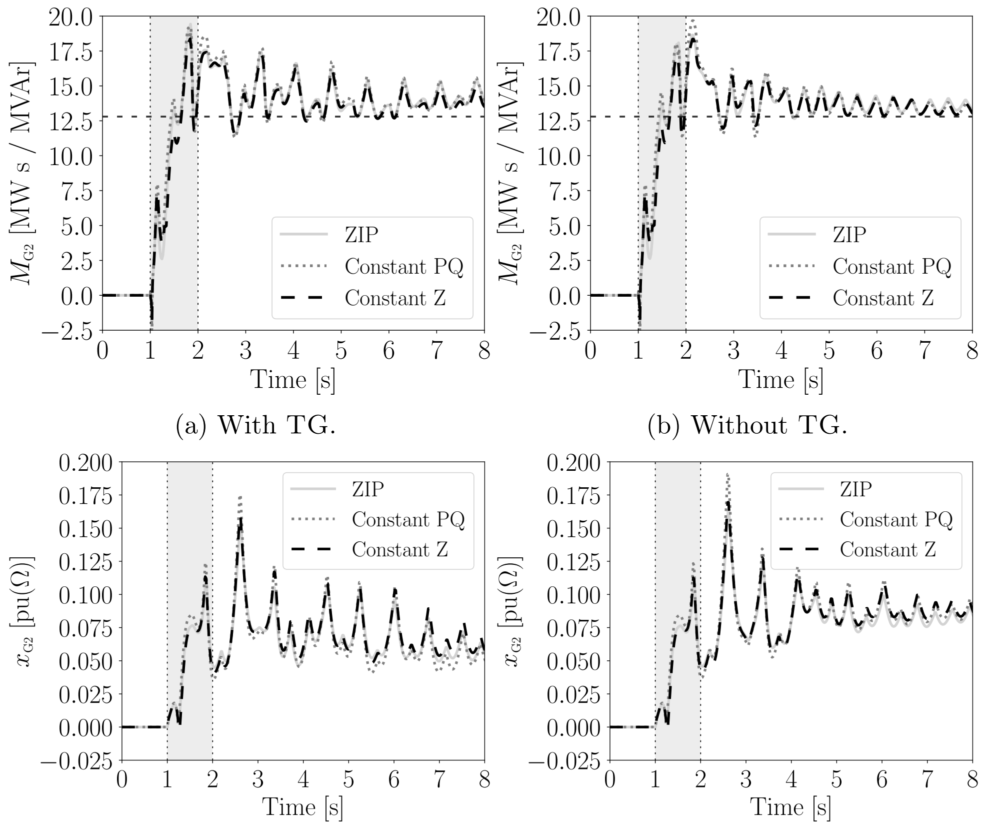

(a) With TG. (b) Without TG.

(c) With TG. (d) Without TG.

Figure 5.5: 50% increase of load connected to bus 6. Impact of load model and TGs.

equipped with a TGs. The latter case is not realistic but it is considered for illustration purposes.

The disturbance consists in a 50% increase of the load connected to bus 6, occurring at $t = 1$ s. Simulation results are shown in Figure 5.5. This figure shows that the inclusion of the PFC leads to a small increase of the deviation from the exact value of the inertia. This effect is stronger the larger is the power imbalance in the system, which is to be expected, due to the overlap in the time scales of the inertial response and the PFC. Regarding the effect on the estimation of load models is in general negligible, with constant power loads having the most significant impact among the examined models.

5.4.2 Subnetwork with Multiple Machines

This section evaluates the proposed inertia estimation for multiple SMs. The original SM connected to bus 2 in WSCC 9-bus system is substituted by a subnetwork with the same power injection. The subnetwork consists of two SMs in parallel with total starting time and damping of 18.82 s and 4.0, and one ZIP load with $P_{L,2,o} = 0.3$ pu, $Q_{L,2,o} = 0.1$ pu.

The examined contingency is the increase by 20% of the load connected to bus 8 at $t = 1$ s. The accuracy of the proposed inertia estimation method is compared to the method proposed in [51] and results are presented in Figure 5.6. Figure 5.6a indicates that the proposed estimator can accurately track the inertia of the SMs in the subnetwork.

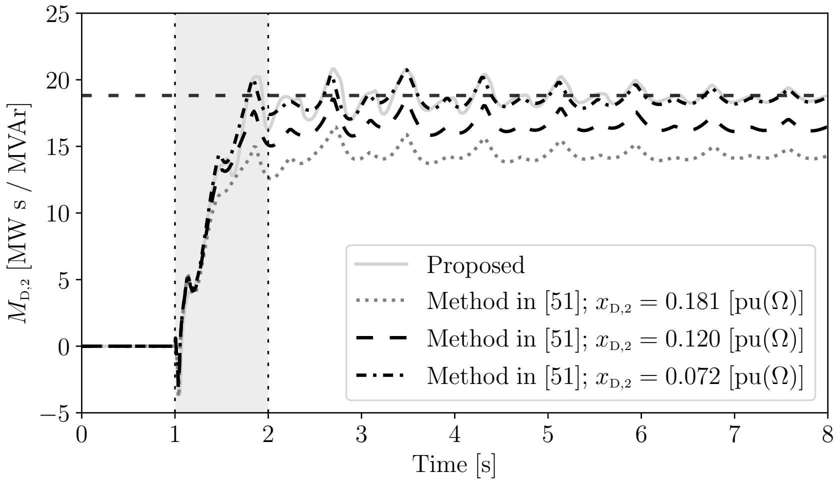

(a) Estimated inertia of subnetwork.

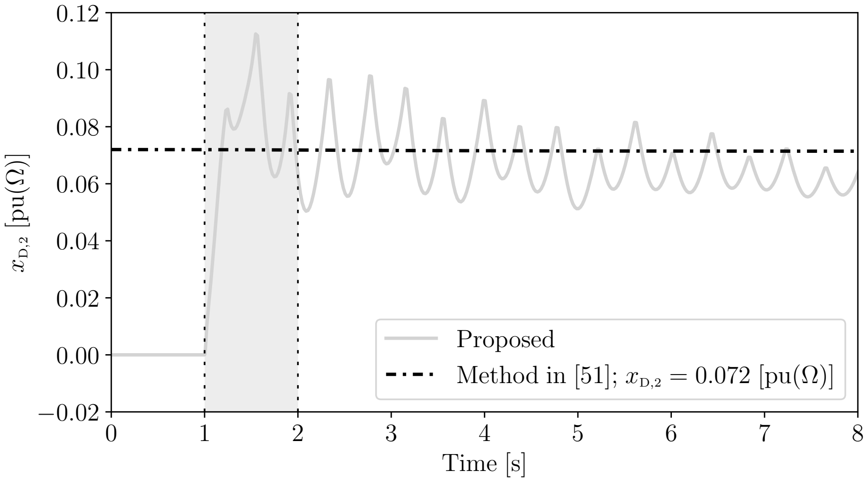

(b) Estimated internal reactance of subnetwork.

Figure 5.6: 20% increase of load connected to bus 8.

The method in [51] requires, for the estimation of the inertia, to assign a value to the equivalent internal reactance of the subnetwork. Apparently, for the simple topology examined in this example, i.e. two SMs in parallel, a proper selection of $x_{D,2}$ is simply the parallel of the transient reactances of the two machines, which yields $x_{D,2} = 0.07$ pu. However, for more complex topologies, comprising several nodes and devices of varying complexity, the selection is not straightforward. Figure 5.6 shows the effect on the estimator in [51] of choosing different values for the equivalent reactance. In particular, apart from $x_{D,2} = 0.07$ pu, two more values are assumed, i.e. the internal reactance is set equal to the transient reactance of each of the SMs in the subnetwork, which gives $x_{D,2} = 0.12$ pu and $x_{D,2} = 0.18$ pu. Results indicate that an improper selection of $x_{D,2}$ has a significant impact on the accuracy of the inertia estimation. The estimation of the equivalent reactance provided by the proposed method is shown in Figure 5.6b.

The estimated inertia and damping of the subnetwork are shown in Figure 5.7. As expected, the estimator can accurately track both the inertia and damping of the SMs. Moreover, as expected, inclusion of the PFC impacts more on the damping than on the inertia estimation.

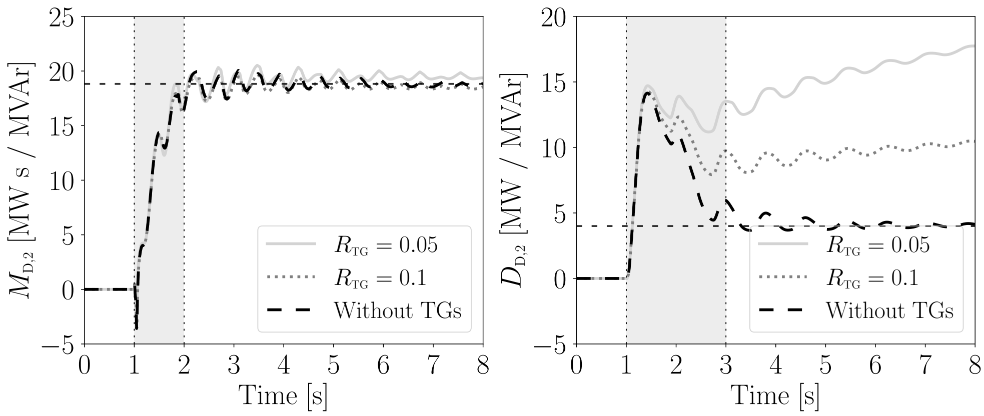

(a) Estimated inertia of D, 2. (b) Estimated Damping of D, 2.

Figure 5.7: 20% increase of load connected to bus 8 at $t = 1$ s.

5.4.3 Non-Synchronous Device

This section evaluates the accuracy of the proposed estimator when applied to non-synchronous device. To this aim, a 45 MW DER (denoted as D, 6) is connected to bus 6 of the WSCC 9-bus system, which has the ability to provide frequency control. The DER frequency control is implemented as the parallel of a droop and a RoCoF control channel. At $t = 1$ s, a 20% increase of the load at bus 8 occurs. Figure 5.8 shows the estimated trajectories of the equivalent inertia and FFR gain of the DER, as obtained with and without the frequency control (denoted as FC_{DER}). When FC_{DER} is off, it is obtained that $M_{D,6} \approx 0$ s and $D_{D,6} \approx 0$, which is as expected. When the DER frequency control is active, it can be seen that both the estimated equivalent inertia and FFR droop gain are time-varying.

A relevant remark is that, in practice, the precision of the estimation is impacted by how much the frequency and active power vary in the time scale of interest. That is, faster and oscillatory variations of $\dot{p}'_h$ and ω_h lead to higher accuracy, whereas slower and smoother variations lead to lower accuracy in the estimation.

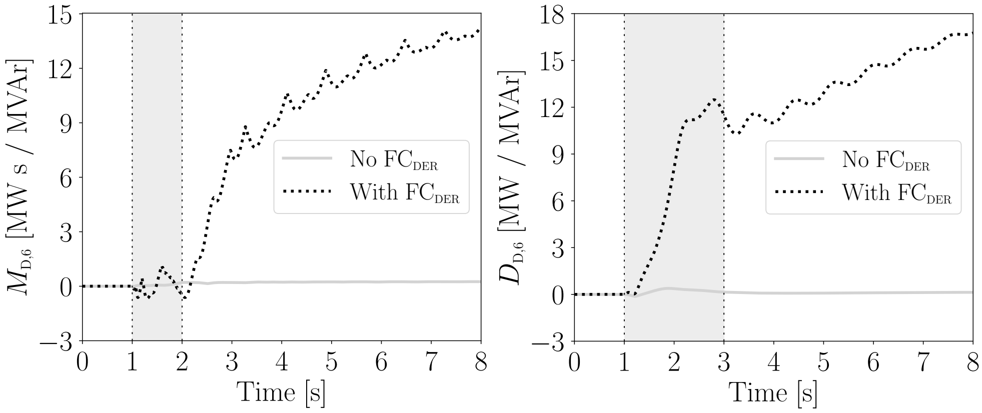

(a) Estimated DER inertia. (b) Estimated DER FFR droop gain.

Figure 5.8: 20% increase of load connected to bus 8 at $t = 1$ s.

5.4.4 Virtual Power Plant

In this section, the proposed method is applied for the estimation of the equivalent inertia provided by a VPP. To this aim, the load at bus 6 is replaced by a VPP. The single-line diagram and description of the modified test system is given in Appendix D. Stochastic fluctuations of wind speed in this study are modeled as an Ornstein-Uhlenbeck's process with Gaussian distribution [62]. A detailed description of the model of this process is provided in Appendix A.

In this scenario, 20% the load at bus 5 is decreased at $t = 1$ s. Four scenarios within the VPP are evaluated, (i) without ESS nor frequency control provided by the DERs; (ii) without ESS but with DER frequency control (FC_{DER}); (iii) with ESS but without FC_{DER}; and (iv) with both ESS and FC_{DER}.

The estimated VPP equivalent inertia, FFR gain, as well as the frequency at bus 6 following the disturbance, are depicted in Figure 5.9. Results indicate that the VPP has time-varying reactance and provides time-varying inertia and FFR to the system. The VPP without the ESS nor FC_{VPP} does not provide any inertia and FFR support to the system, which is consistent with the discussion of Figure 5.8 provided above. Moreover, the VPP with ESS and FC_{DER} can significantly enhance the frequency response of the

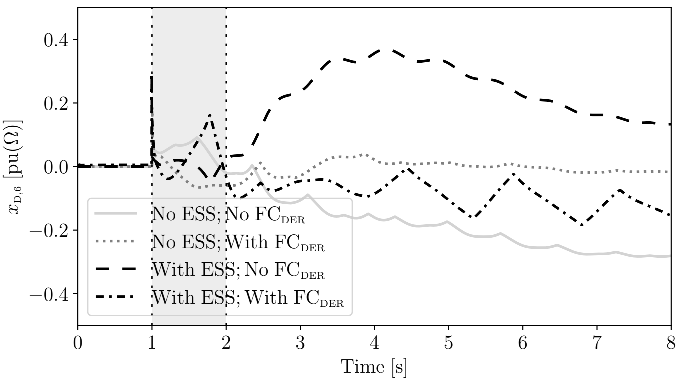

(a) Estimated reactance of VPP.

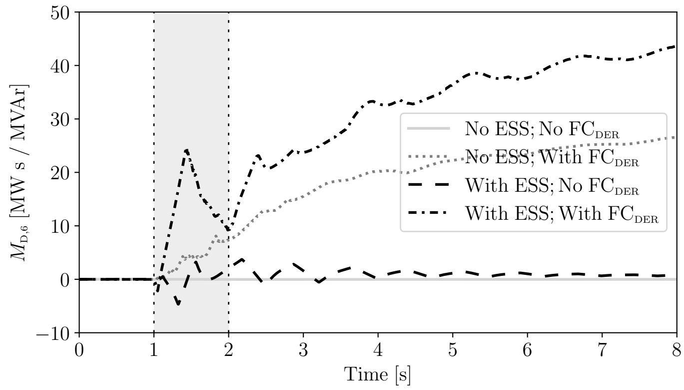

(b) Estimated inertia of VPP.

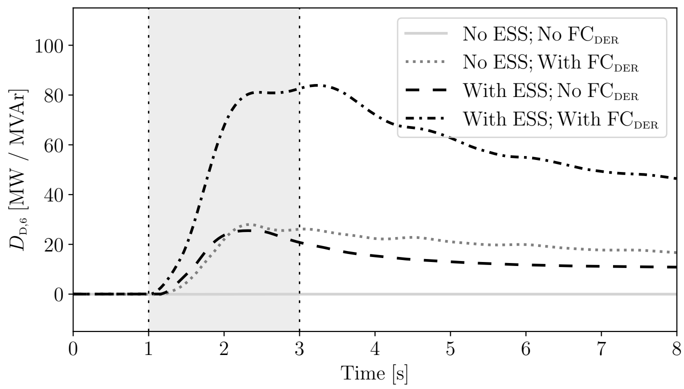

(c) Estimated FFR droop gain of VPP.

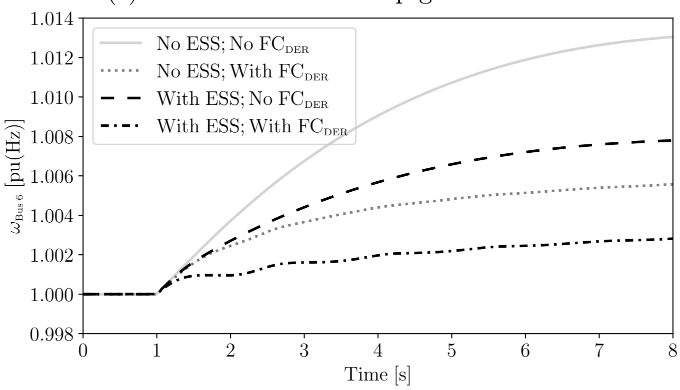

(d) Frequency at bus 6.

Figure 5.9: 20% decrease of load connected to bus 5 at $t = 1$ s.

VPP (see Figure 5.9d). Note that in the scenario that the VPP only utilizes the ESS for frequency regulation, it provides only a small equivalent inertia to the system (see Figure 5.9b). This is because the ESS reaches quickly its maximum power output and, thereon, it loses its capability to regulate the frequency.

5.5 Conclusions

This chapter proposes a method to estimate the equivalent inertia and FFR droop gain of a VPP. The method includes two steps. First, an estimation of the VPP's internal equivalent reactance is obtained, based on the voltage and power variations at the point of connection of the VPP with the grid. Then, the VPP's equivalent inertia is estimated, by considering for the estimation a classical synchronous machine model with inclusion of damping. The inclusion of damping in the estimator allows enhancing the accuracy of the estimation, while it provides, as a byproduct, an estimation of the VPP's equivalent FFR droop gain. Simulation results support the proposed estimator by validating its accuracy and suitability for VPP applications. It is relevant to note that the estimator's accuracy depends on proper choosing time constants, T_M, T_D, of the estimation transfer function. That is, the estimator might not be possible to observe the inertia and FFR droop gain if the inertia response is out of the conventional time scale.

Chapter 6

Conclusions and Future Work

This thesis proposes novel techniques for the coordinated frequency control of VPPs, combined voltage-frequency control of DERs, and inertia and fast frequency control estimation of VPPs. The objective of this chapter is to summarize the conclusions of the thesis and outline future work directions.

- *Coordinated* VPP *control*: The proposed coordinated control of VPPs aims at improving power system frequency response by means of, (i) coordinated ESS control; (ii) coordinated RES control. The performance of the coordinated VPP control approaches is discussed through time domain simulations and Monte Carlo simulations. Analytical results based on the modified WSCC 9-bus system illustrate that both of the control strategies above can significantly improve power system frequency stability. The proposed control approaches perform better than either conventional VPPs that do not regulate the frequency, i.e. utilize a constant power set-point, and VPPs that regulate the frequency through the independent controllers of ESSs and DERs. Moreover, communication delays have a more significant impact on the coordinated control approach of DERs than that on coordinated ESS. This problem can be addressed by utilizing a two-phase coordinated control, such as VPP control Mode 6 described in Chapter 3. In this operating mode, the ESS acts first whereas DERs are included in the coordinated control in a second phase. This reduces the impact of the limited capacity of the ESS and, in turn, improves the transient stability.

  Future work will focus on further improving the short-term frequency control of the DERs and ESSs included in a VPP. For example, *ad hoc* feedback transfer functions for each DER and ESS will be considered. Secondary frequency control of VPPs appears also a relevant topic, as its time scale requires to take into account the SoC of ESSs and short-term weather forecast.

- VPP *topology*: The study on VPP topology concludes that without proper control, DERs deteriorate the dynamic response of the grid, in particular, if they are distributed all over the transmission grid. Interestingly, the averaging effect of stochastic processes helps reducing the negative impact of DERs if they are located at the distribution and connected to the transmission system through a single point of common coupling. The TS-VPP with coordinated control of DERs and ESSs has, in general, a better performance than the DS-VPP. Moreover, the geographical scattering of the resources of the TS-VPP makes the TS-VPPs outperform the DS-VPPs with respect to the reduction of the dynamic impact of communication delays.

  A relevant extension of the work on VPP topology is the study of improving the coordinated control of DERs and ESSs to minimize the impact of noise and delays, as well as taking into account the risk of ICT loss. Apart from this, defining the minimum technical requirements that TS-VPPs and DS-VPPs have to satisfy in order to provide an adequate frequency containment support for the grid appears also an interesting extension of the present work.

- *Combined voltage-frequency control of* DER*s*: The contribution of this work is a systematic study of combined voltage-frequency control of power electronic converter-based DERs to enhance power system stability. A simple yet practical control scheme is proposed, in which both active and reactive power injections are modified to compensate both for frequency and voltage variations. Furthermore, a novel scalar metric that captures the combined effect of frequency/voltage response provided at a bus of the power network is developed. Time domain simulations are carried out considering the effects of load voltage sensitivity, resistance of network lines, and level of DER penetration, and results indicate that, overall, the proposed scheme outperforms other possible active/reactive power control modes and provides a significant improvement to the dynamic response of the system.

A possible future work direction is to evaluate the proposed control scheme using hardware-in-the-loop tests on the effect of different network topology and load models, as well as on the impact of switching between different control modes in transient conditions.

- *Inertia and fast frequency control estimation of* VPP*s*: This work proposes a method to estimate the equivalent inertia and FFR droop gain of a VPP. The specific contributions are twofold. First, the thesis provides a technique to estimate the internal equivalent reactance of any device connected to the grid, based on measurements of the reactive power and by using the concept of the *complex frequency* formula developed in [63]. Then, the estimated reactance is utilised for the estimation formula of the equivalent inertia and FFR droop gain of VPPs comprising a subnetwork and several distributed energy resources and loads.

  A next step that appears relevant is to further improve the accuracy of the proposed method, e.g. against the potential adverse effects due to the PFC provided by resources outside the VPP, as well as to further explore relevant applications of the proposed method, including the deployment of the equivalent estimated inertia to improve the frequency regulation of the grid.

Appendices

Appendix A

Stochastic Models

This appendix presents the Stochastic Delay Differential-Algebraic Equations (SDDAEs) that represent the stochastic processes applied in the thesis to the load demand profile (Section A.1), the wind speed (Section A.2), the solar irradiance (Section A.3), and the delay (Section A.4).

Power system dynamics with inclusion of stochastic processes and delays can be modeled as a set of hybrid non-linear SDDAEs [62, 64]:

$$\begin{aligned}
\dot{\boldsymbol{x}} &= \boldsymbol{f}(\boldsymbol{x}, \boldsymbol{y}, \boldsymbol{y}_d, \boldsymbol{u}, \boldsymbol{\eta})\,, \\
\boldsymbol{0} &= \boldsymbol{g}(\boldsymbol{x}, \boldsymbol{y}, \boldsymbol{y}_d, \boldsymbol{u}, \boldsymbol{\eta})\,, \\
\dot{\boldsymbol{\eta}} &= \boldsymbol{a}(\boldsymbol{x}, \boldsymbol{y}, \boldsymbol{\eta}) + \boldsymbol{b}(\boldsymbol{x}, \boldsymbol{y}, \boldsymbol{\eta})\,\boldsymbol{\xi}\,,
\end{aligned} \tag{A.1}$$

where $\boldsymbol{f}$ and $\boldsymbol{g}$ are the differential and algebraic equations, respectively; $\boldsymbol{x}$ are the state variables, e.g., rotor angles/speeds of synchronous machines, the dynamic states of loads, etc.; $\boldsymbol{y}$ are the algebraic variables, e.g., bus frequency and bus voltage magnitudes/phases, and the active power output of generators; $\boldsymbol{y}_d$ are the delayed algebraic variables; $\boldsymbol{u}$ are the input variables, e.g., load forecasts, faults and line outages; $\boldsymbol{\eta}$ represents the Stochastic Differential Equation (SDE); $\boldsymbol{a}$ and $\boldsymbol{b}$ are the *drift* and the *diffusion* terms of the SDE respectively and $\boldsymbol{\xi}$ represents the white noise, i.e., the formal time derivative of the Wiener processes.

The stochastic variations are modeled by means of the following Itô-type differential equation:

$$dx(t) = a(x(t), t)dt + b(x(t), t)dw(t), \tag{A.2}$$

where $x(t)$ and $w(t)$ are the variable affected by noise and a standard Wiener process respectively; $a(x(t), t)$ and $b(x(t), t)$ are the *drift* and the *diffusion* terms respectively. Both Gaussian and non-Gaussian processes are appropriately considered by (A.2), therefore is applicable to model wind speeds, solar irradiance fluctuations, load power variations as well as delays [62].

A.1 Stochastic Load

The stochastic Voltage-Dependent Load (VDL) is modeled as follows [62]:

$$\begin{aligned} p_{\mathrm{L}}(t) &= (-p_{\mathrm{L}o} + \eta_p(t))(v(t)/v_o)^{\alpha_p} \\ q_{\mathrm{L}}(t) &= (-q_{\mathrm{L}o} + \eta_q(t))(v(t)/v_o)^{\alpha_q} \\ \dot{\eta}_p(t) &= a_p(\mu_p - \eta_p(t)) + b_p\xi_p \\ \dot{\eta}_q(t) &= a_q(\mu_q - \eta_q(t)) + b_q\xi_q, \end{aligned} \tag{A.3}$$

where p_{L} and q_{L} are the active and reactive powers of the loads; $p_{\mathrm{L}o}$ and $q_{\mathrm{L}o}$ are the active and reactive powers at the the rated voltage v_o; $v(t)$ is the voltage magnitude of the bus where the load is connected; and α_p, α_q are the voltage exponents of the active and reactive power, respectively; the *drift* terms (a_p, a_q) are the speed at which the stochastic variables (η_p, η_q) are "attracted" towards the mean values (μ_p, μ_q), and the *diffusion* terms (b_p, b_q) represent the volatility of the processes.

A.2 Stochastic Wind

To emulate the wind speed, $a(\cdot)$ and $b(\cdot)$ in (A.2) must be defined so that the probability distribution of $x(t)$ is a Weibull process [40]. The resulting *drift* and *diffusion* terms are:

$$\begin{aligned} a(x(t)) &= -\alpha \cdot (x(t) - \mu_{\mathrm{W}}) \\ b(x(t)) &= \sqrt{b_1(x(t)) \cdot b_2(x(t))}\ , \end{aligned} \tag{A.4}$$

where α is the autocorrelation coefficient; μ_{W} is the mean of the Weibull distribution; and

$$
\begin{aligned}
b_1(x(t)) &= \frac{2 \cdot \alpha}{p_{\mathrm{W}}(x(t))} \\
b_2(x(t)) &= \lambda \cdot \Gamma\left(1 + \frac{1}{k}, \left(\frac{x(t)}{\lambda}\right)^k\right) - \mu_{\mathrm{W}} \cdot e^{-(x(t)/\lambda)^k} ,
\end{aligned}
$$

where $p_{\mathrm{W}}(\cdot)$ is the Probability Density Function (PDF) of the Weibull distribution; $\Gamma(\cdot, \cdot)$ is the incomplete Gamma function; k and λ are the shape and scale parameters of the Weibull distribution, respectively.

A.3 Stochastic Solar Irradiance

The following clear-sky index is utilized to model the solar irradiance as proposed in [39]:

$$k(t) = x(t) + \kappa(t)G(t), \tag{A.5}$$

where $k(t)$ is the clear-sky index; the stochastic variation $x(t)$ is defined by A.2; $\kappa(t) = \{0, 1\}$ is the duration of a clouding event; and $G(t)$ represents the Poisson jump process of the solar irradiance variability, e.g., the blockage of clouds passing the Solar Photo-Voltaic Generation (SPVG).

A.4 Stochastic Delay

The stochastic Wide-Area Communication (WAC) delay model is proposed in [52], which depends on several manually-set parameters, e.g. τ_f is set *a priori*. The transmission delay $\tau_p(t)$ is represented with a sawtooth function and is defined by the transmission period T and the data packet loss rate $\mathcal{P}$. The jitter η_j is assumed to be Gamma distributed and changes for each data packet. The Gamma distribution is defined by a *drift* factor a and a *diffusion* factor b.

Appendix B

Control Diagrams

This appendix introduces the control diagrams of Energy Storage System (ESS) (Section B.1), Wind Generator (WG) (Section B.2), Solar Photo-Voltaic Generation (SPVG) (Section B.3) and Phase-Locked Loop (PLL) (Section B.4) utilized in this thesis.

B.1 Energy Storage System

ESSs can be utilized to improve the transient behavior of low-inertia systems. In the thesis, the utilized ESS control structure is shown in Fig. B.1, which is proposed in [84]. The controller includes a Storage Input Limiter (SIL) to smooth the transients that derive from the energy saturation/exhaustion of the ESS, which takes the actual value of the energy stored in the device, E, and defines the controlled input variable, P. The input signal is the deviation of the measured frequency ω_i with respect to a reference frequency ω^{ref}. The frequency error is processed by the devices through a Deadband (DB), a Low-Pass Filter (LPF), a frequency controller composed of a Proportional-Integral (PI) controller and droop controller, and a SIL as well as an anti-windup first-order lag filter. A coordinated signal, namely u_i, brings additional information, e.g. the active power output set-point defined by the Transmission System Operator (TSO), is added between the DB and the LPF. The last block of Fig. B.1 represents the actual energy storage device and its output p_{ESS} is the active power injected by the ESS into the grid.

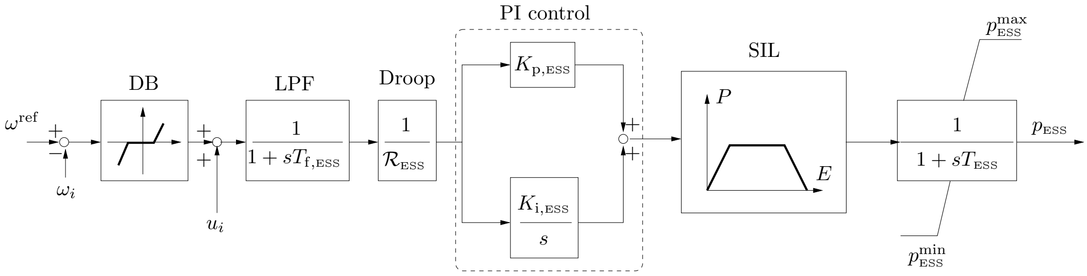

Figure B.1: Frequency control scheme of ESS.

B.2 Wind Generator

The frequency controller of WG adopted in the thesis is shown in Fig. B.2 [72]. This controller to eliminate $\omega^{\text{ref}}-\omega_i$ and u_i is coupled with the Maximum Power Point Tracking (MPPT) output (ω_{WG}) and includes a droop control and a Rate of Change of Frequency (RoCoF) control, where the LPF is used to filter out noises. The RoCoF control is typically faster with an aim to act instantly after a disturbance, while the droop control is slower and aims at providing Primary Frequency Control (PFC). The DB is utilized to enable the frequency control only if its output signal is above a given threshold. The output quantity p_{WG} shown in Fig. B.2 represents the active power reference signal that is utilized in the converter of the WG and that imposes the actual active power generation of the WG.

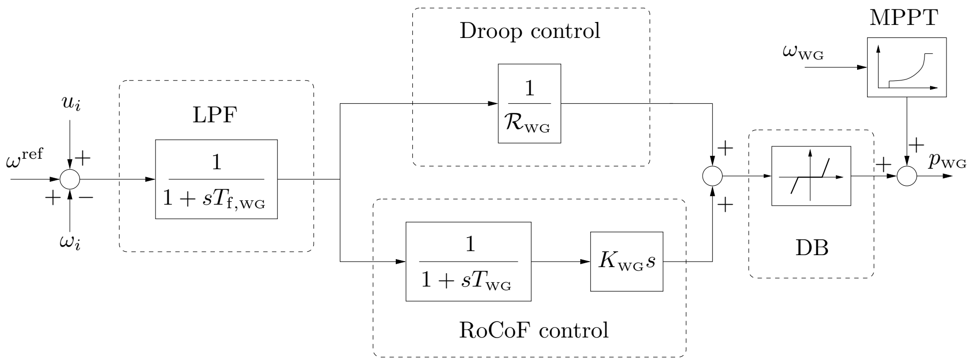

Figure B.2: Frequency control scheme of WG.

B.3 Solar Photo-Voltaic Generation

The SPVG frequency control scheme utilized in this thesis is depicted in Fig. B.3 [103]. The scheme consists of a frequency control composed of droop gain and a LPF to eliminate $\omega^{\rm ref} - \omega_i$ and u_i. The output signal is added to the MPPT reference power and then processed by a PI controller, which imposes the d-axis current of the SPVG converter. The last block of Fig. B.3 represents the converter that connects the Photo-Voltaic (PV) panel to the Alternating Current (AC) grid. Its output is the d-axis component of the current ($i_{\rm d}$) that injected by the PV panel into the grid.

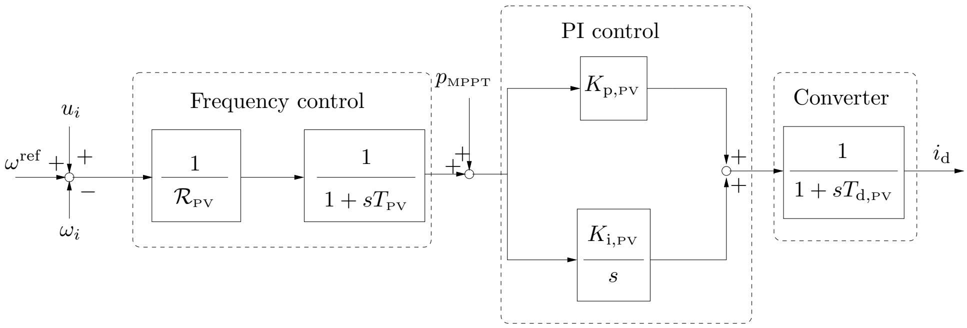

Figure B.3: Frequency control scheme of SPVG.

B.4 Phase-Locked Loop

PLLs are widely-used for the synchronization with the AC grid of the power electronic devices included in the Distributed Energy Resources (DERs). As a byproduct of the synchronization, a PLL can also provide the estimation of the bus frequency at which it is connected. There are several PLL implementations. In particular, the Synchronous Reference Frame Phase-Locked Loop (SRF-PLL) is utilized in the thesis, which is one of the most commonly adopted schemes [80, 86]. The scheme of the SRF-PLL is shown in Fig. B.4.

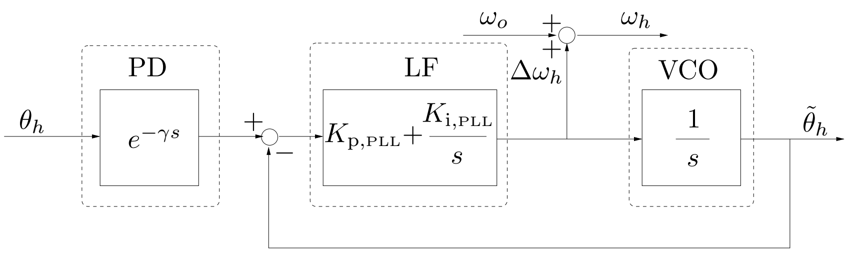

Figure B.4: Scheme of the SRF-PLL.

The SRF-PLL consists of three main components: a Phase Detector (PD) that is modeled as a pure delay; a Loop Filter (LF) that is a PI controller; and a Voltage Controlled Oscillator (VCO) that is implemented as an integrator. The PD measures the bus voltage phase angle (θ_h) at the point of connection through a constant delay. The LF is a PI controller, which produces the estimation of the bus frequency deviation $\Delta\omega_h$. Then the frequency estimation ω_h is obtained by adding the system fundamental frequency ω_o and the $\Delta\omega_h$.

Appendix C

Co-Simulation Framework for Power Systems and Communication Networks

This appendix illustrates the co-simulation framework utilized for the case studies of this thesis [129]. This framework integrates Dome [60], a Python-based power system analysis tool, and NS-3 [92], an open-source discrete-event network simulator, which allows users to customize devices and is particularly suited to education and research (see Section C.1). Examples are provided in Section C.2 to validate the performance of the co-simulation framework.

C.1 Overview of the Co-Simulation Framework

C.1.1 Power System Analysis Tool Dome

The power system analysis tool, Dome, is entirely based on Python scripting language as well as on public domain efficient C and Fortran libraries. Compared with other power system analysis tools, Dome has the advantage to use a semi-implicit formulation of Differential-Algebraic Equations (DAEs) (see Appendix A) [61]. Figure C.1 illustrates the modular structure of Dome.

C.1.2 Communication Network Simulator NS-3

NS-3 is an open-source discrete-event network simulator for internet systems, designed for networking education and research [1]. NS-3 supports Python as a scripting interface,

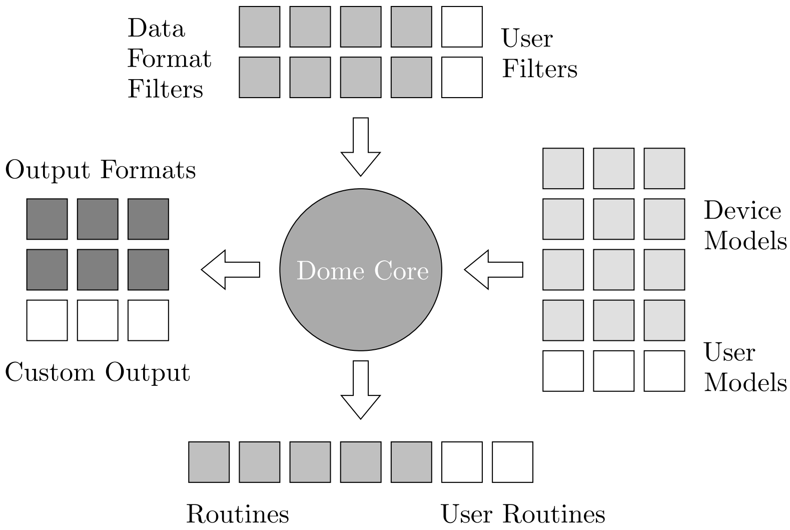

Figure C.1: Modular structure of Dome [60].

which provides the ability to ”cooperate” with Dome. Figure C.2 illustrates the basic architecture of NS-3. The detailed tutorial, manual, and model introduction can be found in the official website of NS-3 [1].

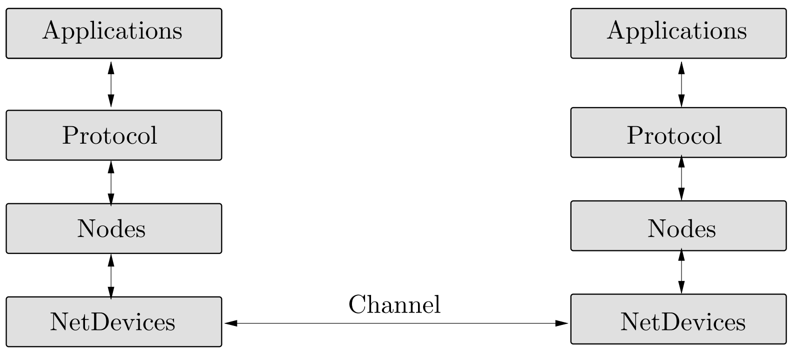

Figure C.2: The basic architecture of NS-3.

C.1.3 Dome/NS-3 Co-Simulation Framework

The design principle of the proposed framework is as follows. Dome is the “master” and NS-3 is the “slave.” All input data are passed to Dome, which takes care of initializing both the power system and the communication network. The latter is sets up in NS-3 and consists a set of the point-to-point communication channel effectively. Then Dome runs the time domain simulations and defines the time steps (fixed or adaptive). At every time step, say t, Dome solves the integration of the differential-algebraic equations that define the power systems and, at the same time passes to NS-3 the current simulation time. NS-3 is run to simulate the each Point-to-Point/Carrier Sense Multiple Access (CSMA) communications and the delays with which the transmitted signals arrive at the destination are passed back to Dome. The signals are then modeled in Dome as delayed variables and properly accounted for in the integration scheme. Figure C.3 illustrates the proposed co-simulation framework.

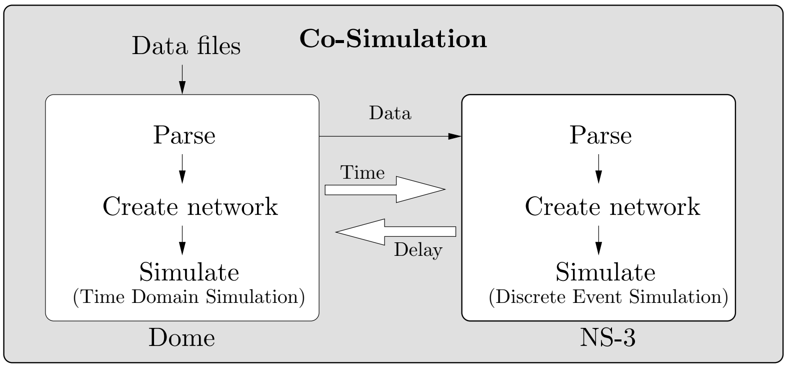

Figure C.3: The architecture of the co-simulation framework.

C.2 Examples

This section illustrates the co-simulation framework described in Section C.1 through a case study that shows the impact of Wide-Area Communication (WAC) delays on a real-world power system. The co-simulation results are compared with the results obtained with an implementation of delay done entirely in Dome.

C.2.1 Wide-Area Communication Delay Model

A realistic WAC delay can be formulated as [79]:

$$\tau(t) = \tau_f + \tau_p(t) + \eta_j(t), \tag{C.1}$$

where $\tau(t)$ is the total delay, τ_f is the fixed delay associated with transducers used, data processing, $\tau_p(t)$ is the transmission delay, and $\eta_j(t)$ is the associated random jitter resulting from network-induced issues, e.g. waiting queue in switches and router.

In an ideal WAC network, the transmission delay $\tau_p(t)$ for each data packet is a constant period:

$$T = t_{k+1} - t_k \ , \tag{C.2}$$

where t_k is the time that k-th data packet arrives. The transmission delay at a specific time t can be derived as:

$$\tau_p(t) = t - t_k \ . \tag{C.3}$$

In a real-world WAC network the $k+1$-th packet can be lost. If the packet drop-out occurs, the zero-order holder will hold the latest state as the feedback signal to the controllers until the next packet has been received, which means that the delay of the last lost packet is automatically added to the next packet. Figure C.4 shows the case when the packet $k+1$ is lost.

The time-varying WAC delays can be obtained through the proposed co-simulation framework or the mathematical model developed in [52].

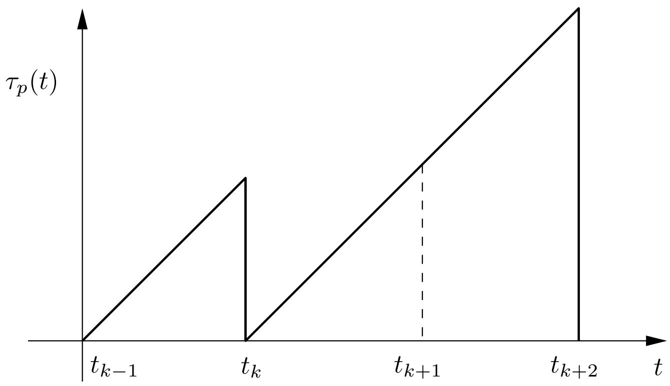

Figure C.4: Transmission delay $\tau_p(t)$ including packet loss.

C.2.1.1 Delay Generated by Co-Simulation Framework

In the co-simulation framework, the fixed delay τ_f is directly set as a parameter in Dome, as this is a feature of the PMU not a part of the communication network. The other terms of (C.1) depends on the communication network and are determined with NS-3.

In NS-3, the transmission delay model is considered as:

$$\tau_p = \tau_{po} + \frac{\mathcal{S}}{\mathcal{B}}, \tag{C.4}$$

where τ_{po} is the propagation delay decided by the transmission medium (e.g. optical fiber, Wireless Fidelity (WiFi), or Wireless Local Area Network (WLAN)), $\mathcal{S}$ is the size of each packet, and $\mathcal{B}$ is the data rate in the transmission channel.

The jitter η_j in (C.1) is decided according to the background traffic, network topology and routing protocol considered in NS-3.

C.2.1.2 Delay Generated with the Stochastic WAC Delay Model

The stochastic WAC delay model utilized in the case study is the one proposed in [52], which includes pseudo-periodic, stochastic and constant components (see Appendix A).

C.2.1.3 Comparison of Delay Models

Consider the following settings of the WAC delay in NS-3:

- The fixed delay $\tau_f = 50$ ms, considering the PMU reporting rate at 25 frames per second PMU time, namely 40 ms for each packet extra 10 ms for data processing [12].

- The PMU-sent data packet size in this simulation is set to 100 Bytes.
- A Point-to-Point link is utilized to connect PMUs to Phasor Data Concentrators (PDCs). The data rate is set as 5 Mbps, and the propagation delay of the channel is 5 ms.
- A CSMA link is utilized to connect PDCs to the control center. The CSMA link simulates the high-speed Ethernet network; the data rate is set as 34 Mbps, and the propagation delay of the channel is 2 ms.
- As the CSMA channel is established to simulate the high-speed Ethernet channel, other data are simultaneously transferred over this network. The Remote Terminal Unit (RTU) data and the video surveillance data streams are considered as the background traffic. The destination of these background traffic is the same as PMU data.
- Assume the communication network is weak for a high packet dropout rate.

In the remainder of this appendix, the delay model obtained with the co-simulation is called "Ethernet delay", as it is based on a model of a high-speed Ethernet network, whereas the model defined in [52] is called "stochastic WAC delay."

With above settings, NS-3 generates a Ethernet delay with packet loss rate 19.04%, magnitude of transmission delay of each packet $\tau_{p,\max} = 23.8$ ms, mean jitter $\bar{\eta}_j = 3.05$ ms. The corresponding settings for the stochastic WAC delay model are the following: $\tau_f = 50$ ms, $T = 23.8$ ms, $\mathcal{P} = 19.04\%$, $a = 3.05/2$, and $b = 2$. Sample trajectories of the Ethernet delay and the stochastic WAC delay are shown in Figure C.5.

According to Figure C.5, the Ethernet delay model and the mathematical delay model proposed in [52] show small but not negligible differences. The major reason for these differences is the modeling of the jitter η_j. In the co-simulation framework, the network-induced delay is a consequence of the background traffic, network topology and routing protocol. While in the stochastic WAC delay model, the jitter is simplified with a gamma-distributed stochastic value for each data packet.

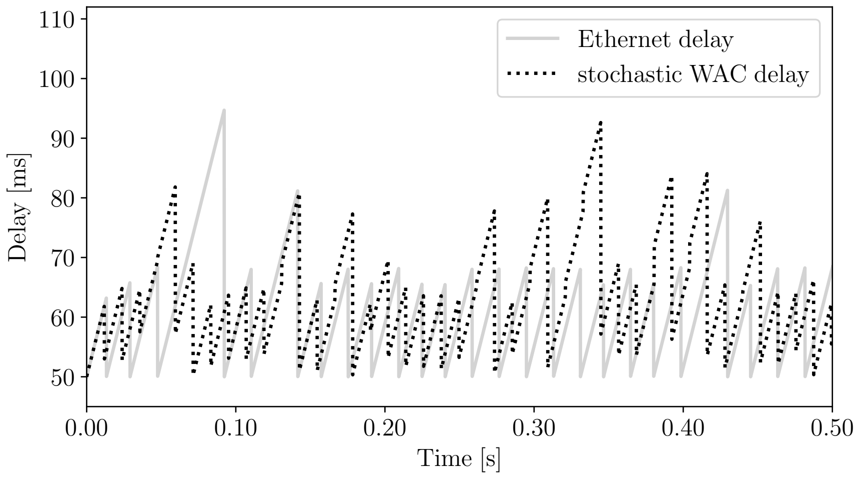

Figure C.5: Time-varing WAC delay models.

C.2.2 Time domain Simulations

This section compares the impact of the two delay models discussed above on a real-world power system, i.e., the AIITS that consists of 1479 buses, 1851 transmission lines, 176 wind power plants, 22 conventional synchronous power plants, and 6 PSSs. The schematic map of the AIITS is provided in Appendix E.

The feeding signals of the PSSs included in the AIITS are assumed to be obtained from the wide-area networks with the WAC delays discussed in Section C.2.1.3. The contingency is the outage of the synchronous power plant connected to bus 1378. The time step of time domain simulation is 1 ms. The other settings of Dome are the same as [52].

The AIITS has a very good stability margin. Therefore, to study the effect of the difference of communication delays generated by the co-simulation and stochastic model proposed in [52], the gains of the PSSs are artificially increased 70 times, thus leading to a high sensitivity of the dynamic response of the system to the delays.

Figure C.6 shows the transient behavior of the frequency of the CoI for the Irish system for various scenarios without and with inclusions of the delays. The running time for the delayed scenario under the co-simulation framework is 593 s and 451 s for Dome implemented with the stochastic WAC delay model.

Compared with the no-delay scenario, both delay models impact on the stability of the power system. However, their impact is significantly different. The scenario tested under the co-simulation framework damps the dynamic oscillation within 50 s, while the

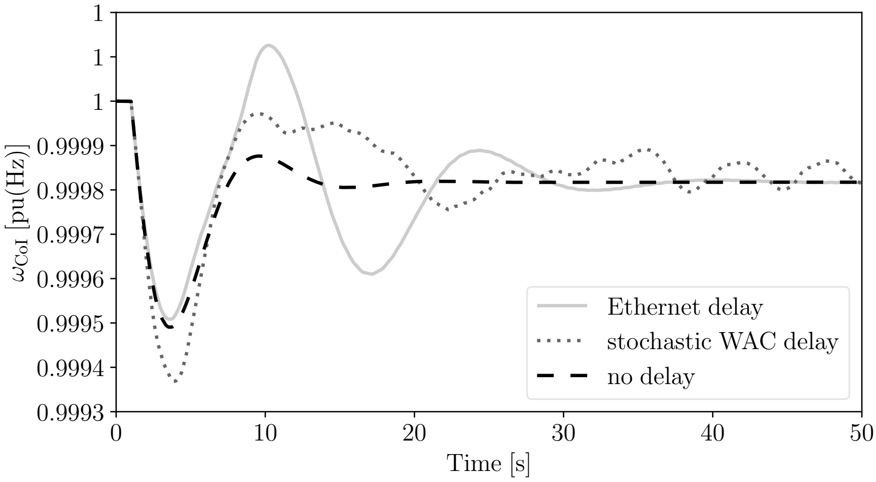

Figure C.6: Transient behavior of the frequency of the CoI for the AIITS following a power plant outage, with high PSS gains.

scenario considering the model proposed in [52] shows an irregular behavior due to the stochastic jitter included in the model.

The developed co-simulation framework appears to be a promising tool to study the impact of WAC delays on power system dynamics but clearly has a higher computational burden with respect to delay models that are directly embedded into the power system equations. This co-simulation framework can be thus utilized as a guideline to develop mathematical models that better represent real-world communication delays, since the related references and measurement data are very limited.

Appendix D

Data

This appendix describes the test systems used in the thesis. These are the Western Systems Coordinating Council (WSCC) 9-bus system (Section D.1); a modified version of the WSCC 9-bus system (Section D.2); and a communication system (Section D.3).

D.1 WSCC 9-Bus System

The single line diagram of the WSCC 9-bus, 3-machine system utilized in this thesis is shown in Figure D.1 [94]. The power and frequency bases of the system are 100 MVA

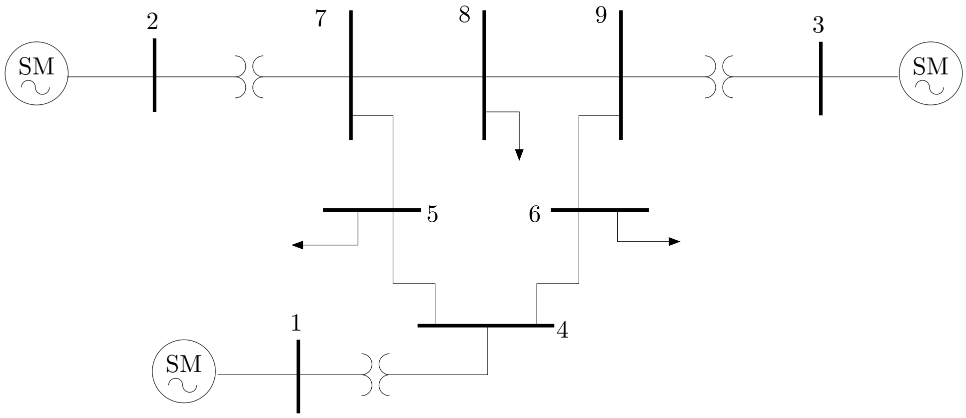

Figure D.1: WSCC 9-bus, 3-machine system.

and 60 Hz, respectively. The grid consists of 9 branches, 3 step-up transformers that connect the Synchronous Machines (SMs) to the transmission grid and 6 transmission lines. The system includes 3 loads and 3 SMs, where the SMs are represented by 4-th order (two-axis) models and are equipped with Turbine Governors (TGs) and Automatic Voltage Regulators (AVRs). The nominal voltage of the transmission system is 230 kV, while the SMs connected to buses 1, 2 and 3 have nominal voltages 16.5 kV, 18 kV and 13.8 kV, respectively. Bus 1 is the slack. The static and dynamic data of the system can be found in [94] and [6].

D.2 Modified WSCC 9-Bus System

Figure D.2 depicts the single line diagram of the modified WSCC 9-bus, 3-machine system utilized in this thesis. In particular, the load connected to bus 6 in the original system is replaced with a 8-bus, 38 kV distribution system that includes a Distribution System Virtual Power Plant (DS-VPP) [78]. The topology of the overall system is shown in Figure D.2. Specific setups are as follows.

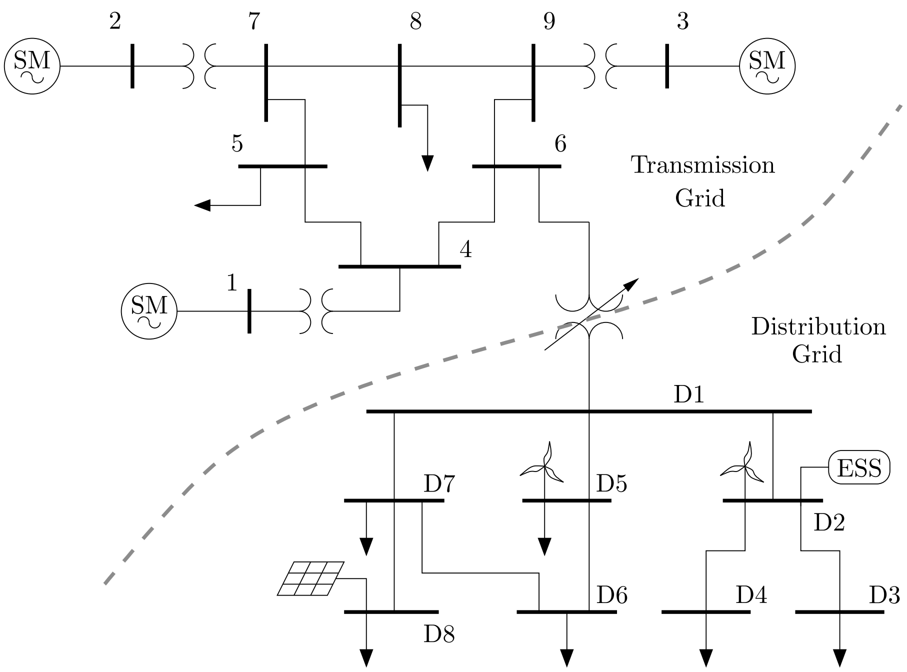

Figure D.2: Modified WSCC 9-bus, 3-machine system includes a DS-VPP.

- The DS-VPP is connected through an Under-Load Tap Changer (ULTC) type step down transformer with transmission grid.
- One Solar Photo-Voltaic Generation (SPVG), two Wind Generators (WGs), and one Energy Storage System (ESS) are connected to buses D8, D5, D2, and D2, respectively, of the distribution network. The dynamic model used to represent the frequency control structure of each Distributed Energy Resource (DER) is described in Appendix B.

- Each DER utilizes the bus frequency signal by an Synchronous Reference Frame Phase-Locked Loop (SRF-PLL) installed at Bus D1 for frequency control. The dynamic model used to represent the SRF-PLL is presented in Appendix B. The frequency signal obtained with the SRF-PLL is transmitted to the DERs that compose the DS-VPP. The model employed to represent communication network induced phenomena is described in Section D.3.

- The initial total active and reactive power consumption of loads in the DS-VPP are 57.8 MW and 11.7 MVAr, respectively. The initial active power generation of the WG and the SPVG are 15 MW each, whereas the power rate of the ESS is 10 MW.

- The focus is on the short-term transient behavior of the power system (few tens of seconds), and thus the impact of the SoC of the ESS is neglected.

Note that the total load level of the DS-VPP is lower than the initial load connected to bus 6 of Figure D.2. Hence, the active power generation of the SMs in this system is reduced to keep the power balance at the initial operating point. The power flow data and solution for the base-case operating point, and the branch data of the DS-VPP are shown in Tables D.1 and D.2.

Table D.1: Base-case power flow solution of the DS-VPP.

Bus #	V_n [kV]	V [pu(kV)]	θ [rad]	p_{G} [pu(MW)]	q_{G} [pu(MVAr)]	p_{Load} [pu(MW)]	q_{Load} [pu(MVAr)]
D1	38.0	1.0010	−0.0631	0	0	0	0
D2	38.0	0.9978	−0.0500	0.1500	0	0	0
D3	38.0	0.9642	−0.0737	0	0	0.0935	0.0190
D4	38.0	0.9918	−0.0542	0	0	0.0510	0.0105
D5	38.0	0.9871	−0.0645	0.1500	0	0.0575	0.0115
D6	38.0	0.9039	−0.1162	0	0	0.2925	0.0595
D7	38.0	0.9421	−0.0841	0	0	0.0355	0.0070
D8	38.0	1.0093	0.0124	0.1500	0	0.0480	0.0095

Table D.2: Branch data, base-case power flows and losses of the DS-VPP.

Branch #	From h	To k	Resistance [pu(Ω)]	Reactance [pu(Ω)]	p_{hk} [pu(MW)]	q_{hk} [pu(MVAr)]	p_{Loss} [pu(MW)]	q_{Loss} [pu(MVAr)]
1	D1	D2	0.377	0.396	−0.0021	0.0330	0.0004	0.0004
2	D1	D5	0.169	0.181	0.0678	0.0643	0.0014	0.0015
3	D1	D7	0.439	0.461	0.0972	0.0565	0.0054	0.0057
4	D2	D3	0.283	0.302	0.0963	0.0220	0.0028	0.0030
5	D2	D4	0.096	0.102	0.0513	0.0108	0.0003	0.0003
6	D5	D6	0.390	0.416	0.1588	0.0513	0.0112	0.0119
7	D7	D6	0.205	0.217	0.1502	0.0258	0.0054	0.0057
8	D7	D8	0.785	0.825	−0.0939	0.0180	0.0081	0.0085

D.3 Communication System

Adopting a centralized control scheme is expected to introduce delays and communication issues, e.g. data packet dropouts, which can limit the ability of the VPP to stabilize the grid. In general, a power system that is impacted by measurement and communication delays can be modeled as a set of Delay Differential-Algebraic Equations (DDAEs) [52, 64], whereas in this thesis, the delays are modeled through the co-simulation framework for power systems and communication networks given in Appendix C.1.3.

The speed of the communication network has a significant effect on the frequency response of a VPP. To take this phenomenon into account, the following three levels of communication networks, namely high-speed, middle-speed, and low-speed network, are utilized in the thesis. The settings of the communication networks are as follows. Remote signals are considered as Phasor Measurement Unit (PMU) data, transmitting through a Point-to-Point communication link. The packet size of PMU data is 100 bytes, and the reporting rate is 25 frames per second. The communication protocol is User Datagram Protocol (UDP)/Internet Protocol (IP) to avoid the data retransmission and reduce the communication delay. Background traffic, e.g. the Remote Terminal Unit (RTU) data and video surveillance streams, are also considered. The packet size and data rate are 500 bytes and 2 packets per second for RTU data, and 1024 bytes and 200 packets per second for video streams, respectively. Table D.3 shows the parameters of the communication networks.

Table D.3: Parameters of the communication networks.

Levels	Bandwidth	PMU data rate	Background traffic
High-speed	20 Mbps	25 frames/s	RTU, Video Stream
Middle-speed	5 Mbps	25 frames/s	RTU, Video Stream
Low-speed	1 Mbps	25 frames/s	N/A

Appendix E

Map of the All-Island Irish Transmission System

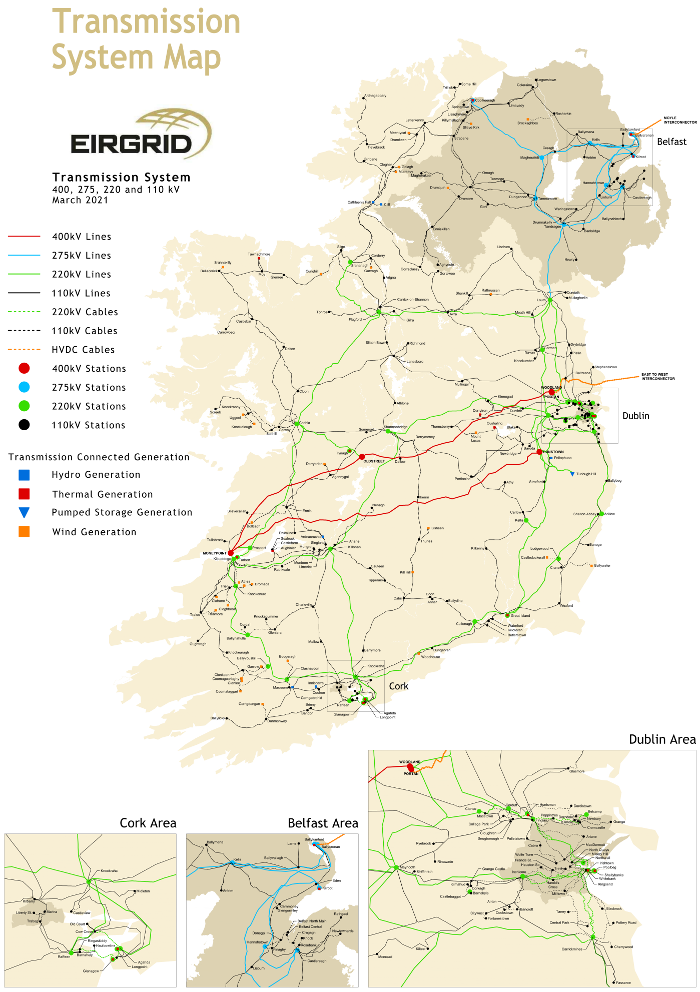

Figure E.1: AIITS: transmission system map, March 2021.

Bibliography

[1] "The ns-3 network simulator," available at https://www.nsnam.org/. 105, 106

[2] S. Acharya, M. S. El-Moursi, A. Al-Hinai, A. S. Al-Sumaiti, and H. H. Zeineldin, "A control strategy for voltage unbalance mitigation in an islanded microgrid considering demand side management capability," *IEEE Transactions on Smart Grid*, vol. 10, no. 3, pp. 2558–2568, 2018. 31

[3] R. A. Ahangar and A. Sheykholeslami, "Bulk virtual power plant, a novel concept for improving frequency control and stability in presence of large scale RES," *International Journal of Mechatronics, Electrical and Computer Technology*, vol. 4, no. 10, pp. 1017–1044, 2014. 12, 19, 22, 25, 26, 27, 31

[4] C. Ahumada, R. Cárdenas, D. Sáez, and J. M. Guerrero, "Secondary control strategies for frequency restoration in islanded microgrids with consideration of communication delays," *IEEE Transactions on Smart Grid*, vol. 7, no. 3, pp. 1430–1441, 2016. 31

[5] H. H. Alhelou, P. Siano, M. Tipaldi, R. Iervolino, and F. Mahfoud, "Primary frequency response improvement in interconnected power systems using electric vehicle virtual power plants," *World Electric Vehicle Journal*, vol. 11, no. 2, p. 40, 2020. 17, 19, 22, 25, 26, 27

[6] P. M. Anderson and A. A. Fouad, *Power system control and stability*, 2nd ed. New York, NY: Wiley-IEEE Press, 2002. 114

[7] M. F. M. Arani and E. F. El-Saadany, "Implementing virtual inertia in DFIG-based wind power generation," *IEEE Transactions on Power Systems*, vol. 28, no. 2, pp. 1373–1384, 2012. 55

[8] A. Arestova and Y. Sidorkin, "The use of wind farms and virtual power plants for emergency control in the future smart super grids," in *Proceedings of 2011 6th International Forum on Strategic Technology*, vol. 1. IEEE, 2011, pp. 437–442. 36

[9] F. Arrigo, C. Mosca, E. Bompard, and P. Cuccia, "Frequency models and control in normal operation: the Sardinia case study," in *55th International Universities Power Engineering Conference (UPEC)*, 2020, pp. 1–6. 10

[10] J. Arrillaga and N. Watson, *Computer Modelling of Electrical Power Systems*. New York: John Wiley & Sons, 2001, ch. 4, pp. 81–128. 58

[11] P. M. Ashton, C. S. Saunders, G. A. Taylor, A. M. Carter, and M. E. Bradley, "Inertia estimation of the GB power system using synchrophasor measurements," *IEEE Transactions on Power Systems*, vol. 30, no. 2, pp. 701–709, 2014. 78

[12] I. S. Association, "IEEE standard for synchrophasor data transfer for power systems," *IEEE Std C*, vol. 37. 109

[13] A. Berizzi, "The italian 2003 blackout," in *IEEE PES General Meeting*, 2004, pp. 1673–1679 Vol.2. 10

[14] H. Bevrani and S. Shokoohi, "An intelligent droop control for simultaneous voltage and frequency regulation in islanded microgrids," *IEEE Transactions on Smart Grid*, vol. 4, no. 3, pp. 1505–1513, 2013. 16, 23, 25, 27

[15] F. Bignucolo, R. Caldon, V. Prandoni, S. Spelta, and M. Vezzola, "The voltage control on MV distribution networks with aggregated DG units (VPP)," in *Proceedings of the 41st International Universities Power Engineering Conference*, vol. 1, 2006, pp. 187–192. 30

[16] L. Casasola-Aignesberger and S. Martínez, "Electric vehicle recharge strategies for frequency control in electrical power systems with high wind power generation," in *IEEE International Conference on Environment and Electrical Engineering and IEEE Industrial and Commercial Power Systems Europe (EEEIC / I CPS Europe)*, 2020, pp. 1–5. 18, 19, 22, 25, 27

[17] K. De Brabandere, B. Bolsens, J. Van den Keybus, A. Woyte, J. Driesen, and R. Belmans, “A voltage and frequency droop control method for parallel inverters,” *IEEE Transactions on power electronics*, vol. 22, no. 4, pp. 1107–1115, 2007. 78

[18] G. Delille, B. François, and G. Malarange, “Dynamic frequency control support by energy storage to reduce the impact of wind and solar generation on isolated power system’s inertia,” *IEEE Transactions on Sustainable Energy*, vol. 3, no. 4, pp. 931–939, 2012. 17, 25, 27, 31

[19] X. Domínguez, M. Pozo, C. Gallardo, and L. Ortega, “Active power control of a virtual power plant,” in *IEEE Ecuador Technical Chapters Meeting (ETCM)*. IEEE, 2016, pp. 1–6. 17, 19, 22, 25, 26, 27

[20] ENTSO-E, “Interim report system disturbance on 4 November 2006,” URL: https://eepublicdownloads.azureedge.net/clean-documents/pre2015/publications/ce/otherreports/IC-Interim-Report-20061130.pdf. 10

[21] N. Etherden, M. H. Bollen, and J. Lundkvist, “Quantification of ancillary services from a virtual power plant in an existing subtransmision network,” in *IEEE PES ISGT Europe 2013*. IEEE, 2013, pp. 1–5. 14, 19, 22, 25, 26, 27

[22] N. Etherden, V. Vyatkin, and M. H. Bollen, “Virtual power plant for grid services using IEC 61850,” *IEEE Transactions on Industrial Informatics*, vol. 12, no. 1, pp. 437–447, 2015. 15, 19, 22, 26, 27, 31

[23] M. Farrokhabadi, C. A. Cañizares, and K. Bhattacharya, “Frequency control in isolated/islanded microgrids through voltage regulation,” *IEEE Transactions on Smart Grid*, vol. 8, no. 3, pp. 1185–1194, 2017. 4, 56

[24] A. Fathi, Q. Shafiee, and H. Bevrani, “Robust frequency control of microgrids using an extended virtual synchronous generator,” *IEEE Transactions on Power Systems*, vol. 33, no. 6, pp. 6289–6297, 2018. 16, 25, 27

[25] A. Ghafouri, J. Milimonfared, and G. B. Gharehpetian, “Classification of microgrids for effective contribution to primary frequency control of power system,” *IEEE Systems Journal*, vol. 11, no. 3, pp. 1897–1906, 2015. 15, 19, 25, 27

[26] M. Giuntoli and D. Poli, "Optimized thermal and electrical scheduling of a large scale virtual power plant in the presence of energy storages," *IEEE Trans. on Smart Grid*, vol. 4, no. 2, pp. 942–955, 2013. 30

[27] J. M. Guerrero, L. G. de Vicuña, J. Matas, M. Castilla, and J. Miret, "Output impedance design of parallel-connected UPS inverters with wireless load-sharing control," *IEEE Transactions on Industrial Electronics*, vol. 52, no. 4, pp. 1126–1135, 2005. 56

[28] H. Haes Alhelou, M. E. Hamedani-Golshan, T. C. Njenda, and P. Siano, "A survey on power system blackout and cascading events: Research motivations and challenges," *Energies*, vol. 12, no. 4, p. 682, 2019. 10

[29] A. Hajizadeh, M. A. Golkar, and A. Feliachi, "Voltage control and active power management of hybrid fuel-cell/energy-storage power conversion system under unbalanced voltage sag conditions," *IEEE Transactions on Energy Conversion*, vol. 25, no. 4, pp. 1195–1208, 2010. 4, 56

[30] S. Han, S. Han, and K. Sezaki, "Development of an optimal vehicle-to-grid aggregator for frequency regulation," *IEEE Transactions on Smart Grid*, vol. 1, no. 1, pp. 65–72, 2010. 18, 25, 27

[31] N. Hatziargyriou *et al.*, "Contribution to bulk system control and stability by distributed energy resources connected at distribution network," IEEE, Tech. Rep., 2017. 55

[32] G.-C. Hsieh and J. C. Hung, "Phase-locked loop techniques. A survey," *IEEE Transactions on industrial electronics*, vol. 43, no. 6, pp. 609–615, 1996. 85

[33] Illinois Center for a Smarter Electric Grid (ICSEG), "IEEE 39-Bus System," URL: http://publish.illinois.edu/smartergrid/ieee-39-bus-system/. 62

[34] T. Inoue, H. Taniguchi, Y. Ikeguchi, and K. Yoshida, "Estimation of power system inertia constant and capacity of spinning-reserve support generators using measured frequency transients," *IEEE Transactions on Power Systems*, vol. 12, no. 1, pp. 136–143, 1997. 78

[35] P. Jampeethong and S. Khomfoi, "Coordinated control of electric vehicles and renewable energy sources for frequency regulation in microgrids," *IEEE Access*, 2020. 15, 19, 22, 25

[36] B. Jansen, C. Binding, O. Sundstrom, and D. Gantenbein, "Architecture and communication of an electric vehicle virtual power plant," in *First IEEE International Conference on Smart Grid Communications*. IEEE, 2010, pp. 149–154. 18, 19, 22, 23, 26, 27

[37] Z. Jiang and X. Yu, "Active power-voltage control scheme for islanding operation of inverter-interfaced microgrids," in *Proceedings of the IEEE PES General Meeting*, 2009, pp. 1–7. 56

[38] K. Jimma, A. Tomac, K. Vu, and C. Liu, "A study of dynamic load models for voltage collapse analysis," in *Proc. Bulk Power System Voltage Phenomena, Voltage Stability and Security NFS Workshop*, Deep Creek Lake, Maryland, August 1991. 74

[39] G. M. Jónsdóttir and F. Milano, "Modeling solar irradiance for short-term dynamic analysis of power systems," in *2019 IEEE Power & Energy Society General Meeting (PESGM)*. IEEE, 2019, pp. 1–5. 100

[40] G. M. Jónsdóttir and F. Milano, "Data-based continuous wind speed models with arbitrary probability distribution and autocorrelation," *Renewable Energy*, vol. 143, pp. 368–376, 2019. 99

[41] V. Kekatos, G. Wang, A. J. Conejo, and G. B. Giannakis, "Stochastic reactive power management in microgrids with renewables," *IEEE Transactions on Power Systems*, vol. 30, no. 6, pp. 3386–3395, 2014. 31

[42] T. Kërçi, M. T. Devine, M. A. A. Murad, and F. Milano, "Impact of the aggregate response of distributed energy resources on power system dynamics," in *IEEE PES General Meeting*. IEEE, 2020, pp. 1–5. 14, 19, 22, 23, 25, 26, 27

[43] H. Khan, S. Dasouki, V. Sreeram, H. H. Iu, and Y. Mishra, "Universal active and reactive power control of electronically interfaced distributed generation sources in virtual power plants operating in grid-connected and islanding modes," *IET*

Generation, Transmission & Distribution, vol. 7, no. 8, pp. 885–897, 2013. 15, 19, 22, 26, 27

[44] R. Khan, N. Gogoi, J. Barman, A. Latif, and D. C. Das, "Virtual power plant enabled co-ordinated frequency control of a grid connected independent hybrid microgrid using firefly algorithm," in *IEEE Region 10 Symposium (TENSYMP)*. IEEE, 2019, pp. 795–800. 18, 19, 22, 23, 25, 26, 27

[45] J. Kim, E. Muljadi, V. Gevorgian, M. Mohanpurkar, Y. Luo, R. Hovsapian, and V. Koritarov, "Capability-coordinated frequency control scheme of a virtual power plant with renewable energy sources," *IET Generation, Transmission & Distribution*, vol. 13, no. 16, pp. 3642–3648, 2019. 15, 19, 22, 25, 26, 27

[46] J.-Y. Kim, J.-H. Jeon, S.-K. Kim, C. Cho, J. H. Park, H.-M. Kim, and K.-Y. Nam, "Cooperative control strategy of energy storage system and microsources for stabilizing the microgrid during islanded operation," *IEEE Trans. on Power Electronics*, vol. 25, no. 12, pp. 3037–3048, 2010. 31

[47] D. Koraki and K. Strunz, "Wind and solar power integration in electricity markets and distribution networks through service-centric virtual power plants," *IEEE Trans. on Power Systems*, vol. 33, no. 1, pp. 473–485, 2018. 31

[48] P. Kundur, *Power System Stability and Control.* New York: McGraw-Hill, 1994. 2, 56

[49] Y. W. Li and C. Kao, "An accurate power control strategy for power-electronics-interfaced distributed generation units operating in a low-voltage multibus microgrid," *IEEE Transactions on Power Electronics*, vol. 24, no. 12, pp. 2977–2988, 2009. 56

[50] H. Liu, Z. Hu, Y. Song, and J. Lin, "Decentralized vehicle-to-grid control for primary frequency regulation considering charging demands," *IEEE Transactions on Power Systems*, vol. 28, no. 3, pp. 3480–3489, 2013. 18, 25, 27

[51] M. Liu, J. Chen, and F. Milano, "On-line inertia estimation for synchronous and non-synchronous devices," *IEEE Transactions on Power Systems*, vol. 36, no. 3, pp. 2693–2701, 2021. xi, 11, 78, 80, 81, 82, 86, 87, 89

[52] M. Liu, I. Dassios, G. Tzounas, and F. Milano, "Stability analysis of power systems with inclusion of realistic-modeling of wams delays," *IEEE Transactions on Power Systems*, 2018. 48, 100, 108, 109, 110, 111, 112, 117

[53] W. Liu, W. Gu, W. Sheng, X. Meng, Z. Wu, and W. Chen, "Decentralized multi-agent system-based cooperative frequency control for autonomous microgrids with communication constraints," *IEEE Trans. on Sustainable Energy*, vol. 5, no. 2, pp. 446–456, 2014. 31

[54] Y. Liu, H. Xin, Z. Wang, and D. Gan, "Control of virtual power plant in microgrids: a coordinated approach based on photovoltaic systems and controllable loads," *IET Generation, Transmission & Distribution*, vol. 9, no. 10, pp. 921–928, 2015. 2, 13, 19, 22, 23, 25, 27, 31

[55] R. Majumder, B. Chaudhuri, A. Ghosh, R. Majumder, G. Ledwich, and F. Zare, "Improvement of stability and load sharing in an autonomous microgrid using supplementary droop control loop," *IEEE transactions on power systems*, vol. 25, no. 2, pp. 796–808, 2009. 78

[56] U. Markovic, O. Stanojev, P. Aristidou, E. Vrettos, D. S. Callaway, and G. Hug, "Understanding small-signal stability of low-inertia systems," *IEEE Transactions on Power Systems*, 2021. 29

[57] E. Mashhour and S. M. Moghaddas-Tafreshi, "Bidding strategy of virtual power plant for participating in energy and spinning reserve markets – Part I: Problem formulation," *IEEE Transactions on Power Systems*, vol. 26, no. 2, pp. 949–956, 2010. 1, 5, 30, 78

[58] J. M. Mauricio, A. Marano, A. Gómez Expósito, and J. L. Martínez Ramos, "Frequency regulation contribution through variable-speed wind energy conversion systems," *IEEE Transactions on Power Systems*, vol. 24, no. 1, pp. 173–180, 2009. 2, 55

[59] F. Milano, *Power System Modelling and Scripting.* London: Springer, 2010. 62, 85

[60] F. Milano, "A Python-based software tool for power system analysis," in *Proceedings of the IEEE PES General Meeting*, Jul. 2013, pp. 1–5. xiii, 5, 105, 106

[61] F. Milano, "Semi-implicit formulation of differential-algebraic equations for transient stability analysis," *IEEE Transactions on Power Systems*, vol. 31, no. 6, pp. 4534–4543, Nov 2016. 105

[62] F. Milano and R. Zárate-Miñano, "A systematic method to model power systems as stochastic differential algebraic equations," *IEEE Transactions on Power Systems*, vol. 28, no. 4, pp. 4537–4544, 2013. 75, 91, 98, 99

[63] F. Milano, "Complex frequency," *IEEE Transactions on Power Systems*, pp. 1–1, 2021. 58, 79, 96

[64] F. Milano and M. Anghel, "Impact of time delays on power system stability," *IEEE Trans. on Circuits and Systems I: Regular Papers*, vol. 59, no. 4, pp. 889–900, 2011. 48, 98, 117

[65] F. Milano, F. Dörfler, G. Hug, D. J. Hill, and G. Verbič, "Foundations and challenges of low-inertia systems," in *2018 Power Systems Computation Conference (PSCC)*. Dublin, Ireland, 2018, pp. 1–25. 1, 4, 5, 9, 34, 55, 77

[66] F. Milano and Á. Ortega, *Frequency Variations in Power Systems: Modeling, State Estimation, and Control*. John Wiley & Sons, 2020. 9

[67] F. Milano and Á. Ortega, "A method for evaluating frequency regulation in an electrical grid – Part I: Theory," *IEEE Transactions on Power Systems*, vol. 36, no. 1, pp. 183–193, 2020. 58, 78

[68] F. Milano and Á. Ortega Manjavacas, *Converter-Interfaced Energy Storage Systems: Context, Modelling and Dynamic Analysis*. Cambridge University Press, 2019. 3

[69] J. V. Milanovic, K. Yamashita, S. M. Villanueva, S. Ž. Djokic, and L. M. Korunović, "International industry practice on power system load modeling," *IEEE Transactions on Power Systems*, vol. 28, no. 3, pp. 3038–3046, 2012. 62

[70] A. Moeini and I. Kamwa, "Analytical concepts for reactive power based primary frequency control in power systems," *IEEE Transactions on Power Systems*, vol. 31, no. 6, pp. 4217–4230, 2016. 56

[71] J. M. Morales, A. J. Conejo, H. Madsen, P. Pinson, and M. Zugno, "Virtual power plants," in *Integrating renewables in electricity markets*. Springer, 2014, pp. 243–287. 1, 30, 36

[72] J. Morren, S. W. De Haan, W. L. Kling, and J. Ferreira, "Wind turbines emulating inertia and supporting primary frequency control," *IEEE Transactions on Power Systems*, vol. 21, no. 1, pp. 433–434, 2006. 12, 25, 27, 102

[73] P. Moutis, A. Vassilakis, A. Sampani, and N. Hatziargyriou, "DC switch driven active power output control of photovoltaic inverters for the provision of frequency regulation," *IEEE Transactions on Sustainable Energy*, vol. 6, no. 4, pp. 1485–1493, 2015. 12

[74] P. Moutis, P. S. Georgilakis, and N. D. Hatziargyriou, "Voltage regulation support along a distribution line by a virtual power plant based on a center of mass load modeling," *IEEE Trans. on Smart Grid*, vol. 9, no. 4, pp. 3029–3038, 2018. 31

[75] P. Moutis and N. D. Hatziargyriou, "Decision trees-aided active power reduction of a virtual power plant for power system over-frequency mitigation," *IEEE Transactions on Industrial Informatics*, vol. 11, no. 1, pp. 251–261, 2014. 12, 19, 22, 23, 25, 26, 27

[76] E. Munkhchuluun, L. Meegahapola, and A. Vahidnia, "Reactive power control of PV for improvement of frequency stability of power systems," in *Proceedings of the IEEE PES General Meeting*, 2020, pp. 1–5. 56

[77] M. A. A. Murad, G. Tzounas, M. Liu, and F. Milano, "Frequency control through voltage regulation of power system using SVC devices," in *Proceedings of the IEEE PES General Meeting*, 2019, pp. 1–5. 56

[78] C. Murphy and A. Keane, "Local and remote estimations using fitted polynomials in distribution systems," *IEEE Transactions on Power Systems*, vol. 32, no. 4, pp. 3185–3194, 2016. 38, 74, 114

[79] B. Naduvathuparambil, M. C. Valenti, and A. Feliachi, "Communication delays in wide area measurement systems," in *System Theory, 2002. Proceedings of the Thirty-Fourth Southeastern Symposium on*. IEEE, 2002, pp. 118–122. 108

[80] A. Nicastri and A. Nagliero, "Comparison and evaluation of the PLL techniques for the design of the grid-connected inverter systems," in *ISIE*, 2010, pp. 3865–3870. 103

[81] K. S. Nielsen, "Test system for determining a frequency response of a virtual power plant," Sep. 1 2015, uS Patent 9,122,274. 13, 19, 22, 25, 26, 27

[82] D. Ochoa and S. Martínez, "Fast-frequency response provided by DFIG-wind turbines and its impact on the grid," *IEEE Transactions on Power Systems*, vol. 32, no. 5, pp. 4002–4011, 2016. 55

[83] Á. Ortega and F. Milano, "Design of a control limiter to improve the dynamic response of energy storage systems," in *IEEE PES General Meeting*, 2015, pp. 1–5. 39

[84] Á. Ortega and F. Milano, "Generalized model of VSC-based energy storage systems for transient stability analysis," *IEEE Transactions on Power Systems*, vol. 31, no. 5, pp. 3369–3380, 2015. 3, 12, 25, 27, 101

[85] Á. Ortega and F. Milano, "Modeling, simulation, and comparison of control techniques for energy storage systems," *IEEE transactions on Power Systems*, vol. 32, no. 3, pp. 2445–2454, 2016. 3

[86] Á. Ortega and F. Milano, "Impact of frequency estimation for VSC-based devices with primary frequency control," in *ISGT-Europe*, 2017, pp. 1–6. 103

[87] Á. Ortega and F. Milano, "Frequency control of distributed energy resources in distribution networks," *IFAC-PapersOnLine*, vol. 51, no. 28, pp. 37–42, 2018. 13, 19, 22, 25, 26, 27

[88] A. Oudalov, D. Chartouni, and C. Ohler, "Optimizing a battery energy storage system for primary frequency control," *IEEE Transactions on Power Systems*, vol. 22, no. 3, pp. 1259–1266, 2007. 17, 25, 27, 31

[89] O. Palizban, K. Kauhaniemi, and J. M. Guerrero, "Microgrids in active network management—Part I: Hierarchical control, energy storage, virtual power plants, and market participation," *Renewable and Sustainable Energy Reviews*, vol. 36, pp. 428–439, 2014. 16, 19, 22, 25, 27

[90] D. Pudjianto, C. Ramsay, and G. Strbac, "Virtual power plant and system integration of distributed energy resources," *IET Renewable Power Generation*, vol. 1, no. 1, pp. 10–16, 2007. 15, 19, 22, 26, 77, 78

[91] G. Ramtharan, N. Jenkins, and J. Ekanayake, "Frequency support from doubly fed induction generator wind turbines," *IET Renewable Power Generation*, vol. 1, no. 1, pp. 3–9, 2007. 12, 25, 27

[92] G. F. Riley and T. R. Henderson, "The ns-3 network simulator," in *Modeling and tools for network simulation.* Springer, 2010, pp. 15–34. 5, 105

[93] N. Ruiz, I. Cobelo, and J. Oyarzabal, "A direct load control model for virtual power plant management," *IEEE Transactions on Power Systems*, vol. 24, no. 2, pp. 959–966, 2009. 2, 14, 19, 22, 26, 27, 30

[94] P. W. Sauer and M. A. Pai, *Power System Dynamics and Stability.* Prentice hall Upper Saddle River, NJ, 1998, vol. 101. 38, 48, 85, 113, 114

[95] J. Schiffer, T. Seel, J. Raisch, and T. Sezi, "Voltage stability and reactive power sharing in inverter-based microgrids with consensus-based distributed voltage control," *IEEE Transactions on Control Systems Technology*, vol. 24, no. 1, pp. 96–109, 2015. 31

[96] C. Schwaegerl and L. Tao, "The microgrids concept," *Microgrids*, pp. 1–24, 2013. 15

[97] E. A. Setiawan, *Concept and Controllability of Virtual Power Plant.* Kassel University press GmbH, 2007. 14, 19, 31

[98] T. Sikorski *et al.*, "A case study on distributed energy resources and energy-storage systems in a virtual power plant concept: Technical aspects," *Energies*, vol. 13, no. 12, p. 3086, 2020. 16, 19, 22, 26, 31

[99] J. W. Simpson-Porco, Q. Shafiee, F. Dörfler, J. C. Vásquez, J. M. Guerrero, and F. Bullo, "Secondary frequency and voltage control of islanded microgrids via distributed averaging," *IEEE Transactions on Industrial Electronics*, vol. 62, no. 11, pp. 7025–7038, 2015. 31

[100] Sustainable Energy Authority of Ireland, "Energy in ireland 2020 report," 2020, available at https://www.seai.ie/publications/Energy-in-Ireland-2020.pdf. 1

[101] M. Świerczyński, D. I. Stroe, R. Lærke, A. I. Stan, P. C. Kjær, R. Teodorescu, and S. K. Kær, "Field experience from Li-ion BESS delivering primary frequency regulation in the Danish energy market," *ECS Transactions*, vol. 61, no. 37, p. 1, 2014. 17, 19, 22, 25, 26, 27

[102] M. Świerczyński, D. I. Stroe, A. I. Stan, and R. Teodorescu, "Primary frequency regulation with Li-ion battery energy storage system: A case study for Denmark," in *IEEE ECCE Asia Downunder*. IEEE, 2013, pp. 487–492. 14, 19, 22, 25, 26, 27

[103] B. Tamimi, C. Cañizares, and K. Bhattacharya, "Modeling and performance analysis of large solar photo-voltaic generation on voltage stability and inter-area oscillations," in *IEEE PES General Meeting*. IEEE, 2011, pp. 1–6. 103

[104] C. Tu, J. Cao, L. He, and Y. Fang, "Combined active and reactive power control strategy to improve power system frequency stability with DFIGs," *The Journal of Engineering*, vol. 2017, no. 13, pp. 2021–2025, 2017. 56

[105] G. Tzounas and F. Milano, "Improving the frequency response of DERs through voltage feedback," in *Proceedings of the IEEE PES General Meeting*, 2021, accepted in Mar. 2021, available at http://faraday1.ucd.ie/. 56

[106] M. Vasirani, R. Kota, R. L. Cavalcante, S. Ossowski, and N. R. Jennings, "An agent-based approach to virtual power plants of wind power generators and electric vehicles," *IEEE Transactions on Smart Grid*, vol. 4, no. 3, pp. 1314–1322, 2013. 18, 19, 22, 23, 26, 27, 31

[107] K. Vidyanandan and N. Senroy, "Primary frequency regulation by deloaded wind turbines using variable droop," *IEEE Transactions on Power Systems*, vol. 28, no. 2, pp. 837–846, 2012. 12, 25, 27

[108] P. N. Vovos, A. E. Kiprakis, A. R. Wallace, and G. P. Harrison, "Centralized and distributed voltage control: Impact on distributed generation penetration," *IEEE Transactions on Power Systems*, vol. 22, no. 1, pp. 476–483, 2007. 31

[109] P. Wall, F. González-Longatt, and V. Terzija, "Estimation of generator inertia available during a disturbance," in *2012 IEEE Power and Energy Society General Meeting*. IEEE, 2012, pp. 1–8. 78

[110] P. Wall and V. Terzija, "Simultaneous estimation of the time of disturbance and inertia in power systems," *IEEE Transactions on Power Delivery*, vol. 29, no. 4, pp. 2018–2031, 2014. 78

[111] Y. Wan, M. A. A. Murad, M. Liu, and F. Milano, "Voltage frequency control using SVC devices coupled with voltage dependent loads," *IEEE Transactions on Power Systems*, vol. 34, no. 2, pp. 1589–1597, 2018. 4, 56

[112] Y. Wang, X. Ai, Z. Tan, L. Yan, and S. Liu, "Interactive dispatch modes and bidding strategy of multiple virtual power plants based on demand response and game theory," *IEEE Trans. on Smart Grid*, vol. 7, no. 1, pp. 510–519, 2016. 31

[113] F. Wilches-Bernal, J. H. Chow, and J. J. Sanchez-Gasca, "A fundamental study of applying wind turbines for power system frequency control," *IEEE Transactions on Power Systems*, vol. 31, no. 2, pp. 1496–1505, 2016. 56

[114] X. Wu, C. Shen, and R. Iravani, "A distributed, cooperative frequency and voltage control for microgrids," *IEEE Transactions on Smart Grid*, vol. 9, no. 4, pp. 2764–2776, 2016. 16, 25, 27

[115] H. Xin, D. Gan, N. Li, H. Li, and C. Dai, "Virtual power plant-based distributed control strategy for multiple distributed generators," *IET Control Theory & Applications*, vol. 7, no. 1, pp. 90–98, 2013. 31

[116] H. Yang, D. Yi, J. Zhao, and Z. Dong, "Distributed optimal dispatch of virtual power plant via limited communication," *IEEE Trans. on Power Systems*, vol. 28, no. 3, pp. 3511–3512, 2013. 31

[117] J. Yang, Q. Zheng, J. Zhao, X. Guo, and C. Gao, "Control strategy of virtual power plant participating in the system frequency regulation service," in *4th International*

Conference on Systems and Informatics (ICSAI). IEEE, 2017, pp. 324–328. 14, 19, 22, 25, 26, 27

[118] L. Yavuz, A. Önen, S. Muyeen, and I. Kamwa, "Transformation of microgrid to virtual power plant–a comprehensive review," *IET Generation, Transmission & Distribution*, vol. 13, no. 11, pp. 1994–2005, 2019. 14, 19, 22, 23, 25, 26, 27

[119] A. Yazdani and P. P. Dash, "A control methodology and characterization of dynamics for a photovoltaic (PV) system interfaced with a distribution network," *IEEE Transactions on Power Delivery*, vol. 24, no. 3, pp. 1538–1551, 2009. 12, 27

[120] M. Zeraati, M. E. H. Golshan, and J. M. Guerrero, "A consensus-based cooperative control of PEV battery and PV active power curtailment for voltage regulation in distribution networks," *IEEE Transactions on Smart Grid*, vol. 10, no. 1, pp. 670–680, 2017. 4, 56

[121] J. Zhao, X. Lyu, Y. Fu, X. Hu, and F. Li, "Coordinated microgrid frequency regulation based on DFIG variable coefficient using virtual inertia and primary frequency control," *IEEE Transactions on Energy Conversion*, vol. 31, no. 3, pp. 833–845, 2016. 16, 25, 27

[122] X. Zhao-Xia, Z. Mingke, H. Yu, J. M. Guerrero, and J. C. Vásquez, "Coordinated primary and secondary frequency support between microgrid and weak grid," *IEEE Transactions on Sustainable Energy*, vol. 10, no. 4, pp. 1718–1730, 2018. 16, 25, 27

[123] W. Zhong, G. Tzounas, M. Liu, and F. Milano, "On-line inertia estimation of virtual power plants," *Electric Power Systems Research*, 2022, accepted in February 2022. Available online at: faraday1.ucd.ie/vppinert.pdf. 78, 82, 87

[124] W. Zhong, G. Tzounas, and F. Milano, "Real-time estimation of vpp equivalent inertia and fast frequency control," in *IEEE PES General Meeting*, 2022, pp. 1–5, accepted in February 2022. Available online at: faraday1.ucd.ie/inertiavppffr.pdf. 78

[125] W. Zhong, J. Chen, M. Liu, M. A. A. Murad, and F. Milano, "Coordinated control of virtual power plants to improve power system short-term dynamics," *Energies*, vol. 14, no. 4, p. 1182, 2021. 5, 48, 71, 78

[126] W. Zhong, T. Kërçi, and F. Milano, "On the impact of topology on the primary frequency control of virtual power plants," in *2021 IEEE Madrid PowerTech*. IEEE, 2021, pp. 1–6. 37

[127] W. Zhong, M. A. A. Murad, M. Liu, and F. Milano, "Impact of virtual power plants on power system short-term transient response," *Electric Power Systems Research*, vol. 189, p. 106609, 2020. 4, 13, 19, 22, 25, 26, 27, 34, 71

[128] W. Zhong, G. Tzounas, and F. Milano, "Improving the power system dynamic response through a combined voltage-frequency control of distributed energy resources," *IEEE Transactions on Power Systems*, 2022. 55

[129] W. Zhong, M. Liu, and F. Milano, "A co-simulation framework for power systems and communication networks," in *2019 IEEE Milan PowerTech*, 2019, pp. 1–6. 105